NOTICE

The quality of this microform is heavily dependent upon the quality of the original thesis submitted for microfilming. Every effort has been made to ensure the highest quality of reproduction possible.

If pages are missing, contact the university which granted the degree.

Some pages may have indistinct print especially if the original pages were typed with a poor typewriter ribbon or if the university sent us an inferior photocopy.

Reproduction in full or in part of this microform is governed by the Canadian Copyright Act, R.S.C. 1970, c. C-30, and subsequent amendments.

AVIS

La qualité de cette microforme dépend grandement de la qualité de la thèse soumise au microfilmage. Nous avons tout fait pour assurer une qualité supérieure de reproduction.

S'il manque des pages, veuillez communiquer avec l'université qui a conféré le grade.

La qualité d'impression de certaines pages peut laisser à désirer, surtout si les pages originales ont été dactylographiées à l'aide d'un ruban usé ou si l'université nous a fait parvenir une photocopie de qualité inférieure.

La reproduction, même partielle, de cette microforme est soumise à la Loi canadienne sur le droit d'auteur, SRC 1970, c. C-30, et ses amendements subséquents.

Canada

RESPONSE OF STRUCTURES TO IMPACT LOADS USING ELASTIC AND PLASTIC ANALYSIS

Gautam Mundkur

A Thesis

in

The Department

of

Mechanical Engineering

Presented in Partial Fulfillment of the Requirements

for the Degree of Master of Applied Science at

Concordia University

Montreal, Quebec, Canada

May 1992

ISBN 0-315-84647-X

Canada

ABSTRACT

RESPONSE OF STRUCTURES TO IMPACT LOADS USING ELASTIC AND PLASTIC ANALYSIS

GAUTAM MUNDKUR

The objective of this work is to study the response of structures to impact loads. Depending on the magnitude of impact the structural response may need elastic or plastic analysis When the deformations are within the elastic region, normal mode analysis is used to find the response. Structures considered in this study are Beams and Rectangular Plates. The Rayleigh-Ritz method is used to obtain the natural frequency and mode shape coefficients. Different types of displacement shape functions are employed in the analysis in the past such as beam characteristic functions and beam characteristic orthogonal polynomials. An approximate plate function is arrived at by reduction of the plate partial differential equation and solving the resulting ordinary differential equation as in Kantarovich method, and then used in the Rayleigh-Ritz method. The same reduction procedure is also used along with successive iteration until convergence to obtain the natural frequencies and mode shape functions directly. This method takes much less time for response evaluation than that is required by using the Rayleigh-Ritz method. Structural response to impact loads is also carried out using rigid plastic analysis. A cantilever beam with impulsive load applied at the free end is considered with finite blade radius and varying centrifugal forces are considered in the investigation.

Experimental simulation of impact loading is carried out in the laboratory using a mass falling from a known height onto the structure under investigation. The elastic response of a plate with two adjacent edges clamped and the other two free are observed, and a equivalent mathematical model formulated by using flexible edge supports.

ACKNOWLEDGEMENT

The author wishes to express deep sense of gratitude and appreciation to his supervisor, Dr. R. B. Bhat for his continued support and encouragement, invaluable guidance, and great patience during the course of this work.

Thanks are also due to Dr. C. Rajalingham for his help and guidance.

I appreciate the help and suggestions by staff of Mechanical Engineering Department at the Concordia University.

Special thanks must go to my friends and family for their abundant moral support all along.

TABLE OF CONTENTS

CHAPTER 3

ELASTIC RESPONSE OF BEAMS AND PLATES

CHAPTER 4

PLASTIC ANALYSIS OF STRUCTURES TO IMPACT LOADING

CHAPTER 5

EXPERIMENTAL INVESTIGATIONS

CHAPTER 6

CONCLUSIONS AND SCOPE FOR FURTHER RESEARCH

NOMENCLATURE

a, b	Dimensions of a rectangular plate in x and y directions, respectively
C_1, C_2, C_3, C_4	Constants of integration in x direction
C_1^*, C_2^*, C_3^*, C_4^*	Constants of integration in y direction
D	Plate flexural rigidity, $[Eh^3/[12(1-\nu^2)]]$
E	Modulus of elasticity of the plate material
G	Modulus of rigidity, $[E/2(1+\nu)]$
h	Plate thickness
$M(x)$,$M(y)$	Plate bending moments in x and y directions, respectively
$V(x)$, $V(y)$	Plate shear forces in x and y directions, respectively
m, n	Number of half waves in x and y directions, respectively
$p_{1,2}$, $q_{1,2}$	Roots of reduced equation in x and y directions, respectively
T_{max}	Maximum kinetic energy
U_{max}	Maximum potential energy
w	Transverse plate deflection, $[w(x,y,t)]$
x	Dimensionless plate cartesian coordinate$[\xi/a]$
y	Dimensionless plate cartesian coordinates$[\eta/b]$
α	Plate aspect ratio, $[a/b]$
δ	Variation symbol
ν	Poisson's ratio for the plate material
∇	Laplacian operator
ρ	Mass density of plate material
σ, τ	Coefficients of functions
ω	Circular natural frequency of plate vibration
Ω	Non-dimensional frequency parameter, $\left[\omega a^2\sqrt{\frac{\rho h}{D}}\right]$
ϕ	Deflection shape of plate in x direction

ψ	Deflection shape of plate in y direction
$\xi,\ \eta$	Cartesian coordinates along plate edges

LIST OF FIGURES

LIST OF TABLES

Chapter 1

INTRODUCTION

1.1 General

A good understanding of the dynamic behavior of structures under impulsive loads is very important in engineering design. Impulsive loads are characterized by their suddenness of application and brevity of duration. Loads of this nature are generally experienced in cases of sudden impact on structures due to collision with a metallic or non-metallic mass. Ships and submarines experience such loads due to blast of mines, sudden variation in velocity of water flow or collision with external particles such as rocks or floating ice. Aircraft compressor fan blades are prone to bird impacts during take-off. Blades in aircraft turbine engines may fail during operation causing serious damage to the casing when the broken piece impacts at very high speeds, and may sometimes even penetrate through the fuselage. All these structures must be designed to withstand such impact loads. Various approaches involving elastic and plastic analysis are being used to design such structures to withstand impact loads. Aerospace structures are subjected to such loading due to meteoroid impact,and from a variety of sources including dropped tools, runway debris, and munitions. In advanced composite materials, impact loading can cause significant internal structural damage, and therefore, development of an accurate means of calculating structural response due to impact loading is of critical importance in the analysis and design of advanced space structures[9].

There are dynamic effects on stationary structures such as bridges, the railway tracks, and cranes due to moving loads which may cause impact conditions. Japanese Railway Technical Research Institute (RTRI) uses Impact Testing results on bridges to monitor the integrity of bridge foundations. Permanent damage inelastic collisions can occur in moving vehicles. Ground accelerations during earthquakes[10] are in the

form of sudden pulses and buildings must be designed to withstand such loads. Civil Engineering structures such as buildings and bridges are subjected to blast loadings during bombing. Design of Nuclear reactors must take care of withstanding such loads due to impact from missiles or aircrafts. Engineering structures are analysed for impulse loading by observing response to pulse loading of various shapes. Response of structures reduced to a simple spring mass system are studied in terms of dynamic load factor with different ratios of pulse period to natural period of the system. These provide a good insight into the dynamic behaviour of structures for such loads. These can be used for any ratio of peak force to stiffness combinations which are called dynamic magnification factors of the system under study.

It is also interesting to find the structural response due to high rates of loading experienced by structures when an unintentional explosion takes place in a piece of equipment. Not much is known about the phenomenon of localized bending which accompanies the impact of a projectile travelling at a high velocity. There is considerable evidence based on observation of points which have been hit by bullets, shells, or bombs to indicate that dominant effects are localized, and that structures as a whole do not have time to react to the sudden blow because of their inertia. However, the containment tests indicate that there is failure of secondary attachment structure.

1.2 Review of Literature

Impact problems on beams and plates have been studied quite extensively. Extension of Hertz Theory of colliding solids to include vibration of one of the colliding body involves study of transverse impact of a solid sphere upon a beam or a plate. The coefficient of restitution is an important element in any analysis of motion ensuing after the collision of two bodies[1].

Experimental results verify the theory when the limitations of the theory are not violated. The velocity of impact must be sufficiently small to avoid plastic deformation. When the collision involves steel on steel, the velocity must be usually less than 0.3 meters per second. However, useful Engineering results can be obtained with

this approach even though plastic deformation does occur locally [2]. Experiments also show that the low velocity impact can also leave permanent craters at the impact point[3].

1.2.1 Elastic Response of Mechanical systems

Response Analysis of mechanical systems involving elastic components such as bars, beams, plates, and shells subjected to harmonic loading is generally carried out by analytical methods. However, in case of complicated structures it is necessary to formulate a discretized model. These elements have continuously distributed mass and stiffness properties which need to be discretized when there is no exact solution available in some cases. There are various methods of formulating such problems, one of them being Finite Element Analysis. Modal Analysis Techniques are widely used in the case of complicated structures due to its versatility and ease of operation along with experimental methods.

Timoshenko initiated the basic approach by combining Hertz's contact force law with the Bernoulli-Euler Beam Theory to predict the transient dynamic response of a beam to the impact of an elastic sphere. The impact of a mass on a plate was first investigated by Karas [4] using the classical plate theory and assuming Hertzian force deflection relationship at the contact point. Zener pointed out that the central displacement is proportional to the impulse of the contact force[5].

Classical methods of solution of response by using the mode summation procedure is carried out by Hoppmann[6, 7, 8]. He studied the response of a damped elastically supported beam subjected to a central impact. Similar study was carried out by the same author for transverse impact of a mass on a column with elastic support throughout its length, and response of a multispan beam with simply-supported ends subjected to an impulsive load at the center of the mid-span due to a collision of a solid sphere. The simply-supported plate response is analysed along with permanent indentation effects by Chattopadhyay [3] using Zener's approach. By using experimental data obtained for permanent indentation due to impact of an elastic

sphere on an elastic beam he evaluated displacement time histories for a plate with elastic and inelastic impacts. The energy absorbed in the plate due to these responses have also been obtained to predict additional energy contribution due to permanent indentation.

A non-linear force-displacement relationship is used to calculate the transient force and local deformation at the point of contact by Trowbridge et al. [9] by using NASTRAN to define a finite element model that behaves globally linearly elastic, and locally non-linear elastic. A computational technique is developed to predict the dynamic response of a structure to a low velocity elastic impact by using a triangular pulse to simulate the impact force.

Low velocity impact of an elastic plate resting on sand was carried out by Chen et al. [10] by using an experimental set-up that measures contact duration of the steel ball impacting the plate. The analysis and the experiments resulted in comparable values of arrival time, the duration, and magnitude. The radial strain at the bottom of the target plate and the acceleration of sand beneath the center of the target plate were evaluated.

Sansalone et al.[11] have carried out extensive tests on thick circular plates for transient response due to impact.

With the advent of composites as the material in Engineering designs, the impact tests and analysis on such anisotropic laminated plates are carried out extensively. Ramkumar et al.[12] have presented response of such plates due to low velocity impact loads considering Mindlin's theory and the governing equations are solved by Fourier Integral Transforms.

Structural response evaluation by normal mode analysis uses the normal modes and natural frequencies of structures. In the case of bars and beams there are exact solutions for natural frequencies and natural modes depending on the boundary conditions. The natural frequency parameters and mode shape coefficients for beams in

case of bending vibrations are well documented by Young and Felgar Jr. [13].

There is no exact solution for the natural frequencies and normal modes of rectangular plates unless at least two opposite edges of the plate are simply-supported. The Rayleigh-Ritz method of analysis is widely used in cases where there are no exact solutions available. In this method, the mass and stiffness matrices are formulated by assuming deflection shape functions that satisfy the boundary conditions of the plate. The eigenvalue problem is then solved to obtain natural frequency and mode shape coefficients. A detailed review is presented in Leissa's monograph [14].

Shape functions that satisfy at least the geometrical boundary conditions are essential in solving an eigenvalue problem by the Rayleigh-Ritz method. Beam characteristic functions were used by Leissa [15] to study plates with several combinations of boundary conditions. Vijayakumar and Ramaiah [16] used modified Bolotin's solutions as admissible shape functions. Bhat[17] proposed beam characteristic orthogonal polynomials to study the vibration of rectangular plates. He used the simplest polynomial that satisfied the boundary conditions at the two opposite edges of the plate and constructed the other members of the orthogonal polynomial set using Gram - Schmidt process [18]. Products of beam characteristic orthogonal polynomials on either direction were used as assumed shape functions. Dickinson and Di Blasio [21], Kim and Dickinson [22] used boundary characteristic orthogonal polynomials in Rayleigh-Ritz method to study vibration of plates of various configurations. Laura and Cortinez [23] and Cortinez and Laura [24] used optimized Kantorovich method, essentially reducing the partial differential equation into an ordinary differential equation to obtain the fundamental frequency coefficients of plates. Simply-supported plate functions were employed by Dickinson[25] to study vibration of plates by Rayleigh-Ritz method. In this technique, he arbitrarily assumed simply-supported conditions on two opposite edges to get exact solution for the perpendicular direction. Repeating this procedure on the remaining two opposite edges he obtained another set of exact solutions in the first direction. Using these functions in the Rayleigh-Ritz method he obtained very good results when all the plate edges were supported in some manner. However, when one or more edges were free, the results were sometimes

worse than those obtained using beam characteristic functions.

Results obtained by the Rayleigh-Ritz method were used by Warburton[28] to analyse the plate response. For harmonic excitation, amplitudes of displacements and bending moment were combined with values from a modal solution of the plate equation. He pointed out that determination of resonant response is less accurate than a comparable evaluation of the corresponding natural frequency by Rayleigh Ritz method. He concluded that the results from Rayleigh-Ritz method can be used for response calculations of beams, plates, and shells, but for acceptable accuracy appropriate number of deflection shape functions may have to be included.

1.2.2 Plastic Analysis

Rigid plastic analysis is used by various researchers in analysing permanent deformations of a cantilever beam. When subjected to transverse impact at the tip, a rigid plastic cantilever will bend at a discrete plastic hinge that moves away from the impact site toward the root[43]. All permanent deformations of the beam develops at these plastic hinges[42, 43]. Numerical solutions of the analysis presented in [13] gives deflection after elapse of time after the impact, and after the force is removed from the beam tip.

Parkes [42] considered a cantilever of rigid plastic material transversely struck at the tip by a falling mass, but he considers a rigid body impact. The analysis with a finite magnitude of a time dependent force is considered by Stronge[43]. The formulations of rigid plastic cantilever and definitions are used by Ting[47] except that the body force due to rotation is not considered.

Bodner and Symonds[46] have considered strain rate dependence of the yield stress and geometry changes unlike Parkes, who neglected them. Ting[47] has also pointed out this affect and shown comparisons and discrepancies.

All authors[42, 46, 47] have discussed their experimental set-ups of varying

complexity and the results obtained with them.

Kennedy et al.[41] investigated the deformation response of floating ice sheets under high intensity short duration loads by using rigid plastic theory together with Tresca yield criterion.

Normal impact and perforation of thin plates by hemispherically - tipped projectiles are analysed and experimentally investigated for determination of the force and central plate deflection histories by Levy and Goldsmith [44, 45].

Extensive work on Impact dynamics is also presented in the monographs by Goldsmith [2], Jones [48], and Brach [49].

The deformations at or near the impact point is not accurately evaluated with these formulations. However, Stronge concludes that his formulation represents deformations near the impact point when the force is large.

1.3 Scope of Present Study

Structural response to impact loads using both elastic and plastic analysis is investigated in this thesis. An experimental investigation is also carried out to verify some of the analytical findings.

The elastic analysis part consists of consideration of response of beams and rectangular plates to pulse type loads using normal mode analysis technique. In the case of beams, the natural frequencies and the mode shapes are readily available. However in the case of plates exact natural frequencies and normal mode information is available only for plates which are simply-supported at least on one pair of opposite edges. When this is not true, approximate techniques such as the Rayleigh-Ritz method or Finite Element Method must be used to obtain the natural frequencies and normal modes. Since the normal modes affect the resulting response significantly, considerable effort has been devoted in this thesis in developing techniques that obtain

better approximations for the natural frequencies and normal modes for the plate type structures considered in the study.

Structural response to pulse loads using plastic analysis is limited to beams only. Closed form solutions are given when a rigid plastic model is used for the beam. Numerical investigations are carried out for large deformations, finite blade radius, and varying centrifugal force is incorporated and are reported in this thesis.

Experimental investigations are done on beams and plates using impact loads due to a falling mass. An experimental set-up was designed and fabricated for this purpose. Some analytical findings are verified using the experimental results.

Chapter 2 discusses the various approaches used to obtain better approximations for the natural frequencies and natural modes of plates (i) using Rayleigh-Ritz methods with boundary characteristic orthogonal polynomials, (ii) using plate characteristic functions obtained by reducing the plate partial differential equation using Kantorovich method.

Chapter 3 deals with the response of beam and plate structures using the natural frequencies and normal modes developed in chapter 2, in normal mode analysis.

Chapter 4 gives the details of plastic analysis on beams subjected to impact loads at the tip. The cantilever type of beams are subjected to centrifugal loads thus simulating a rotating turbine blade.

Chapter 5 deals with the experimental investigations on plates subject to impact loads due to falling mass.

Chapter 6 gives the conclusions and suggestions for future work.

Chapter 2

NATURAL FREQUENCIES AND NORMAL MODES OF BEAMS AND RECTANGULAR PLATES

In this chapter, the natural frequencies and normal modes of beams and plates are developed for use in the response evaluation using normal mode analysis. In order to analyse any system for its response behavior due to a particular loading it is essential to obtain the characteristic properties of the system in terms of the natural frequencies, mode shapes and damping. This is done by solving a free vibration problem. For beams such information is readily available, whereas when rectangular plates do not have at least two opposite edges simply-supported, exact solutions for natural frequencies and normal modes are not known. The Rayleigh-Ritz method is one of the most popular methods to solve free vibration problems of rectangular plates. The accuracy of natural frequencies and mode shapes play an important role in obtaining the response of any system. The Rayleigh-Ritz method predicts displacements of acceptable accuracy, but for a given number of terms accuracy is less for response calculations than for determination of eigenvalues[28]. Shape functions that exactly satisfy the boundary conditions are essential in Rayleigh-Ritz method.

The general equation of motion of an elastic system is given as,

$$D_1(w) + D_2(\dot{w}) + \rho(\ddot{w}) = f(x, y, t) \tag{2.1}$$

where D_1, D_2, and ρ are operators and f(x,y,t) is the external load.

Solution of homogeneous part of the equation of motion without the damping term will result in undamped natural frequencies and mode shapes (complimentary solution). These are required to obtain the response of the system due to any load (the particular integral) acting on it. Once the natural frequencies and normal modes are known, the response is evaluated for a given forcing function *f(x,y,t)*. The

Rayleigh-Ritz method using boundary characteristic orthogonal polynomials, beam characteristic functions, and the method of approximate plate functions by reduction of plate partial differential equation are used to obtain the natural frequencies and natural modes.

The solution of the homogeneous part of equation (2.1) gives the eigenvalues and eigenvectors which are characteristic of the system. The eigenvectors thus obtained are orthogonal to each other and are generally normalized by a condition $\left\{u^{(r)}\right\}^T [M] \left\{u^{(r)}\right\} = 1$ for convenience, but this is without any physical significance. The normal mode vector is in terms of ratios of the amplitudes of each modes. The normal modes only show the system characteristic property which is the shape of the system in vibration at corresponding natural frequency. In a continuous system, when the system is excited by a force as in the case of a sudden impact, all modes are excited and they contribute to the total response of the system.

The modal vectors can be arranged in a square matrix of order n known as the modal matrix $[\phi]$, and used in modal analysis to uncouple the mass and stiffness matrices to reduce them into n single degree of freedom system equations. This shows that the normal modes provide a good description of the dynamical properties of a system and its response. However this is valid only when response does not exceed the linear elastic limit of the material.

2.1 BEAM PROBLEM:

The equation of motion for the bending vibrations of an undamped beam as shown in Fig.2.1 is given by [33],

$$EI\frac{\partial^4 y}{\partial x^4} + m\frac{\partial^2 y}{\partial t^2} = f(x,t) \tag{2.2}$$

where m is the mass per unit length and EI is the flexural rigidity of the beam material.

The natural frequencies and natural modes of the beam are obtained by solving

the homogeneous part of equation (2.2) given by

$$EI\frac{\partial^4 y}{\partial x^4} + m\frac{\partial^2 y}{\partial t^2} = 0 \tag{2.3}$$

Assuming harmonic motion the equation can be written as.

$$\frac{\partial^4 y}{\partial x^4} - \beta^4 y = 0 \tag{2.4}$$

where

$$\begin{aligned} \beta^4 &= \omega^2 \frac{m}{EI} \\ or \quad \omega_n &= (\beta_n l)^2 \sqrt{\frac{EI}{ml^4}} \qquad n = 1, 2, 3 \ldots \end{aligned} \tag{2.5}$$

The solution of equation (2.4) is.

$$y(x) = C_1 \sin \beta_n x + C_2 \cos \beta_n x + C_3 \sinh \beta_n x + C_4 \cosh \beta_n x \tag{2.6}$$

where constants C_1, C_2, C_3, C_4 are evaluated based on the boundary conditions of the beam and β_n are the roots of the frequency equation. The beam has infinite number of degrees of freedom ($n \longrightarrow \infty$), and is reduced to n degrees by choosing finite value of n depending on requirements in design and analysis.

Beam frequency equations with their roots and corresponding shape functions are available for different boundary conditions in standard literature [13]. The natural frequencies can be calculated using β_n values in equation (2.5).

However, in case of plates when at least two opposite edges are not simply-supported Rayleigh-Ritz is the most frequently used method to estimate natural frequencies and mode shapes.

2.2 PLATE PROBLEM:

The kinetic and potential energy expressions of the plate as shown in Fig. 2.2 are given by

$$T_{max} = \frac{1}{2}\rho h a b \omega^2 \int_0^1 \int_0^1 W^2(x, y) dx\, dy.$$

$$U_{max} = \frac{1}{2} Dab \int_0^1 \int_0^1 \left[W_{xx}^2 + \alpha^4 W_{yy}^2 + 2\nu\alpha^2 W_{xx} W_{yy} + 2(1-\nu)\alpha^2 W_{xy}^2 \right] dx\, dy$$

where ρ is the density of the plate material, h is the thickness of the plate, D is the flexural rigidity of the plate, α is the side ratio a/b, ν is the Poisson's ratio, and the subscripts x and y refer to the differentiation with respect to the subscript and the number of times the subscript appears denotes the order of differentiation.

The deflection of rectangular plate undergoing free flexural vibration can be expressed in separable form as,

$$w(x,y) = \sum_m \sum_n A_{mn} X_m(x) Y_n(y) \tag{2.7}$$

where $x = \xi/a$ and $y = \eta/b$, and ξ and η are the coordinates along two sides of the plate where a and b are plate dimensions.

Substituting the deflection function in the kinetic and potential energy expressions the Rayleigh's quotient is obtained as $\omega^2 = \frac{U_{max}}{T_{max}}$ where $T_{max}\omega^2 \quad T_{max}$. Minimizing ω^2 with respect to the coefficients A_{ij} yields the eigenvalue equation

$$\sum_m \sum_n \left[C_{mnij} - \lambda E_{mi}^{(0,0)} F_{nj}^{(0,0)} \right] A_{mn} = 0$$

where

$$C_{mnij} = E_{mi}^{(2,2)} F_{nj}^{(0,0)} + \alpha^4 E_{mi}^{(0,0)} F_{nj}^{(2,2)} + \nu\alpha^2 \left[E_{mi}^{(0,2)} F_{nj}^{(2,0)} + E_{mi}^{(2,0)} F_{nj}^{(0,2)} \right] + 2(1-\nu)\alpha^2 E_{mi}^{(1,1)} F_{nj}^{(1,1)}$$

$$E_{mi}^{(r,s)} = \int_0^1 (d^r X_m/dx^r)(d^s X_i/dx^s)\, dx, \qquad F_{nj}^{(r,s)} = \int_0^1 (d^r Y_n/dy^r)(d^s Y_j/dy^s)\, dy \tag{2.8}$$

where $\lambda^2 = \rho h \omega^2 a^4/D$ and $m, n, i, j = 1, 2, 3 \ldots \qquad r, s = 0, 1, 2.$

The solution of the eigenvalue equation will yield the natural frequency coefficients (λ) and mode shapes (A_{mn}) of the plate.

2.2.1 BOUNDARY CHARACTERISTIC ORTHOGONAL POLYNOMIALS:

Natural frequencies of rectangular plates can be obtained by employing a set of beam characteristic orthogonal polynomials in Rayleigh-Ritz method. The orthogonal polynomials are generated by Gram-Schmidt process [18], after the first member is constructed so as to satisfy all the boundary conditions. This method yields good results for lower modes, but the results are not accurate for higher modes[17].

The orthogonal polynomials are generated from a first member $\phi_0(x)$ in the interval $a \leq x \leq b$ by using Gram-Schmidt process as follows[17]:

$$\phi_1(x) = (x - B_1)\phi_0(x), \qquad \phi_k(x) = (x - B_k)\phi_{k-1}(x) - C_k\phi_{k-2}(x),$$

$$B_k = \frac{\int_a^b x g(x)\phi_{k-1}^2(x)dx}{\int_a^b g(x)\phi_{k-1}^2(x)dx}$$

$$C_k = \frac{\int_a^b x g(x)\phi_{k-1}\phi_{k-2}()dx}{\int_a^b g(x)\phi_{k-2}^2(x)dx}$$

$g(x)$ being the weighting function. The polynomials $\phi_k(x)$ satisfy the orthogonality condition

$$\int_a^b g(x)\phi_k(x)\phi_l(x)dx = 0 \;\; if \;\; k \neq l$$

The weight function is taken as unity when the plate is uniform and the integral is from 0 to 1 and the coefficients of the polynomials are chosen in such a way so as to make the polynomials orthonormal by,

$$\int_0^1 \phi_k^2(x)dx = 1$$

The first member of the polynomial $\phi_0(x)$ is constructed so as to satisfy all the boundary conditions of the beam problems accompanying the plate problem. Even though $\phi_0(x)$ satisfies all the boundary conditions, both geometrical and natural, the other members of the orthogonal set satisfy only geometric boundary conditions, which can easily be checked from the way the set is constructed by using equations above.

The first member polynomial is constructed so as to satisfy all the boundary conditions. For example, in case of a plate with all its edges simply-supported (SSSS), beam problems both in x and y directions have same boundary conditions, namely,

$$X(0) = X''(0) = X(1) = X''(1) = 0.$$

Assuming the beam deflection function as

$$X(x) = a_0 + a_1 x + a_2 x^2 + a_3 x^3 + a_4 x^4$$

and applying the boundary conditions, the deflection shape can be written as,

$$X(x) = a_4 (x - 2x^3 + x^4),$$

where a_4 is an arbitrary constant. The normalized mode function is obtained as

$$\phi_0(x) = \frac{(x - 2x^3 + x^4)}{\left(\int_0^1 X^2(x)dx\right)^{1/2}}$$

2.2.2 APPROXIMATE PLATE FUNCTIONS IN RAYLEIGH-RITZ METHOD

In order to improve the estimation of higher frequencies and corresponding mode shape coefficients, reduction of partial differential equation of plate to ordinary differential equation is carried out. Solving the resulting ordinary differential equation for the roots, the shape functions are formed which are more realistic plate deflection shapes, and are used in Rayleigh-Ritz method.

Vibration of a plate is associated with the minimum of the integral

$$I = \iint_A \left\{ (\nabla w)^2 - 2(1-\nu)\left[\frac{\partial^2 w}{\partial \xi^2}\frac{\partial^2 w}{\partial \eta^2} - \left(\frac{\partial^2 w}{\partial \xi \partial \eta}\right)^2\right] + \frac{m}{D}\left(\frac{dw}{dt}\right)^2 \right\} d\xi d\eta$$
$$-2\int_l V(s) w ds + 2\int_\Gamma M(s)\frac{\partial w}{\partial n} ds \qquad (2.9)$$

where $\nabla = \frac{\partial^2}{\partial \xi^2} + \frac{\partial^2}{\partial \eta^2}$ is the Laplacian operator, and

$$D = \frac{Eh^3}{12(1-\nu^2)}$$

is the plate flexural rigidity, E is the modulus of elasticity, m is the mass per unit area of the plate, ν is the Poisson's ratio, w is the plate deflection, and ξ and η are the Cartesian coordinates. The double integral is over the area of the plate whereas the line integral is along the boundaries of the plate, where s is along the boundary and n is a direction normal to the boundary. The necessary condition for the minimum of the integral I is obtained by considering a small variation in the deflection w as $w + g\varepsilon$ and then the derivative with respect to g is equated to zero. This results in [27],

$$\iint_A \left(\nabla\nabla w + \frac{m}{D}\frac{\partial^2 w}{\partial t^2} \right) \varepsilon d\xi d\eta + \int_\Gamma M(s)\frac{\partial \varepsilon}{\partial n} ds - \int_\Gamma V(s)\varepsilon ds = 0 \qquad (2.10)$$

where

$$\nabla\nabla w = \frac{\partial^4 w}{\partial \xi^4} + 2\frac{\partial^4 w}{\partial \xi^2 \partial \eta^2} + \frac{\partial^4 w}{\partial \eta^4}$$

When the plate is rectangular and the boundaries are parallel to the coordinate axes, the moment and shear force distribution along boundaries are given by

$$M(\xi) = \left\{ \frac{\partial^2 w}{\partial \xi^2} + \nu \frac{\partial^2 w}{\partial \eta^2} \right\}_{at\ \xi=0,\,a}$$

$$V(\xi) = \left\{ \frac{\partial^3 w}{\partial \xi^3} + (2-\nu)\frac{\partial^3 w}{\partial \xi \partial \eta^2} \right\}_{at\ \xi=0,\,a} \qquad (2.11)$$

Similar expressions describe the moments and shear forces along $\eta = 0$ and b also. For free harmonic vibration, the solution is assumed in the separable form

$$w(x,y) = X(x)Y(y)e^{\omega t} \qquad (2.12)$$

where $x = \xi/a$ and $y = \eta/b$.

In order to reduce the partial differential equation to an ordinary differential equation, the deflection shape along one direction, say y, is assumed *a priori*. Such a deflection expression can be any function of y satisfying all the boundary conditions along y. In the present analysis beam characteristic functions [13] are employed.

Substituting $Y(y)$ into equation (2.10), and since $\varepsilon = \delta w = Y\delta X + X\delta Y$, where $\delta Y = 0$, since Y is assumed *a priori*, the resulting differential equation in the x direction is given by

$$\frac{ab}{a^4}\int_0^1\int_0^1 \left[X''''Y + 2\alpha^2 X''\ddot{Y} + \alpha^4 X\ddot{Y} - \frac{\omega^2 mXY}{D}\right] Y\delta X dx dy$$
$$+\frac{ab}{a^4}\int_0^1 [\alpha^4 X\ddot{Y} + \nu\alpha^2 X''Y]\dot{Y}\delta X dx$$
$$-\frac{ab}{a^4}\int_0^1 [\alpha^4 X\ddot{Y} + (2-\nu)\alpha^2 X''\dot{Y}]\dot{Y}\delta X dx = 0 \qquad (2.13)$$

We have $\varepsilon = \delta w = Y\delta X$ and $\frac{\partial \varepsilon}{\partial y} = \delta \dot{w} = \dot{Y}\delta X$. Further, $()' = \frac{\partial}{\partial x}$ and $\dot{()} = \frac{\partial}{\partial y}$. $\alpha = a/b$ is the plate aspect ratio where a and b are the side lengths of the plate along ξ and η directions respectively. After performing the integration, the ordinary differential equation in the x direction is obtained as

$$X'''' + 2\alpha^2[B - (1-\nu)(G_0 + G_1)]X'' + \alpha^4\left[C - \frac{\Omega^2}{\alpha^4} + H_0 + H_1 - J_0 - J_1\right]X = 0 \qquad (2.14)$$

with

$$A = \int_0^1 Y^2 dy,\ B = \frac{1}{A}\int_0^1 Y\ddot{Y} dy,\ C = \frac{1}{A}\int_0^1 Y\ddot{Y} dy,\ G_0 = \frac{1}{A}(Y\dot{Y})_{y=0},$$

$$G_1 = \frac{1}{A}(Y\dot{Y})_{y=1},\ H_0 = \frac{1}{A}(\dot{Y}\ddot{Y})_{y=0},\ H_1 = \frac{1}{A}(\dot{Y}\ddot{Y})_{y=1},\ J_0 = \frac{1}{A}(Y\ddot{Y})_{y=0},\ J_1 = \frac{1}{A}(Y\ddot{Y})_{y=1}$$

and $\Omega^2 = \frac{\omega^2 m a^4}{D}$

Equation (2.14) can be put in the form

$$X'''' + 2\beta X'' + \gamma X = 0 \qquad (2.15)$$

where

$$\beta = \alpha^2[B - (1-\nu)(G_0 + G_1)]$$
$$\gamma = \alpha^4\left[C - \frac{\Omega^2}{\alpha^4} + H_0 + H_1 - J_0 - J_1\right]$$

Similarly by assuming *a priori* $X(x)$ and substituting this in the partial differential equation with $\delta w = X\delta Y$, $\delta w' = X'\delta Y$, it is possible to obtain an ordinary differential Equation along y direction in the form

$$\ddot{Y} + 2\beta^* \ddot{Y} + \gamma^* Y = 0 \tag{2.16}$$

where

$$\beta^* = \frac{1}{\alpha^2}[B^* - (1-\nu)(G_0^* + G_1^*)]$$

$$\gamma^* = \frac{1}{\alpha^4}[C^* + H_0^* + H_1^* - J_0^* - J_1^* - \Omega^2]$$

The quantities B^*, C^*, G_0^*, G_1^*, H_0^*, H_1^*, J_0^* and J_1^* must be evaluated appropriately along y, using equations similar to (2.14). Assuming $Y = X_0 e^{\lambda\tau}$ as the solution of equation (2.15) results in

$$\lambda^4 + 2\beta\lambda^2 + \gamma = 0 \tag{2.17}$$

The roots of this equation are given by

$$\lambda_{1,2}^2 = -\beta \pm \left(\beta^2 - \gamma\right)^{1/2} \tag{2.18}$$

Further, the solution of equation (2.15) can be written as

$$X(x) = C_1 \sin p_1 x + C_2 \cos p_1 x + C_3 \sinh p_2 x + C_4 \cosh p_2 x \tag{2.19}$$

where p_1 and p_2 are defined as

$$p_{1,2} = \pm\left[\pm\beta + \left(\beta^2 - \gamma\right)^{1/2}\right]^{1/2} \tag{2.20}$$

Similarly in y direction, solution of equation (2.16) can be expressed as

$$Y(y) = C_1^* \sin q_1 y + C_2^* \cos q_1 y + C_3^* \sinh q_2 y + C_4^* \cosh q_2 y \tag{2.21}$$

where q_1 and q_2 are given as

$$q_{1,2} = \pm\left[\pm\beta^* + \left(\beta^{*2} - \gamma^*\right)^{1/2}\right]^{1/2} \tag{2.22}$$

The boundary conditions at a plate edge for different cases are:

Clamped:

$$X(x) = X'(x) = 0 \tag{2.23}$$

Simply-supported:

$$\begin{aligned} X(x) &= 0 \\ X''(x) + \nu\alpha^2 B X(x) &= 0 \end{aligned} \tag{2.24}$$

Free:

$$\begin{aligned} X''(x) + \nu\alpha^2 B X(x) &= 0 \\ X'''(x) + (2-\nu)\alpha^2 B X'(x) &= 0 \end{aligned} \tag{2.25}$$

The different boundary conditions at the plate edges in y direction are:

Clamped:

$$Y(y) = \dot{Y}(y) = 0 \tag{2.26}$$

Simply-supported:

$$\begin{aligned} Y(y) &= 0 \\ \alpha^2 \ddot{Y}(y) + \nu B^* Y(y) &= 0 \end{aligned} \tag{2.27}$$

Free:

$$\begin{aligned} \alpha^2 \ddot{Y}(y) + \nu B^* Y(y) &= 0 \\ \alpha^2 \dddot{Y}(y) + (2-\nu) B^* \dot{Y}(y) &= 0 \end{aligned} \tag{2.28}$$

The line integrals in equation (2.13) are zero if the edges are not simply supported or free involving natural boundary conditions, i.e. in case of clamped edge.

It is not possible to satisfy the boundary conditions at the free edge, therefore, the work done by the moment and shear force at the edge, say $x = 0$, in equations (2.24) and (2.25), integrated along y direction is equated to zero. Similarly in equations (2.27) and (2.28) work done by moment and shear forces at the edge, say $y = 0$, integrated along x direction is equated to zero. Substituting corresponding conditions in the equation (2.19) and (2.21), two frequency equations are obtained consisting of infinite number of roots for Ω. These roots by themselves are very good approximations for some of the natural frequencies. Roots corresponding to solution in equation (2.19) in the x direction are good approximations to natural frequencies $\Omega_{11}, \Omega_{12} \ldots \Omega_{1i}$ and those corresponding to equation (2.21) are good approximations to natural frequencies Ω_{11} , Ω_{21} , $\ldots \Omega_{j1}$, respectively. The subscripts in Ω_{ij} correspond to the number of half waves in x and y directions respectively.

For each of the roots, solutions (2.19) and (2.21) will yield a set of plate characteristic functions $\phi_i(x)$ and $\psi_j(y)$ respectively. Using these approximate plate characteristic functions $\phi_i(x)$ and $\psi_j(y)$ as shape functions in Rayleigh-Ritz method, better approximations for all the natural frequencies and the corresponding mode shapes can be obtained.

Natural frequencies of rectangular plates with different combinations of boundary conditions are obtained using this method. Beam characteristic functions are assumed *a priori* along one direction to obtain approximate plate functions in the other direction. Six roots of the frequency equations in each of x and y directions are obtained for α values of 0.5, 1.0 and 2.0. These roots are obtained by applying plate boundary conditions given in equations (2.23,2.24,2.25) into the exact solutions (2.19,2.21). Roots obtained by using beam boundary conditions instead of the plate conditions are observed to differ only when the edge is free. Application of beam boundary conditions result in lower roots than the natural frequencies calculated by Rayleigh-Ritz method using beam characteristic orthogonal polynomials.

The form of beam characteristic function is same as that of plate function

given in equations (2.19) and (2.21) with $p = p_1 = p_2$ *and* $q = q_1 = q_2$. In the course of computations it was noted that p_1 and p_2 values are distinct for a given case, and comparison between the plate functions and the corresponding beam characteristic functions showed that even though the functions themselves do not differ significantly, the moments and shear forces calculated using them do differ considerably.

Using six plate characteristic functions corresponding to six roots of the frequency equations on either side, 36 natural frequencies are obtained using Rayleigh Ritz analysis and are presented in Tables 2.1 - 2.10. The cases studied are represented by referring to the edge condition of the plate in a counter - clockwise sequence starting at x = 0. using the notation of C for a clamped edge, S for simply-supported and F for a free edge. For example, CCSF is a plate with clamped edges at x = 0 and y = 0, simply-supported at x = 1 and free at y = 1. Even though several cases such as CCCC, CSCS, CCSF, CCFF, SSSS, CCSC, CCSS and CCCF are studied, results for only first four cases are presented. The 36 natural frequencies obtained with this method are compared with those obtained using (i) beam characteristic functions [13], (ii) boundary characteristic orthogonal polynomials [17, 19, 20], and (iii) plate functions obtained using corresponding beam boundary conditions in equations (2.24) and (2.25), as assumed deflection shapes in Rayleigh-Ritz method. A comparison shows that the results from the present method using the plate boundary conditions in equations (2.24) and (2.25) are the best except for the first two or three natural frequencies which are lower when orthogonal polynomials are used. In addition to these, in the case of square CCCC plate, comparison with Rayleigh Ritz results using Bolotin functions as displacement shapes [16] and simply- supported plate functions [26] are also tabulated in Table 2.2. For the CCFF plate in Table 2.10, comparisons with Rayleigh-Ritz results using simply-supported plate functions [26] are also shown. The results compare favorably. For higher frequencies the orthogonal polynomial shape functions provide poor results. This may be due to the difficulty in representing the higher modes using the orthogonal polynomials. Plate functions provide very good approximations even for the higher frequencies, better than those obtained by the use of beam characteristic functions; the orthogonal poly-

nomial results go on deteriorating for the higher frequencies. The present results show that the 36^{th} eigenvalue using (6×6) plate functions are much better than those obtained using same order of orthogonal polynomials and slightly superior to those obtained by beam characteristic functions.

The 36^{th} natural frequency was also computed using only the sixth deflection function on either side by Rayleigh's method, and the results are tabulated in Table 2.10. These results are always lower than corresponding values obtained by Rayleigh-Ritz method. In addition when one of the plate edges is free, the sixth plate function with beam boundary conditions was also used in evaluating Rayleigh quotient, and the comparison showed that beam conditions applied to plate characteristic function results in lower values than with plate conditions. The one term solution giving sometimes a lower frequency is reported by Leissa[15]. In his results, this is observed to happen only when at least one of the edges is free.

The eigenvalues calculated by using plate characteristic functions do not differ significantly from those calculated by using beam functions. Nevertheless they are lower, and therefore more accurate. A comparison of the functions showed that even though the functions themselves do not differ significantly, the moments and shear forces computed by using them do differ. Hence, the response analysis using the plate functions will be more accurate than those obtained by using beam characteristic functions or orthogonal polynomials.

The approximate plate functions (APF) obtained by reduction of plate partial differential equation and the beam characteristic function[13] are compared for their shapes and higher derivatives in the case of CCSF as given by Figures 2.3 – 2.26.

In the case of CCSF plate, the accompanying beam function along x is CS and along y it is CF. The Figs. 2.3–2.5 show the shape function along x direction (CS). The agreement between the two is very good, and both these curves overlap each other. The higher derivatives of the function is shown in Figs. 2.9– 2.11, 2.15–

2.17, 2.21–2.23. It can be seen that the function as well as their derivatives in all six modes are the same. This indicates that the beam characteristic function and the approximate plate functions are same in the case of clamped and simply-supported edges. This is also proved by the fact that the natural frequency coefficients in the case of plates involving no free edge are same when both beam and plate conditions are applied at the edges as mentioned before. But y direction functions vary significantly at the interior of the plate but are same at the edges as shown in Figs. 2.6 2.8. However the higher derivative shapes vary along the edges also. The difference at the free edges reduces for higher modes as can be seen in Figs. 2.12 2.14 in the case of first derivative. However second and third derivatives vary at both edges, though the trend in reduction of the difference in higher modes is same. This can be seen from Figs. 2.18–2.20, 2.24–2.26. For example if the shape function satisfies *beam conditions* along the y direction, at the free edge the moment and shear force should be zero (second and third derivative). But in the case of APF the work done by the moment and shear force is equated to zero, and therefore the function does not satisfy the beam boundary conditions exclusively. However, further study in computing the exact displacement mode shapes, the moments and the shear forces by taking eigenvectors obtained through Rayleigh-Ritz method should be carried out, which is listed as one of the recommendations for future research in this area.

2.2.3 PLATE CHARACTERISTIC FUNCTIONS BY ITERATIVE CONVERGENCE

In the previous section, the approximate function obtained by reduction of the partial differential equation of the plate into ordinary differential equation along the x and y directions are used in Rayleigh-Ritz method to solve an eigenvalue problem. This is a minimization process and the resulting eigenvalues are the estimates of upper bounds for the actual values.

In this section, reduction of the partial differential equation is carried out sequentially along the x and y directions in an iterative fashion until the resulting natural frequency coefficients converge, and the corresponding plate characteristic

functions are exact. Initially, the beam characteristic function of the j^{th} beam mode along, say, the y direction, is used to reduce the partial differential equation to an ordinary differential equation in the x direction. Substituting the exact solution of this ordinary differential equation into the boundary conditions along the x direction results in a frequency equation. The i^{th} root of the frequency equation corresponds to the natural frequency coefficient $\Omega_{(i,j)}$, and the corresponding solution in the x direction is a first approximation to the plate characteristic function in the x direction. Subsequently, this function along the x direction is used to reduce the partial differential equation into an ordinary differential equation along y direction. The exact solution of this equation is substituted into the boundary conditions of the plate along the y direction and the j^{th} root of the resulting frequency equation will be a better approximation for the natural frequency coefficient $\Omega_{(i,j)}$. The corresponding solution along y direction is the second approximation to the characteristic function along y direction. This process is continued iteratively until $\Omega_{(i,j)}$ value converges to a set criterion. The procedure is repeated to obtain all the required natural frequency coefficients, $\Omega_{(i,j)}$.

Successive iterations along both x and y directions is carried out until the first root converges to the required accuracy to obtain the first natural frequency, $\Omega_{(1,1)}$. Using a similar procedure for the first root in the y direction and the second root in x direction will give natural frequency $\Omega_{(2,1)}$. Continuing in this manner for all the roots will yield frequencies $\Omega_{(1,1)}$, $\Omega_{(2,1)}$, ..., $\Omega_{(i,1)}$. When the same process is used with the second root in y direction and 1, 2, 3, ... in x direction the resulting roots are $\Omega_{(i,2)}$ ($i = 1,2,\ldots$). Likewise, taking subsequent roots in the y direction and $1,2,3,\ldots$ in the x direction will give all the roots $\Omega_{i,j}$ ($i = 1,2,\ldots$ and $j = 1,2,\ldots$).

Rectangular plates (α = 0.5, 1.0, 2.0) with different boundary conditions are analyzed using this method to obtain the natural frequencies. Beam characteristic functions are assumed for the first step of iteration along the y direction and are used to find the first natural frequency, say $\Omega_{(1,1)}$ by alternately reducing the partial differential equation into an ordinary differential equation in the x and y directions,

and solving them.

The relative error criteria for these convergence are taken to be 5×10^{-6}. The results thus obtained up to the sixteenth frequency are tabulated in Tables 2.11–2.13. The three cases studied are CCCC, CSCS and CCSF.

The frequency coefficients obtained by the present method are compared with those obtained by the Rayleigh-Ritz method using (6×6) number of first approximations to the plate characteristic functions. Except for the first two frequencies all others by the present method are lower than those by the Rayleigh Ritz method. It can be seen from Table 2.13 that when $\alpha = 1$, the present method yields identical values for $\Omega_{(i,j)}$ and $\Omega_{(j,i)}$. However, the Rayleigh-Ritz results show one of them to be lower than the present results and the other one to be higher for $\left(\Omega_{(3,1)}, \Omega_{(1,3)}\right)$ and $\left(\Omega_{(4,2)}, \Omega_{(2,4)}\right)$. Tables 2.15 – 2.23 give the converged values of p_1, p_2, σ and q_1, q_2 and τ in the x and y directions, respectively. The Rayleigh-Ritz results using six beam characteristic functions on either side were computed and included in the tables for comparison. The first six of these are presented by Leissa [15]. It can be seen that the difference in the natural frequency coefficients by the two methods are very small. The main advantages of this method are that any natural frequency can be evaluated separately for each mode along with the corresponding plate characteristic function.

Natural frequencies and normal modes of beams and plates discussed in this chapter are employed in normal mode analysis to obtain the elastic response of these structures subjected to impact loads. This is presented in the next chapter

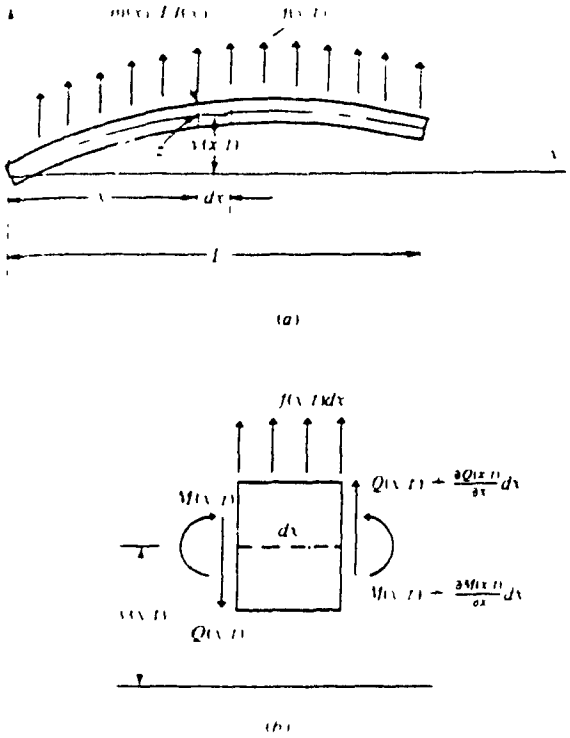

Fig. 2.1 Free Body Diagram of a Beam Element [31]

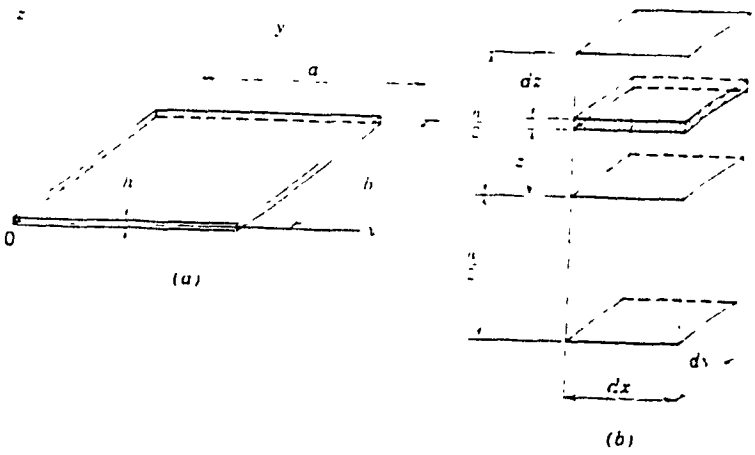

Fig. 2.2 Free Body Diagram of a Plate Element [33]

Table 2.1 **Natural Frequency coefficients of CCCC Plate**

$(\Omega = \omega a^2\sqrt{\frac{m}{D}}, \alpha = 0.5, \nu = 0.3)$

(BF): Beam Characteristic Functions [13], **(OP):** Orthogonal Polynomial Functions [17–21], **(PF):** Approximate Plate Characteristic Function

i	$\Omega_{i(BF)}$	$\Omega_{i(OP)}$	$\Omega_{i(PF)}$
1	24.5820	24.5782	24.5789
2	31.8363	31.8267	31.8298
3	44.7979	44.8082	44.7796
4	63.3631	63.5695	63.3473
5	64.0014	63.9848	63.9916
6	71.1207	71.0786	71.0982
7	83.4076	83.3156	83.3386
8	87.3119	98.9594	87.2815
9	100.9390	100.9639	100.8726
10	116.3914	123.4740	116.3693
11	123.2865	130.5550	123.2723
12	123.9820	131.7782	123.8458
13	130.4531	142.5697	130.4184
14	142.6791	142.6292	142.5743
15	152.0870	159.8170	151.9839
16	159.8518	172.7463	159.7423
17	182.5459	187.3115	182.3265
18	202.2873	203.4865	202.2706
19	209.5312	210.5773	209.4899
20	209.9763	222.6092	209.7974
21	221.8408	225.2537	221.7169
22	238.9179	239.5691	238.7859
23	261.5373	265.0670	261.2743
24	288.5650	300.4879	288.3459
25	301.0185	355.3872	300.9999
26	308.3411	361.2686	308.2931
27	320.7792	371.3549	320.6377
28	337.9139	385.6825	337.7574
29	360.6675	406.8103	360.3625
30	387.6140	436.6223	387.3504
31	419.4729	533.7074	419.4528
32	426.8344	539.3396	426.7841
33	439.3340	548.9855	439.1867
34	456.4652	562.5686	456.3027
35	479.2457	581.9951	478.9290
36	506.0431	609.1000	505.7700

Table 2 2: **Natural Frequency coefficients of CCCC Plate**

$$(\Omega = \omega a^2\sqrt{\frac{m}{D}}, \alpha = 1.0, \nu = 0.3)$$

(BF): Beam Characteristic Functions [13], **(OP)**: Orthogonal Polynomial Functions [17–21], **(PF)**: Plate Characteristic Functions. **(MB)**: Modified Bolotin Functions in Rayleigh-Ritz [16], **(SS)**: Simply Supported Plate Characteristic Functions [25].

i	$\Omega_{i(BF)}$	$\Omega_{i(OP)}$	$\Omega_{i(PF)}$	$\Omega_{i(MB)}$	$\Omega_{i(SS)}$
1	35.9915	35 9855	35.9882	35.9854	35.988
2	73 4133	73 3947	73.4046	73.3942	73.406
3	73.4133	73 3947	73.4046	73.3942	73.406
4	108 2710	108 2179	108 2482	108.2174	108.25
5	131.6365	131.7789	131.6177	131 5807	131.62
6	132 2119	132 4097	132 2323	132.2063	132.23
7	165 1534	165 1597	165 1005	165.0025	—
8	165 1534	165 1597	165 1005	165.0025	—
9	210 6022	211 7061	210.5849	210.5228	—
10	210 6022	211.7061	210.5849	210 5228	—
11	220.5018	220 3199	220.3782	220.0375	—
12	242 4066	243 1353	242.3477	242.1539	—
13	243.3388	244.1539	243.2899	243.1499	—
14	297.0360	297.3216	296.8964	296.3420	—
15	297.0360	297 3216	296.8964	296.3420	—
16	309.0443	361 7988	309 0181	308.9024	—
17	309.2748	362 2325	309.2538	309.1664	—
18	340.9671	372 7805	340 8800	340.5843	—
19	340 9671	388 4898	340 8800	340.5843	—
20	372.2834	388.4898	372.1272	371.3530	—
21	394.1260	433 6726	393.8991	392.7656	—
22	395.0132	435 6811	394.8085	393 9172	—
23	427 4879	502 1155	427.4632	427.3539	—
24	427.4879	502 1155	427.4632	427.3539	—
25	458.6324	539 9153	458.5514	458.2250	—
26	459 1294	539 9153	459 0577	458.8230	—
27	469 0531	564 0803	468 7914	467.2671	—
28	469 0531	565 2631	468 7914	467.2671	—
29	511 8806	607 7885	511.6820	510 6412	—
30	511 8806	607 7885	511.6820	510.6412	—
31	565 5552	617 0781	565.1413	562.1327	—
32	584 9407	669 5149	584.6971	583.1233	—
33	585.8300	671 9394	585.6040	584.3448	—
34	681.2188	774 4492	680.8230	677.7228	—
35	681 2188	774 4492	680.8230	677.7228	—
36	795 7758	920 4339	795 4070	792.4481	—

Table 2.3: **Natural Frequency coefficients of CCCC Plate**

$$(\Omega = \omega a^2 \sqrt{\frac{m}{D}}, a = 2.0, \nu = 0.3)$$

(BF): Beam Characteristic Functions [13], **(OP)**: Orthogonal Polynomial Functions [17 21], **(PF)**: Approximate Plate Characteristic Functions

i	$\Omega_{i(BF)}$	$\Omega_{i(OP)}$	$\Omega_{i(PF)}$
1	98.3279	98.3127	98.3158
2	127.3451	127.3067	127.3190
3	179.1918	179.2330	179.1186
4	253.4523	254.2781	253.3893
5	256.0057	255.9391	255.9663
6	284.4828	284.3143	284.3929
7	333.6303	333.2625	333.3544
8	349.2475	395.8376	349.1258
9	403.7561	403.8556	403.4902
10	465.5656	493.8961	465.4773
11	493.1461	522.2200	493.0893
12	495.9279	527.1128	495.3834
13	521.8123	570.2789	521.6735
14	570.7177	570.5167	570.2973
15	608.3181	639.2682	607.9358
16	639.4073	690.9853	638.9694
17	730.1837	749.2461	729.3058
18	809.1490	813.9158	809.0823
19	838.1249	842.3093	837.9598
20	839.9053	890.4367	839.1896
21	887.3632	901.0146	886.8676
22	955.6714	958.2774	955.1434
23	1046.1492	1060.2678	1045.0972
24	1154.2600	1201.9516	1153.3837
25	1204.0740	1421.5489	1203.9997
26	1233.3643	1445.0743	1233.1726
27	1283.1169	1485.4197	1282.5507
28	1351.6554	1542.7299	1351.0297
29	1442.6698	1627.2410	1441.4501
30	1550.4562	1746.4891	1549.4016
31	1677.8915	2134.8294	1677.8113
32	1707.3375	2157.3583	1707.1364
33	1757.3358	2195.9419	1756.7469
34	1825.8610	2250.2745	1825.2108
35	1916.9828	2327.9805	1915.7159
36	2024.1737	2436.4002	2023.0799

Table 2.4: **Natural Frequency coefficients of CSCS Plate**

$(\Omega = \omega a^2\sqrt{\frac{m}{D}}, \alpha = 0.5, \nu = 0.3)$

(BF): Beam Characteristic Functions [13], **(OP):** Orthogonal Polynomial Functions [17–21], **(PF):** Approximate Plate Characteristic Functions.

i	$\Omega_{i(BF)}$	$\Omega_{i(OP)}$	$\Omega_{i(PF)}$
1	23.8157	23.8156	23.8156
2	28.9521	28.9509	28.9516
3	39.0944	39.1993	39.0933
4	54.7558	55.5439	54.7541
5	63.5346	63.5345	63.5345
6	69.3286	69.3270	69.3279
7	75.8656	79.6013	75.8635
8	79.5323	95.1999	79.5307
9	94.6052	123.1504	94.6026
10	102.2488	123.8027	102.2462
11	114.8213	129.2993	114.8177
12	122.9299	139.8654	122.9296
13	129.0997	155.2668	129.0978
14	139.6416	155.4471	139.6374
15	140.2604	202.7842	140.2558
16	154.8300	203.2287	154.8229
17	174.9019	209.1338	174.8917
18	199.9906	209.5843	199.9773
19	201.9818	220.3726	201.9816
20	208.3948	230.7279	208.3934
21	219.2218	236.0564	219.2186
22	234.6283	279.8531	234.6228
23	254.7829	285.4602	254.7748
24	279.7946	351.4902	279.7837
25	300.7401	355.2032	300.7397
26	307.3233	360.5674	307.3205
27	318.3866	369.7158	318.3800
28	334.0444	383.1013	334.0331
29	354.4220	423.8974	354.4054
30	379.5969	480.1141	379.5747
31	419.2110	533.5515	419.2102
32	425.8907	538.7605	425.8884
33	437.0839	547.5974	437.0791
34	452.8697	560.4294	452.8618
35	473.3406	597.5292	473.3291
36	498.5477	648.0444	498.5322

Table 2.5: **Natural Frequency coefficients of CSCS Plate**

$(\Omega = \omega a^2 \sqrt{\frac{m}{D}})$; $a = 1.0, \nu = 0.3$

(BF): Beam Characteristic Functions [13], **(OP)**: Orthogonal Polynomial Functions [17-21], **(PF)**: Approximate Plate Characteristic Functions

i	$\Omega_{i(BF)}$	$\Omega_{i(OP)}$	$\Omega_{i(PF)}$
1	28.9521	28 9509	28.9508
2	54.7558	54 7432	54.7498
3	69.3286	69.3270	69 3270
4	94.6052	94 5853	94 5960
5	102.2546	102.8070	102 2451
6	129.0997	129.2993	129 0955
7	140.2771	140 6907	140.2597
8	154.8300	154.9387	154 8050
9	170.4221	174.0812	170 4098
10	200.0165	200 3558	199.9668
11	206.8573	209 5843	206 8331
12	208 3948	210 0653	208.3917
13	234 6283	235 6088	234 6088
14	258.7330	268 3394	258.7188
15	265 6614	280 8461	265.5892
16	279.8270	347.9370	279 7860
17	294 0299	360 5674	293.9998
18	307 3233	382 7547	307.3170
19	334 0444	422 1557	334 0042
20	344.9663	463.0489	344 9036
21	351.9123	482 2228	351.8223
22	366.9757	488.9491	366.9599
23	379 6310	533 8095	379 5502
24	401.4581	538.7605	401.4237
25	425.8907	560.1252	425 8849
26	430.4670	597 6007	430.3851
27	444.9178	599 0246	444.7903
28	452.8697	654 3225	452.8416
29	458 5607	707 3249	458.4571
30	498 5877	783 1579	498 5291
31	530 3591	806 7633	530 1934
32	536 3143	847 5589	536 2164
33	563 7342	858.0738	563 6431
34	636 0146	906 6273	635 8178
35	648 7979	1000 2390	648.6764
36	753 9155	1133 7486	753 7677

Table 2.6: **Natural Frequency coefficients of CSCS Plate**

$(\Omega = \omega a^2\sqrt{\frac{m}{D}}, \alpha = 2.0, \nu = 0.3)$

(BF): Beam Characteristic Functions [13], **(OP):** Orthogonal Polynomial Functions [17–21], **(PF):** Approximate Plate Characteristic Functions.

i	$\Omega_{i(BF)}$	$\Omega_{i(OP)}$	$\Omega_{i(PF)}$
1	54.7558	54.7431	54.7431
2	94 6052	94.5853	94.5853
3	154.8300	154.9387	154.7757
4	170 4221	170 3499	170.3819
5	206 8575	206.6996	206.7756
6	234 6283	235 6088	234 5854
7	265.6614	265 3603	265.4212
8	334 0444	345.2892	333.9558
9	344 9664	369.3756	344.7531
10	366 9819	382.7547	366.9272
11	401 4808	403 5016	401.3584
12	444 9178	459 9605	444 4839
13	452 8697	480 0255	452.8081
14	458.6056	537.9276	458.2396
15	536 3816	560 1252	536.0290
16	563 7342	652 4289	563.4211
17	636 1035	658 2058	635.3948
18	642.9802	660 0856	642.9176
19	676 5006	690 9310	676.3539
20	732.5905	745 6709	732.1520
21	754 0218	821.5497	753.4817
22	809.0624	823 4848	808.6187
23	908 3694	934.1839	907.4863
24	998 1080	1087 5720	998.0407
25	1025.1602	1826 1608	1024.4605
26	1031 0897	1849 6368	1030.9283
27	1086 5710	1889.7794	1086.0900
28	1162.1364	1946.3122	1161.6352
29	1261 0911	2027.6714	1260.1009
30	1376.9126	2141.3066	1376.1081
31	1432.2621	3108 9249	1432.1920
32	1464 9030	3130.8542	1464.7322
33	1519 9804	3168 3489	1519.4734
34	1594 8960	3220 6894	1594 3580
35	1693 5458	3293.7499	1692.4884
36	1808.5794	3391.1785	1807.7060

Table 2.7: **Natural Frequency coefficients of CCSF Plate**

$$(\Omega = \omega a^2 \sqrt{\frac{m}{D}}, a = 0.5, \nu = 0.3)$$

(BF): Beam Characteristic Functions [13], **(OP)**: Orthogonal Polynomial Functions [17-21], **(PF)**: Approximate Plate Characteristic Functions, **(BC)**: Beam boundary conditions, **(PC)**: Plate boundary conditions.

i	$\Omega_{i(BF)}$	$\Omega_{i(OP)}$	$\Omega_{i(PF,BC)}$	$\Omega_{i(PF,PC)}$
1	15.8731	15.8125	15.8713	15.8224
2	20.1761	20.1485	20.1727	20.1526
3	29 1878	29.2004	29 1861	29.1707
4	43.2685	44 9489	43 2528	43.2208
5	50.4269	50 2539	50.4234	50 3326
6	54.9620	54 8534	54.9507	54.9035
7	62.4310	64 1723	62 4517	62 3891
8	64.1954	68 3711	64.1730	64.1442
9	78.4056	79 7341	78 3461	78.2553
10	86.7575	102 3857	86 7645	86.6492
11	97.3844	104 7492	97.3794	97.2207
12	104 7129	109 4608	104 7084	104 6075
13	109.3531	118 9708	109.3366	109 2813
14	118.7476	131.2971	118 7109	118.6769
15	121.9934	157 3021	122 0101	121.4149
16	133.2276	181 7645	133.1380	133 0358
17	152.3628	186.5229	152 3236	152.1441
18	178 0811	196 1275	178 1298	177.0861
19	178 7378	211.2044	178.7329	178.6274
20	183.4420	222.4051	183 4222	183.3634
21	192.9524	234 4081	192.9072	192 8707
22	207.6347	251 0919	207.5270	207.4227
23	226 9386	307 0754	226.8730	226 6956
24	253.8176	335 9817	253.8962	252.5287
25	272 5013	339 8664	272 4962	272 3885
26	277.2501	347 7941	277 2285	277.1677
27	286 8447	360.2403	286.7942	286.7558
28	301.6802	379 9486	301 5614	301.4564
29	321 1271	382 6990	321 0437	320.8712
30	348.9478	513 3071	349 0488	347.4594
31	386 0030	783 1213	385 9977	385.8884
32	390.7797	786 6580	390 7567	390.6948
33	400.4296	793 8477	400 3755	400 3358
34	415.3695	804.8298	415 2435	415 1382
35	434.9221	822 3902	434.8263	434 6580
36	463.4420	938 8720	463 5582	461 8178

Table 2.8: **Natural Frequency coefficients of CCSF Plate**

$$(\Omega = \omega a^2\sqrt{\frac{m}{D}}, \alpha = 1.0, \nu = 0.3)$$

(BF): Beam Characteristic Functions [13], **(OP):** Orthogonal Polynomial Functions [17–21], **(PF):** Approximate Plate Characteristic Functions, **(BC):** Beam boundary conditions, **(PC):** Plate boundary conditions.

i	$\Omega_{i(BF)}$	$\Omega_{i(OP)}$	$\Omega_{i(PF,BC)}$	$\Omega_{i(PF,PC)}$
1	17.6153	17.5434	17.6141	17.5632
2	36.0465	36.0275	36.0442	36.0337
3	52.0664	51.8278	52.0637	51.9602
4	71.1950	71.0893	71.1871	71.1486
5	74.3492	74.4454	74.3490	74.3406
6	106.2828	106.1416	106.2790	106.1642
7	109.4732	109.4995	109.4625	109.4377
8	125.6530	125.6576	125.6396	125.5876
9	132.8443	139.4964	132.8384	132.8259
10	164.3474	164.5156	164.3231	164.2920
11	167.5423	174.3358	167.5133	167.4445
12	180.2662	182.9510	180.2616	180.1432
13	199.7017	202.4433	199.6838	199.6253
14	211.3736	229.3822	211.3792	211.3588
15	222.8536	238.0739	222.7959	222.6898
16	238.7260	241.4117	238.6898	238.6562
17	245.3865	269.4049	245.3856	245.2984
18	274.0043	305.7042	273.9993	273.8792
19	293.4752	322.4749	293.4536	293.3916
20	297.8318	336.7827	297.7484	297.6267
21	300.6461	352.7689	300.6316	300.4818
22	309.8255	385.9755	309.8248	309.7929
23	332.6683	398.2468	332.6217	332.5861
24	343.5480	442.3960	343.5356	343.3252
25	375.9493	528.2703	375.9160	375.7287
26	387.4877	783.5378	387.4822	387.3612
27	392.3943	797.8641	392.2890	392.1621
28	399.3043	827.3634	399.2870	398.8192
29	406.9720	857.5694	406.9470	406.8830
30	446.2578	875.5600	446.2018	446.1645
31	470.9253	887.6851	470.8702	470.6656
32	476.2944	938.2690	476.2827	475.5310
33	506.4068	951.9990	506.2823	506.1543
34	573.6491	1009.9706	573.6483	572.6216
35	585.3921	1119.9981	585.3142	585.1070
36	690.7538	1488.9086	690.7640	689.4954

Table 2.9: **Natural Frequency cofficients of CCSF Plate**

$$(\Omega = \omega a^2 \sqrt{\frac{m}{D}}, \alpha = 2.0, \nu = 0.3)$$

(BF): Beam Characteristic Functions [13], **(OP):** Orthogonal Polynomial Functions [17–21], **(PF): Approximate** Plate Characteristic Functions, **(BC):** Beam boundary conditions, **(PC): Plate** boundary conditions.

i	$\Omega_{i(BF)}$	$\Omega_{i(OP)}$	$\Omega_{i(PF,BC)}$	$\Omega_{i(PF,PC)}$
1	26.3372	26.2832	26 3361	26.3006
2	59.9984	59.7508	59 9958	59.8951
3	101.4468	101.4185	101.4408	101 4374
4	113.7198	113.4697	113 7162	113.5956
5	137 8695	137 7547	137 8506	137 8308
6	187 3407	189 7256	187.3360	187.2092
7	193.5957	193.5239	193 5639	193 5293
8	258 6261	259 0593	258 6185	258 6159
9	268.0928	270 2476	268 0493	268 0043
10	280.8257	293 7041	280 8205	280 6914
11	293.4499	341 9240	293 4216	293.4093
12	349 5011	349 7219	349 4463	349.4247
13	361.8380	410.6997	361 7837	361.7315
14	394 1049	427 1897	394 0984	393 9687
15	425 4105	520 9633	425 3304	425.3027
16	475.0210	554 7231	474 9500	474 8928
17	494.9644	556 5180	494 9540	494 9505
18	520 5297	611 5183	520 4235	520 3925
19	528.7990	689.1082	528.7590	528.7333
20	584.3519	787.4009	584.2719	584.2179
21	634 7830	809 0795	634 6429	634.6098
22	660.7720	847.7389	660 6503	660.5690
23	757.2682	920 9194	757.1033	757 0005
24	810.5234	950.4268	810 5154	810.5100
25	843.6557	976 0358	843 6211	843 5938
26	873.2860	1000 3394	873.0693	872.9515
27	898 4955	1071 5372	898 4257	898 3667
28	974.5184	1180 8204	974 4104	974.3156
29	1071.2262	1203 7632	1071.0780	1070.9487
30	1188.0239	1547.7096	1187.8248	1187 6663
31	1205.1486	3400 0552	1205 1384	1205.1302
32	1237.9140	3429.5479	1237.8725	1237.8156
33	1292.4721	3478 9596	1292 3888	1292 2530
34	1368.7278	3548 1373	1368 6005	1368 3596
35	1466.5601	3646 6354	1466 3893	1466.0224
36	1585 6117	3951 7397	1585 3905	1584 8835

Table 2 10: **Natural Frequency coefficients of CCFF Plate**

$$(\Omega = \omega a^2 \sqrt{\frac{m}{D}}, a = 1.0, \nu = 0.3)$$

(BF): Beam Characteristic Functions [13], **(OP)**: Orthogonal Polynomial Functions [17–21], **(SS)**: Simply Supported Plate Characteristic Functions [25], **(BC)**: Beam boundary Conditions. **(PF)**; Approximate Plate Characteristic Functions.

i	$\Omega_{i(BF)}$	$\Omega_{i(OP)}$	$\Omega_{i(PF,BC)}$	$\Omega_{i(SS)}$
1	6 9421	6.9243	6.9421	7.1631
2	24 0344	23.9228	24.0343	23.974
3	26.6808	26 5906	26 6796	26.687
4	47 7848	47 6696	47 7810	47.753
5	63.0388	62.8501	63 0362	62.967
6	65.8326	65 6848	65 8335	65.772
7	85.9148	85 8559	85.9092	—
8	88 6545	88 4713	88.6511	—
9	121 9830	127 4429	121.9818	—
10	124.5729	128 3541	124.5710	—
11	128 8410	131.5511	128.8334	—
12	144.7989	151.2246	144.7903	—
13	147 1953	154.0019	147.1858	—
14	187.1207	193 7504	187.1019	—
15	190 0376	197 2119	190 0201	—
16	200.7420	227 3046	200 7365	—
17	203.7889	230 9771	203.7922	—
18	222.9397	247 8474	222.9317	—
19	225.6819	251 0373	225.6815	—
20	250 5352	262 8661	250.4984	—
21	266.1452	289 1050	266 1333	—
22	268.5798	291.8032	268.5735	—
23	299.3761	354 1255	299 3726	—
24	302 2451	360 0075	302 2455	—
25	321 2552	453 4228	321.2453	—
26	323 7377	792.1026	323 7317	—
27	328.8384	856.2597	328.8090	—
28	333 1346	860 7704	333.1133	—
29	361 3914	882 9777	364.3741	—
30	368.0601	898 2405	368.0512	—
31	411 8144	926 5823	411.8002	—
32	429 9462	958 3966	429.9162	—
33	434.3153	992 9606	434.2914	—
34	513.4252	1044 6685	513.4120	—
35	519 9384	1123 9614	519.9468	—
36	628.8309	1918 7910	628.8720	—

Table 2.11: 36^{th}Natural frequencies ($\Omega_{(6,6)}$)

- - Rayleigh-Ritz analysis with plate characteristic functions.
- ( ) - Rayleigh's method with sixth plate characteristic function
- [ ] - Rayleigh's method with sixth beam characteristic function
- { } - Rayleigh's method with sixth plate characteristic function using beam conditions.

Support Conditions	$\alpha = 0.5$	$\alpha = 1.0$	$\alpha = 2.0$
CCCC	505.7700 (504.9659) [505.0128]	795.4070 (793.0073) [793.0440]	2023.0799 (2019.8637) [2020.0512]
SSSS	444.0475 (444.0475) [444.0475]	710.3998 (710.3998) [710.3998]	1776.1901 (1776.1901) [1776.1901]
CSCS	498.5322 (498.3362) [498.3376]	753.7677 (752.5809) [752 5949]	1807.7060 (1805.0909) [1805 2309]
CCSC	478.2781 (477.4783) [477.5215]	774.5392 (772 3802) [772.4083]	2009.2909 (2006.6511) [2006.7713]
CCSS	474.6798 (474.0284) [474.0559]	753 2283 (751 3037) [751.3244]	1898 7193 (1896.1136) [1896.2236]
CCCF	489.8811 (487.6788) [487.8574] {486.8025}	712.0547 (705.0933) [705.1433] {704.4846}	1601.0649 (1592.7272) [1592.7616] {1592.4632}
CCSF	461.8178 (459.5047) [459.6713] {458.6529}	689.4954 (682.6997) [682 7438] {682.1268}	1584.8835 (1577.4030) [1577.4276] {1577.1600}

Table 2.12: **Natural Frequency coefficients of CCCC Plate**

$(\Omega = \omega a^2 \sqrt{\frac{m}{D}}, \nu = 0.3)$

(PCF): Plate Characteristic Functions By Iteration Until Convergence.
(APF): Approximate Plate Functions Used In Rayleigh-Ritz Method.
(BCF): Beam Characteristic Functions Used In Rayleigh-Ritz Method.

•		$\alpha = 0.5$			$\alpha = 1.0$			$\alpha = 2.0$		
m	n	$\Omega_{mn(PCF)}$	$\Omega_{mn(APF)}$	$\Omega_{mn(BCF)}$	$\Omega_{mn(PCF)}$	$\Omega_{mn(APF)}$	$\Omega_{mn(BCF)}$	$\Omega_{mn(PCF)}$	$\Omega_{mn(APF)}$	$\Omega_{mn(BCF)}$
1	1	24.5809	24.5789	24.5820	35.9990	35.9882	35.9915	98.3236	98.3158	98.3279
2	1	63.9847	63.9916	64.0014	73.4051	73.4016	73.4133	127.3335	127.3190	127.3451
3	1	123.2489	123.8458	123.9820	131.9021	131.6177	131.6365	179.1153	179.1186	179.1918
4	1	202.2285	202.2706	202.2873	210.5263	210.5849	210.6022	253.3597	253.3893	253.4523
1	2	31.8334	31.8298	31.8363	73.4054	73.4046	73.4133	255.9387	255.9663	256.0057
2	2	71.0813	71.0982	71.1207	108.2359	108.2482	108.2710	284.3251	284.3929	284.4828
3	2	130.3534	130.4184	130.4531	165.0230	165.1005	165.1534	333.1250	333.3544	333.6303
4	2	209.3722	209.4899	209.5312	242.6671	242.3477	242.4066	403.2126	403.4902	403.7561
1	3	44.7788	44.7796	44.7979	131.9021	132.2323	132.2449	492.9957	493.0893	493.1461
2	3	83.2812	83.3386	83.4076	165.0230	165.1005	165.1534	521.4138	521.6735	521.8123
3	3	142.3774	142.5743	142.6794	220.0587	220.3782	220.5018	569.5097	570.2973	570.7177
4	3	221.3769	221.7169	221.8408	296.3663	296.8964	297.0360	637.9468	638.9694	639.4073
1	4	63.3399	63.3473	63.3631	210.5263	210.5849	210.6022	808.9208	809.0823	809.1490
2	4	100.8032	100.8726	100.9390	242.6671	243.2899	243.3388	837.4893	837.9598	838.1249
3	4	159.4871	159.7423	159.8518	296.3663	296.8964	297.0360	885.5058	886.8676	887.3632
4	4	238.3470	238.7859	238.9179	371.3759	372.1272	372.2834	953.3880	955.1434	955.6714

Table 2.13: **Natural Frequency coefficients of CSCS Plate**

$$(\Omega = \omega a^2 \sqrt{\frac{m}{D}}, \nu = 0.3)$$

(PCF): Plate Characteristic Functions By Iteration Until Convergence.
(APF): Approximate Plate Functions Used In Rayleigh-Ritz Method.
(BCF): Beam Characteristic Functions Used In Rayleigh-Ritz Method.

b		$\alpha = 0.5$			$\alpha = 1.0$			$\alpha = 2.0$		
m	n	$\Omega_{mn(PCF)}$	$\Omega_{mn(APF)}$	$\Omega_{mn(BCF)}$	$\Omega_{mn(PCF)}$	$\Omega_{mn(APF)}$	$\Omega_{mn(BCF)}$	$\Omega_{mn(PCF)}$	$\Omega_{mn(APF)}$	$\Omega_{mn(BCF)}$
1	1	23.8156	23.8156	23 8157	28 9508	28 9508	28.9521	54.7431	54.7431	54.7558
2	1	63 5345	63 5315	63 5316	69 3270	69 3270	69.3286	94 5853	94 5853	94.6052
3	1	122 9296	122.9296	122.9299	129 0955	129 0955	129 0997	154.7757	154.7757	154.8300
4	1	201.9816	201.9816	201 9818	208 3917	208.3917	208.3948	234.5855	234 5854	234 6283
1	2	28 9508	28 9516	28 9521	54 7431	54 7498	54 7558	170.3465	170.3819	170 4221
2	2	69 3270	69.3279	69 3286	94 5853	94 5960	94 6052	206 6971	206.7756	206.8575
3	2	129.0955	129 0978	129 0997	154 7757	154 8050	154.8300	265 1964	265 4212	265 6611
4	2	208.3917	208 3934	208 3948	234 5855	234 6088	234 6283	344.5379	344.7531	344 9661
1	3	39 0892	39 0933	39 0914	102 2162	102 2451	102 2546	366 8167	366.9272	366 9819
2	3	79.5251	79 5307	79 5323	140 2015	140 2597	140.2771	401 0792	401.3584	401 4808
3	3	139 6224	139.6374	139 6116	199 8105	199 9668	200.0165	457.4395	458 2396	458 6056
4	3	219 2072	219 2186	219 2218	279 6512	279 7860	279 8270	535 1638	536 0290	536 3816
1	4	54 7431	54 7541	54 7558	170 3465	170 4098	170 4221	642 7399	642 9176	642 9802
2	4	94 5853	94 6026	94 6052	206 6971	206 8331	206 8575	675.8317	676.3539	676.5006
3	4	154 7757	154 8229	154 8300	265 1961	265 5892	265 6614	730 5381	732 1520	732 5905
4	4	234 5855	234 6228	234 6283	344 5379	344 9036	344 9663	806 9015	808 6187	809 0624

Table 2.11: **Natural Frequency coefficients of CCSF Plate**

$(\Omega = \omega a^2 \sqrt{\frac{m}{D}}, \nu = 0.3)$

(PCF): Plate Characteristic Functions By Iteration Until Convergence.
APF): Approximate Plate Functions Used In Rayleigh-Ritz Method.
(BCF): Beam Characteristic Functions Used In Rayleigh-Ritz Method.

•		$\alpha = 0.5$			$\alpha = 1.0$			$\alpha = 2.0$		
m	n	$\Omega_{mn(PCF)}$	$\Omega_{mn(APF)}$	$\Omega_{mn(BCF)}$	$\Omega_{mn(PCF)}$	$\Omega_{mn(APF)}$	$\Omega_{mn(BCF)}$	$\Omega_{mn(PCF)}$	$\Omega_{mn(APF)}$	$\Omega_{mn(BCF)}$
1	1	15.8245	15.8224	15.8731	17.5797	17.5632	17.6153	26.4661	26.3006	26.3372
2	1	50.2494	50.3326	50.4269	51.8522	51.9602	52.0664	59.8114	59.8951	59.9981
3	1	101.3674	104.6075	101.7129	105.8285	106.1612	106.2828	113.2145	113.5956	113.7198
4	1	183.0669	183.3631	183.4120	179.5232	180.1132	180.2662	279.4683	280.6914	280.8257
1	2	20.1593	20.1526	20.1761	36.0779	36.0337	36.0465	101.4959	101.4374	101.4168
2	2	54.8501	54.9035	54.9620	71.1364	71.1486	71.1950	137.8585	137.8308	137.8695
3	2	109.1154	109.2813	109.3531	125.3968	125.5876	125.6530	193.3923	193.5293	193.5957
4	2	192.5636	192.8707	192.9521	199.2320	199.6253	199.7017	267.6305	268.0043	268.0928
1	3	29.1837	29.1707	29.1878	71.3105	71.3106	74.3492	258.5934	258.6159	258.6261
2	3	61.0984	64.1442	61.1954	109.1133	109.4377	109.4732	293.2607	293.4093	293.4499
3	3	118.5165	118.6769	118.7176	161.1190	161.2920	164.3474	319.0891	349.4217	319.5011
4	3	206.8509	207.4227	207.6317	238.2677	238.6562	238.7260	424.6490	425.3027	425.4105
1	4	43.2306	43.2208	43.2685	132.8160	132.8259	132.8443	494.8674	494.9505	494.9641
2	4	78.1411	78.2553	78.4056	167.2726	167.4145	167.5423	528.3687	528.7333	528.7990
3	4	132.6975	133.0358	133.2276	222.1791	222.6898	222.8536	583.3668	584.2179	584.3519
4	4	225.9697	226.6956	226.9386	296.6339	297.6267	297.8318	658.9395	660.5690	660.7720

Table 2.15. CCCC Plate Characteristic Function Parameters.

$$(\Omega = \omega a^2 \sqrt{\frac{m}{D}}, \alpha = 0.5, \nu = 0.3)$$

$$X(x) = \cosh p_2 x - \cos p_1 x - \sigma \{p_1/p_2 \sinh p_2 x - \sin p_1 x\}$$

$$Y(y) = \cosh q_2 y - \cos q_1 y - \tau \{q_1/q_2 \sinh q_2 y - \sin q_1 y\}$$

m	n	p_1	p_2	σ	q_1	q_2	τ
1	1	4.6041	5.1895	1.1146	3.8359	10.6032	2.7641
2	1	7.8109	8.1504	1.0441	3.4967	19.4850	5.5724
3	1	10.9742	11.2120	1.0216	3.3791	28.3240	8.3822
4	1	14.1243	14.3076	1.0130	3.3196	37.1953	11.2047
1	2	4.3333	6.4116	1.4748	7.3651	12.2602	1.6647
2	2	7.6995	8.9890	1.1678	6.9413	20.3275	2.9285
3	2	10.9143	11.8393	1.0847	6.7416	28.8968	4.2864
4	2	14.0870	14.8121	1.0515	6.6321	37.6260	5.6733
1	3	4.0743	8.0984	1.9865	10.7000	14.4433	1.3498
2	3	7.5534	10.2483	1.3569	10.3144	21.6376	2.0978
3	3	10.8273	12.8219	1.1842	10.0766	29.8156	2.9589
4	3	14.0290	15.6354	1.1145	9.9319	38.3278	3.8591
1	4	3.8801	10.0263	2.5838	13.9443	16.9312	1.2142
2	4	7.4036	11.8029	1.5942	13.6239	23.3194	1.7117
3	4	10.7261	14.0901	1.3136	13.3804	31.0397	2.3198
4	4	13.9571	16.7273	1.1985	13.2155	39.2759	2.9720

Table 2.16: CCCC Plate Characteristic Function Parameters.

$$(\Omega = \omega a^2 \sqrt{\frac{m}{D}}, \alpha = 1.0, \nu = 0.3)$$

$$X(x) = \cosh p_2 x - \cos p_1 x - \sigma \left\{ p_1/p_2 \sinh p_2 x - \sin p_1 x \right\}$$

$$Y(y) = \cosh q_2 y - \cos q_1 y - \tau \left\{ q_1/q_2 \sinh q_2 y - \sin q_1 y \right\}$$

m	n	p_1	p_2	σ	q_1	q_2	τ
1	1	4.3121	6.5261	1.5090	4.3122	6.5252	1.5088
2	1	7.6902	9.0630	1.1788	3.8585	10.3001	2.6693
3	1	10.9100	11.8859	1.0894	3.6321	14.5105	3.9950
4	1	14.0852	14.8367	1.0534	3.5098	18.8469	5.3697
1	2	3.8583	10.3026	2.6701	7.6903	9.0625	1.1787
2	2	7.3866	12.0012	1.6247	7.3868	11.9989	1.6244
3	2	10.7156	14.2308	1.3280	7.1358	15.7130	2.2020
4	2	13.9549	16.7628	1.2012	6.9607	19.7570	2.8384
1	3	3.6321	14.5121	3.9955	10.9100	11.8858	1.0894
2	3	7.1356	15.7158	2.2024	10.7157	14.2300	1.3280
3	3	10.5088	17.4516	1.6607	10.5089	17.4500	1.6605
4	3	13.7951	19.5560	1.4176	10.3340	21.1425	2.0459
1	4	3.5098	18.8478	5.3700	14.0852	14.8367	1.0534
2	4	6.9606	19.7593	2.8387	13.9549	16.7625	1.2012
3	4	10.3340	21.1445	2.0461	13.7951	19.5552	1.4175
4	4	13.6409	22.8978	1.6786	13.6410	22.8964	1.6785

Table 2.17: CCCC Plate Characteristic Function Parameters.

$$(\Omega = \omega a^2 \sqrt{\frac{m}{D}}, \alpha = 2.0, \nu = 0.3)$$

$$X(x) = \cosh p_2 x - \cos p_1 x - \sigma \{p_1/p_2 \sinh p_2 x - \sin p_1 x\}$$

$$Y(y) = \cosh q_2 y - \cos q_1 y - \tau \{q_1/q_2 \sinh q_2 y - \sin q_1 y\}$$

m	n	p_1	p_2	σ	q_1	q_2	τ
1	1	3.8357	10.6053	2.7647	4.6041	5.1893	1.1146
2	1	7.3649	12.2626	1.6650	4.3335	6.4108	1.4745
3	1	10.6999	14.4443	1.3499	4.0745	8.0972	1.9861
4	1	13.9443	16.9316	1.2142	3.8802	10.0251	2.5834
1	2	3.4967	19.4879	5.5733	7.8109	8.1504	1.0441
2	2	6.9411	20.3325	2.9293	7.6995	8.9887	1.1677
3	2	10.3143	21.6414	2.0982	7.5535	10.2475	1.3567
4	2	13.6238	23.3219	1.7119	7.4037	11.8017	1.5940
1	3	3.3790	28.3312	8.3845	10.9742	11.2120	1.0216
2	3	6.7415	28.8995	4.2868	10.9143	11.8393	1.0847
3	3	10.0765	29.8187	2.9592	10.8273	12.8217	1.1842
4	3	13.3803	31.0427	2.3200	10.7261	14.0897	1.3136
1	4	3.3196	37.1953	11.2047	14.1243	14.3074	1.0130
2	4	6.6321	37.6260	5.6733	14.0871	14.8106	1.0514
3	4	9.9319	38.3275	3.8590	14.0313	15.6012	1.1119
4	4	13.2155	39.2765	2.9720	13.9571	16.7273	1.1985

Table 2.18. CSCS Plate Characteristic Function Parameters.

$$(\Omega = \omega a^2\sqrt{\frac{m}{D}}, \alpha = 0.5, \nu = 0.3)$$

$$X(x) = \cosh p_2 x - \cos p_1 x - \sigma \left\{p_1/p_2 \sinh p_2 x - \sin p_1 x\right\}$$

$$Y(y) = \sinh q_2 y + \tau \sin q_1 y$$

m	n	p_1	p_2	σ	q_1	q_2	τ
1	1	4.6204	5.1267	1.0965	3.1416	10.3787	-0.1313E+21
2	1	7.8145	8.1242	1.0402	3.1416	19.4292	-0.2023E+24
3	1	10.9755	11.1981	1.0202	3.1416	28.2981	-0.1438E+28
4	1	14.1249	14.2986	1.0123	3.1416	37.1800	0.1437E+32
1	2	4.3682	6.2306	1.4207	6.2832	11.6549	0.2518E+22
2	2	7.7109	8.8992	1.1544	6.2832	20.1234	0.5877E+24
3	2	10.9191	11.7883	1.0796	6.2832	28.7977	0.6556E+28
4	2	14.0898	14.7737	1.0485	6.2832	37.5669	0.4217E+32
1	3	4.1088	7.8292	1.9039	9.4248	13.5378	0.4938E+22
2	3	7.5709	10.0862	1.3323	9.4248	21.2414	0.1612E+25
3	3	10.8359	12.7212	1.1740	9.4248	29.6087	-0.2486E+29
4	3	14.0357	15.5375	1.1070	9.4248	38.2006	-0.1339E+33
1	4	3.9070	9.7068	2.4842	12.5664	15.8254	0.8152E+23
2	4	7.4234	11.5786	1.5598	12.5664	22.7315	0.8138E+26
3	4	10.7377	13.9375	1.2980	12.5664	30.7067	-0.6145E+29
4	4	13.9681	16.5549	1.1852	12.5664	39.0678	-0.2628E+33

Table 2.19: CSCS Plate Characteristic Function Parameters

$$(\Omega = \omega a^2\sqrt{\frac{m}{D}}, \alpha = 1.0, \nu = 0.3)$$

$$X(x) = \cosh p_2 x - \cos p_1 x - \sigma \left\{ p_1/p_2 \sinh p_2 x - \sin p_1 x \right\}$$

$$Y(y) = \sinh q_2 y + \tau \sin q_1 y$$

m	n	p_1	p_2	σ	q_1	q_2	τ
1	1	4.3682	6.2306	1.4207	3.1416	5.8275	-0.1483E+20
2	1	7.7109	8.8992	1.1544	3.1416	10.0617	-0.5017E+20
3	1	10.9191	11.7883	1.0796	3.1416	14.3989	-0.7317E+22
4	1	14.0898	14.7737	1.0485	3.1416	18.7834	0.1472E+24
1	2	3.9070	9.7068	2.4842	6.2832	7.9127	0.5968E+20
2	2	7.4234	11.5786	1.5598	6.2832	11.3657	0.1886E+22
3	2	10.7377	13.9375	1.2980	6.2832	15.3533	-0.2640E+23
4	2	13.9681	16.5549	1.1852	6.2832	19.5339	-0.1727E+25
1	3	3.6592	13.8218	3.7773	9.4248	10.5439	0.2474E+21
2	3	7.1678	15.1338	2.1113	9.4248	13.2952	0.3875E+22
3	3	10.5349	16.9893	1.6127	9.4248	16.8292	0.1327E+24
4	3	13.8139	19.1958	1.3896	9.4248	20.7208	0.6503E+25
1	4	3.5260	18.1180	5.1384	12.5664	13.4060	0.7254E+22
2	4	6.9845	19.0948	2.7339	12.5664	15.6324	0.6721E+23
3	4	10.3577	20.5696	1.9859	12.5664	18.7172	-0.3816E+24
4	4	13.6610	22.4154	1.6408	12.5664	22.2809	-0.5960E+25

Table 2.20: CSCS Plate Characteristic Function Parameters.

$$(\Omega = \omega a^2\sqrt{\frac{m}{D}}, \alpha = 2.0, \nu = 0.3)$$

$$X(x) = \cosh p_2 x - \cos p_1 x - \sigma \left\{p_1/p_2 \sinh p_2 x - \sin p_1 x\right\}$$

$$Y(y) = \sinh q_2 y + \tau \sin q_1 y$$

m	n	p_1	p_2	σ	q_1	q_2	τ
1	1	3.9070	9.7068	2.4842	3.1416	3.9563	-0.2283E+19
2	1	7.4234	11.5786	1.5598	3.1416	5.6829	-0.1284E+20
3	1	10.7377	13.9375	1.2980	3.1416	7.6767	0.2448E+20
4	1	13.9681	16.5549	1.1852	3.1416	9.7669	0.1980E+21
1	2	3.5260	18.1180	5.1384	6.2832	6.7030	0.1780E+20
2	2	6.9845	19.0948	2.7339	6.2832	7.8162	0.5420E+20
3	2	10.3577	20.5696	1.9859	6.2832	9.3586	0.2534E+21
4	2	13.6610	22.4154	1.6408	6.2832	11.1405	-0.1730E+21
1	3	3.3928	26.8723	7.9205	9.4248	9.7016	0.1065E+21
2	3	6.7656	27.5025	4.0650	9.4248	10.4850	0.2332E+21
3	3	10.1061	28.5087	2.8209	9.4248	11.6664	0.7601E+21
4	3	13.4111	29.8407	2.2251	9.4248	13.1319	0.3291E+22
1	4	3.3275	35.6985	10.7284	12.5664	12.7719	0.3847E+22
2	4	6.6468	36.1592	5.4401	12.5664	13.3664	0.6972E+22
3	4	9.9515	36.9099	3.7090	12.5664	14.3080	0.1788E+23
4	4	13.2380	37.9283	2.8651	12.5664	15.4723	0.5727E+23

Table 2.21: CCSF Plate Characteristic Function Parameters.

$$(\Omega = \omega a^2\sqrt{\frac{m}{D}}, \alpha = 0.5, \nu = 0.3)$$

$$X(x) = \cosh p_2 x - \cos p_1 x - \sigma \{p_1/p_2 \sinh p_2 x - \sin p_1 x\}$$

$$Y(y) = \cosh q_2 y - \cos q_1 y - \tau \{q_1/q_2 \sinh q_2 y - \sin q_1 y\}$$

m	n	p_1	p_2	σ	q_1	q_2	τ
1	1	3.9505	3.7652	0.9541	1.4650	9.7201	6.6339
2	1	7.0886	6.8097	0.9607	1.1499	18.5642	16.1447
3	1	10.2274	9.8811	0.9661	0.7292	27.4379	37.6252
4	1	13.3480	13.4486	1.0075	4.5494	36.6061	8.0464
1	2	3.8343	4.6194	1.2050	4.8466	10.7065	2.2091
2	2	7.0410	7.4409	1.0568	4.7354	19.1124	4.0361
3	2	10.2000	10.4098	1.0206	4.6345	27.8142	6.0016
4	2	13.3240	14.0845	1.0571	7.8378	37.1542	4.7404
1	3	3.6870	6.0762	1.6480	7.9855	12.3767	1.5499
2	3	6.9707	8.4883	1.2177	7.9714	20.1354	2.5260
3	3	10.1607	11.2194	1.1042	7.9026	28.5322	3.6105
4	3	13.2883	15.0927	1.1358	11.0553	37.9533	3.4331
1	4	3.5656	7.8985	2.2152	11.0917	14.5153	1.3087
2	4	6.8919	9.8873	1.4346	11.1384	21.5471	1.9345
3	4	10.1111	12.3436	1.2208	11.1047	29.5615	2.6621
4	4	13.2668	15.7387	1.1863	14.2415	38.9928	2.7380

Table 2.22: CCSF Plate Characteristic Function Parameters.

$$(\Omega = \omega a^2\sqrt{\frac{m}{D}}, \alpha = 1.0, \nu = 0.3)$$

$$X(x) = \cosh p_2 x - \cos p_1 x - \sigma \{p_1/p_2 \sinh p_2 x - \sin p_1 x\}$$

$$Y(y) = \cosh q_2 y - \cos q_1 y - \tau \{q_1/q_2 \sinh q_2 y - \sin q_1 y\}$$

m	n	p_1	p_2	σ	q_1	q_2	τ
1	1	3.9642	3.6750	0.9282	1.6606	5.0846	3.0294
2	1	7.0969	6.7054	0.9448	1.4774	9.3819	6.3491
3	1	10.2349	9.7410	0.9517	1.3227	13.7780	10.4162
4	1	13.3737	12.7987	0.9570	1.1638	18.1988	15.6378
1	2	3.6689	6.3007	1.7174	4.8233	6.7486	1.4023
2	2	6.9601	8.6611	1.2444	4.8490	10.4369	2.1525
3	2	10.1550	11.3428	1.1170	4.7981	14.5223	3.0267
4	2	13.3209	14.1709	1.0638	4.7399	18.7666	3.9593
1	3	3.4692	10.2091	2.9428	7.9113	9.1709	1.1590
2	3	6.8059	11.8132	1.7357	7.9832	12.1737	1.5249
3	3	10.0484	13.9672	1.3900	7.9960	15.8464	1.9818
4	3	13.2454	16.4117	1.2391	7.9738	19.8197	2.4856
1	4	3.3705	14.4683	4.2927	11.0272	11.9434	1.0831
2	4	6.6882	15.6003	2.3325	11.0889	14.3678	1.2957
3	4	9.9469	17.2879	1.7380	11.1297	17.6063	1.5819
4	4	13.1638	19.3463	1.4697	11.1387	21.2699	1.9096

Table 2.23: CCSF Plate Characteristic Function Parameters.

$$(\Omega = \omega a^2 \sqrt{\frac{m}{D}}, \alpha = 2.0, \nu = 0.3)$$

$$X(x) = \cosh p_2 x - \cos p_1 x - \sigma \left\{ p_1/p_2 \sinh p_2 x - \sin p_1 x \right\}$$

$$Y(y) = \cosh q_2 y - \cos q_1 y - \tau \left\{ q_1/q_2 \sinh q_2 y - \sin q_1 y \right\}$$

m	n	p_1	p_2	σ	q_1	q_2	τ
1	1	4.0504	3.1446	0.7792	1.7884	3.0053	1.5450
2	1	7.1147	6.4874	0.9118	1.6691	4.9241	2.9137
3	1	10.2453	9.5506	0.9322	1.5693	7.0348	4.4749
4	1	16.5218	15.6076	0.9447	1.4056	11.3907	8.1035
1	2	3.4503	10.8210	3.1363	4.7442	5.2786	1.1240
2	2	6.7879	12.2876	1.8102	4.8201	6.6563	1.3844
3	2	10.0342	14.3755	1.4327	4.8537	8.3852	1.7283
4	2	13.2343	16.7769	1.2677	4.8502	10.2861	2.1209
1	3	3.3101	19.4580	5.8784	7.8706	8.1932	1.0404
2	3	6.5974	20.3035	3.0775	7.9094	9.1218	1.1530
3	3	9.8523	21.6220	2.1946	7.9517	10.4620	1.3156
4	3	13.0775	23.3194	1.7832	7.9818	12.0614	1.5111
1	4	3.2561	28.3208	8.6979	11.0038	11.2335	1.0209
2	4	6.5047	28.8822	4.4402	11.0263	11.9155	1.0807
3	4	9.7408	29.7935	3.0586	11.0567	12.9637	1.1725
4	4	12.9622	31.0223	2.3933	11.0873	14.2887	1.2887

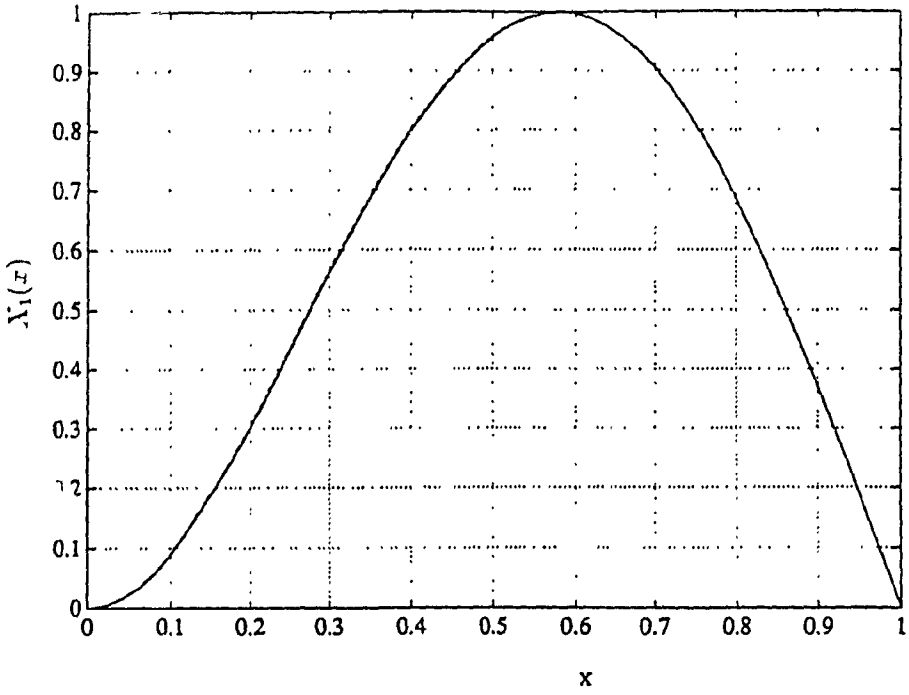

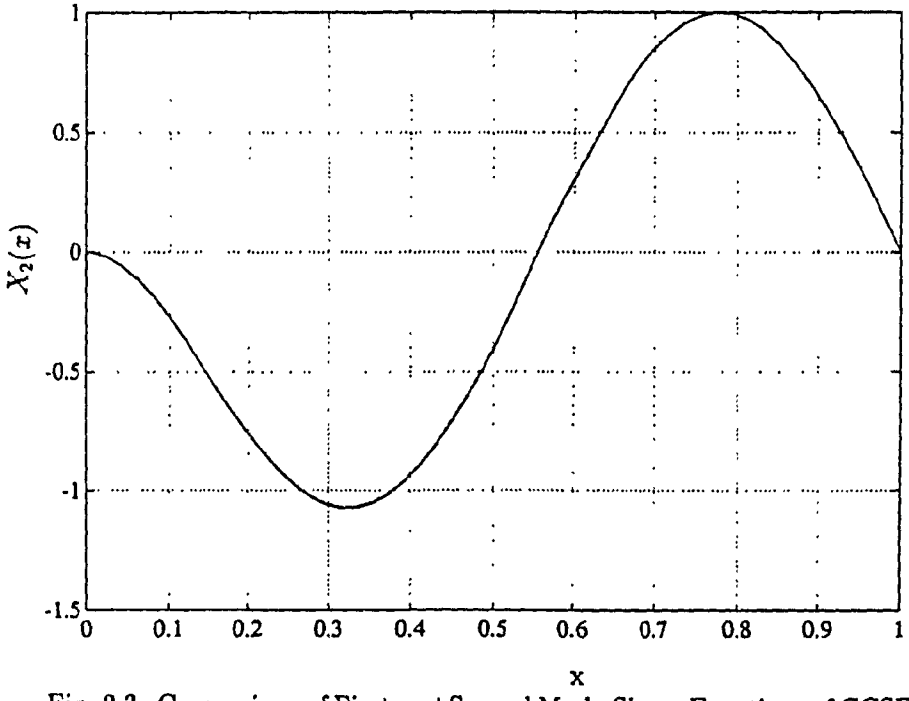

Fig. 2.3 Comparison of First and Second Mode Shape Functions of CCSF plate along x direction (— Beam Characteristic Function and - - - Approximate Plate Function)

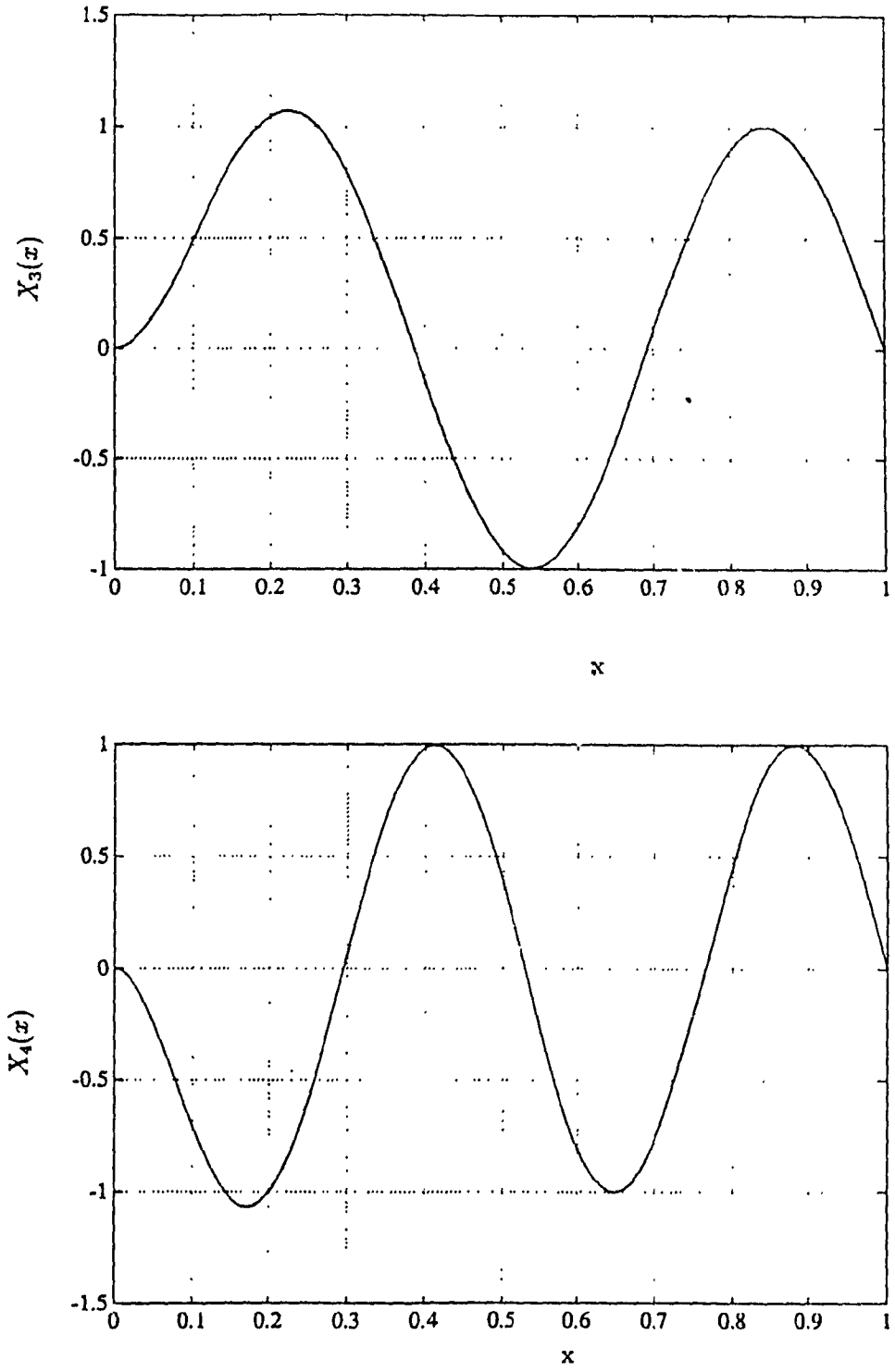

Fig. 2.4 Comparison of Third and Fourth Mode Shape Functions of CCSF plate along x direction (— Beam Characteristic Function, and - - - Approximate Plate Function)

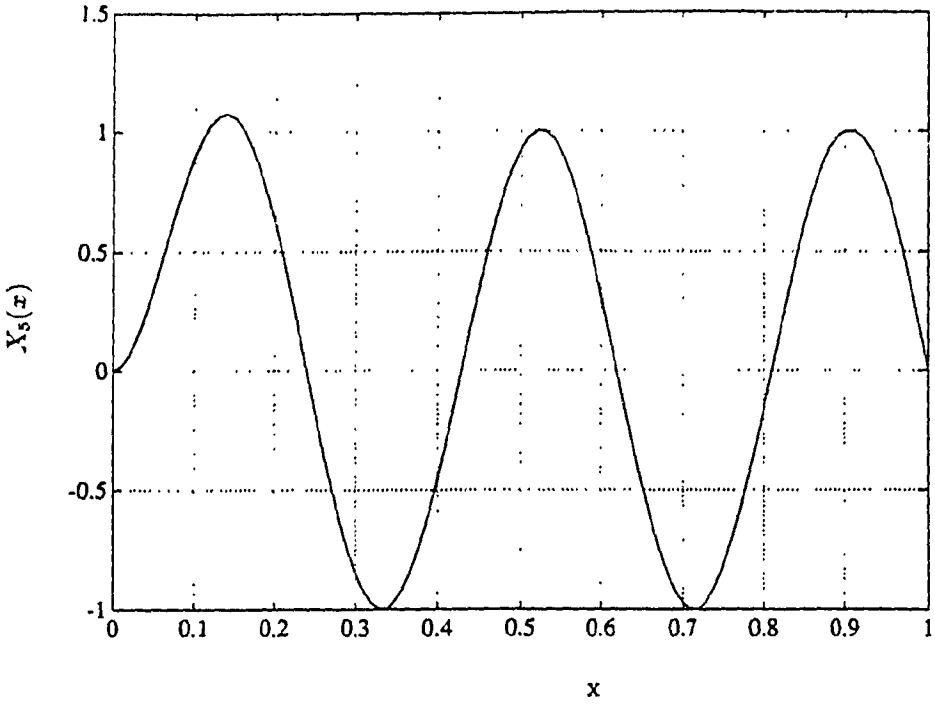

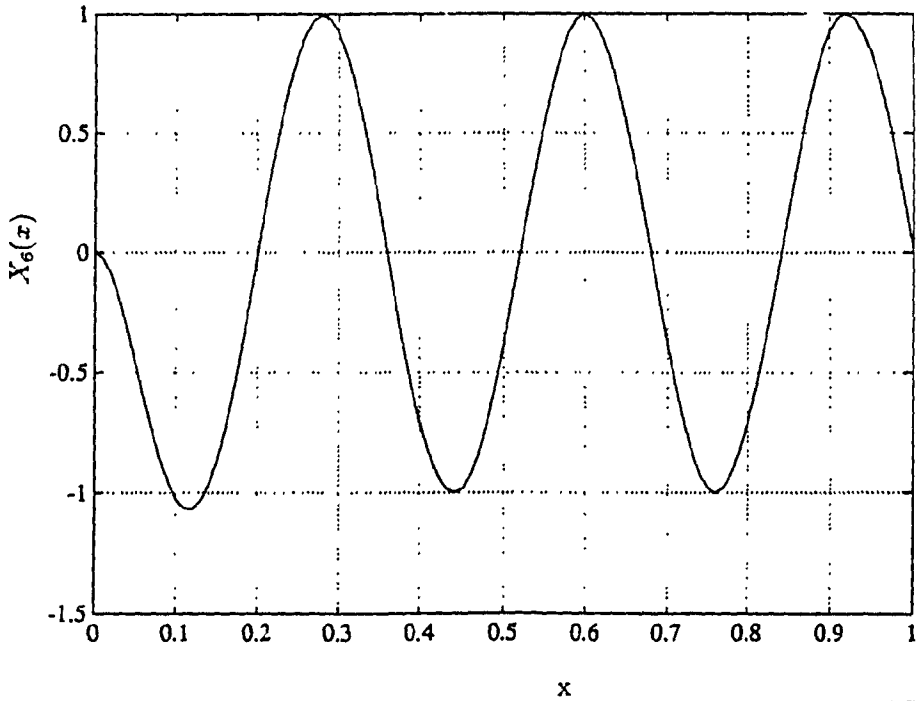

Fig. 2.5 Comparison of Fifth and Sixth Mode Shape Functions of CCSF plate along x direction (— Beam Characteristic Function, and - - - Approximate Plate Function)

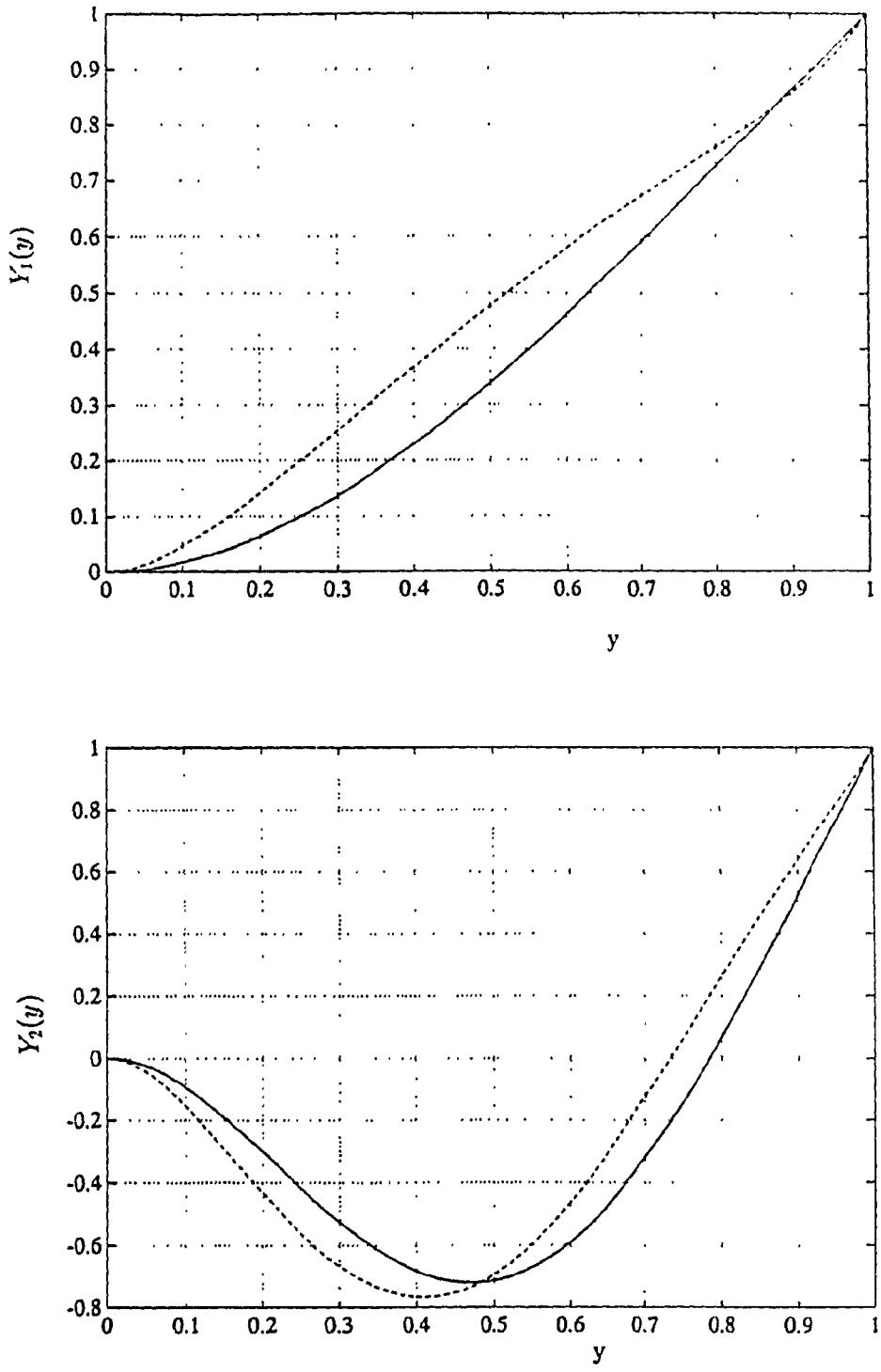

Fig. 2.6 Comparison of First and Second Mode Shape Functions of CCSF plate along y direction (— Beam Characteristic Function, and - - - Approximate Plate Function)

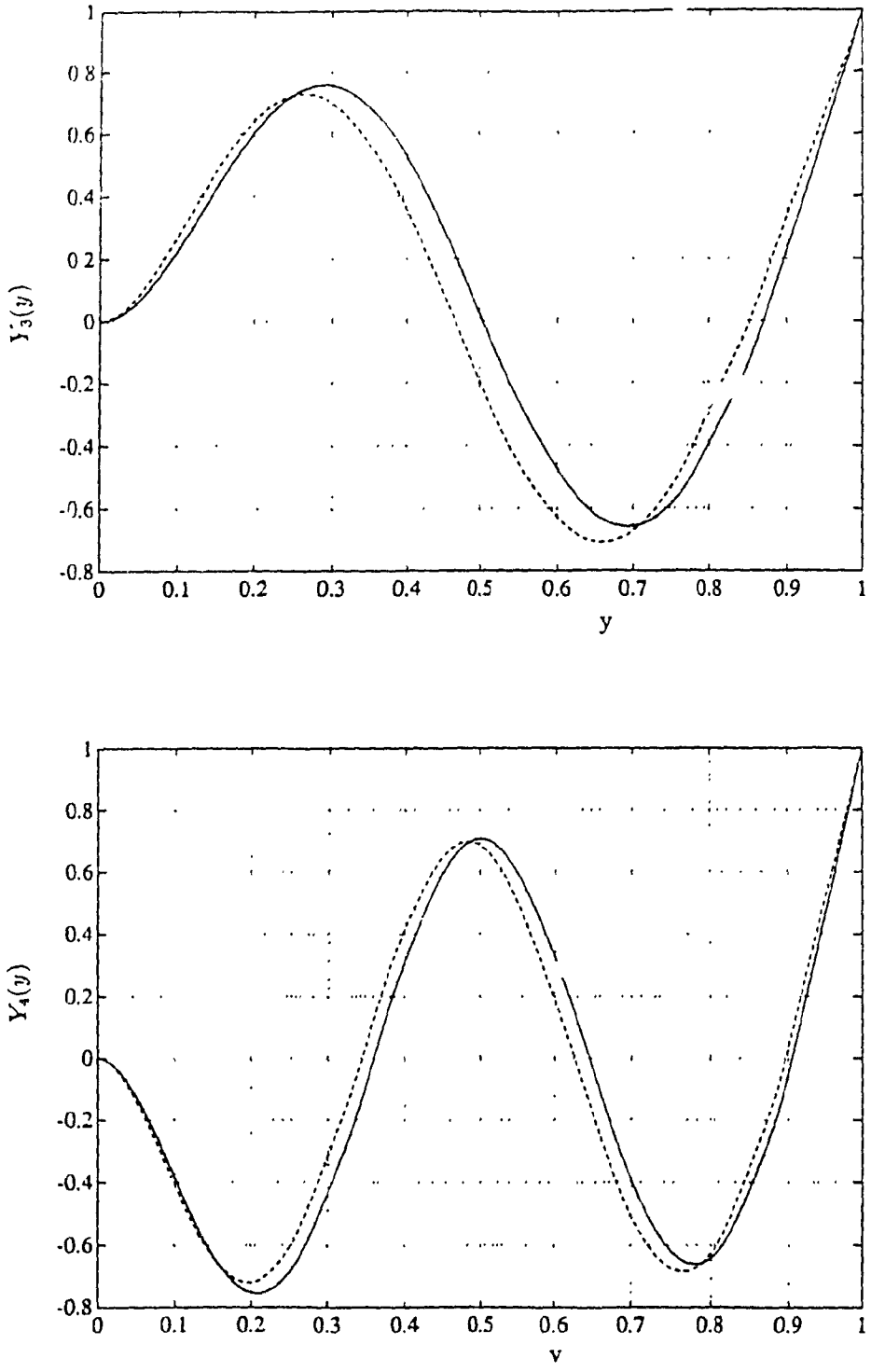

Fig. 2.7 Comparison of Third and Fourth Mode Shape Functions of CCSF plate along y direction (— Beam Characteristic Function, and - - - Approximate Plate Function)

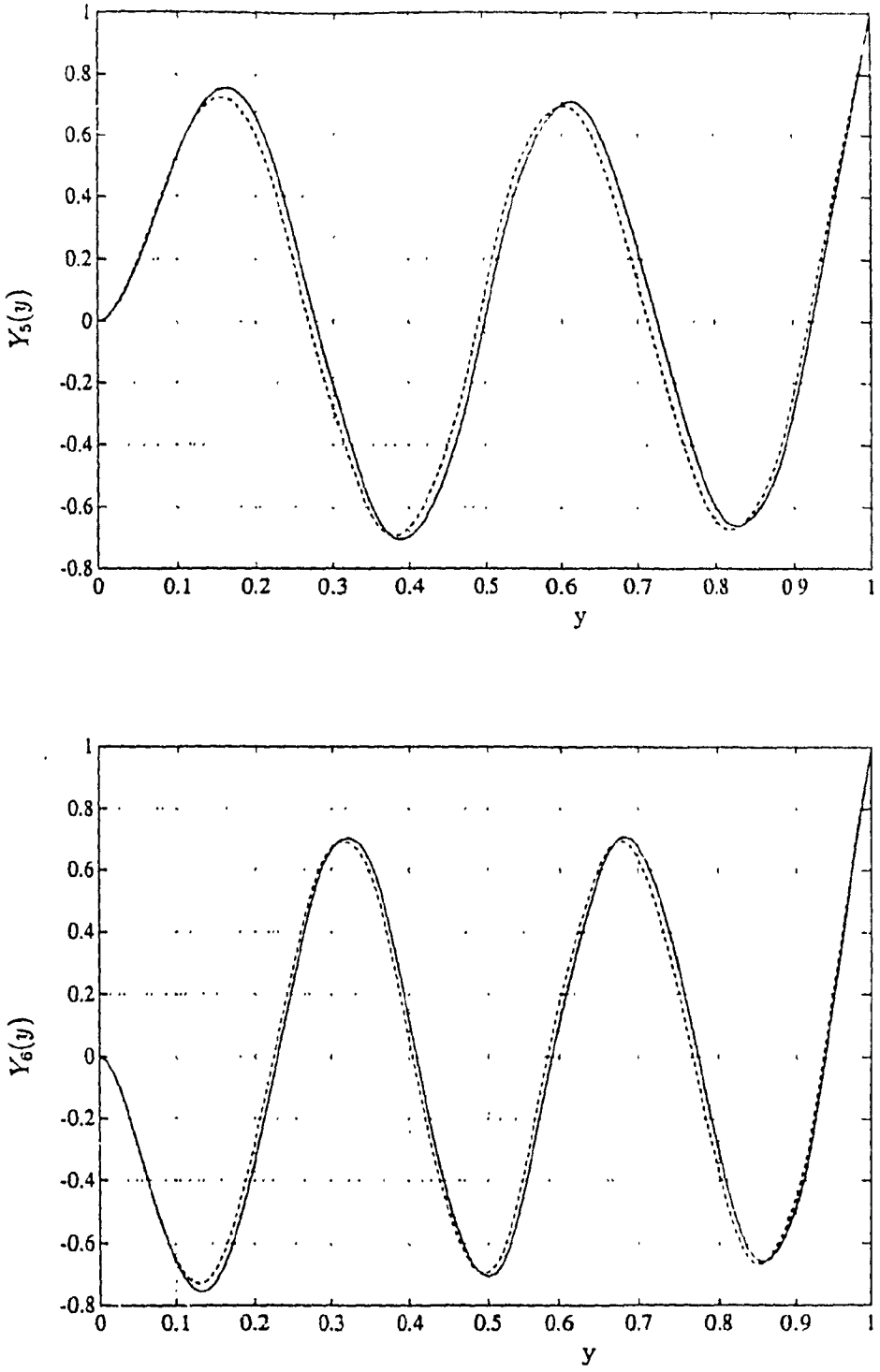

Fig. 2.8 Comparison of Fifth and Sixth Mode Shape Functions of CCSF plate along y direction (— Beam Characteristic Function, and - - - Approximate Plate Function)

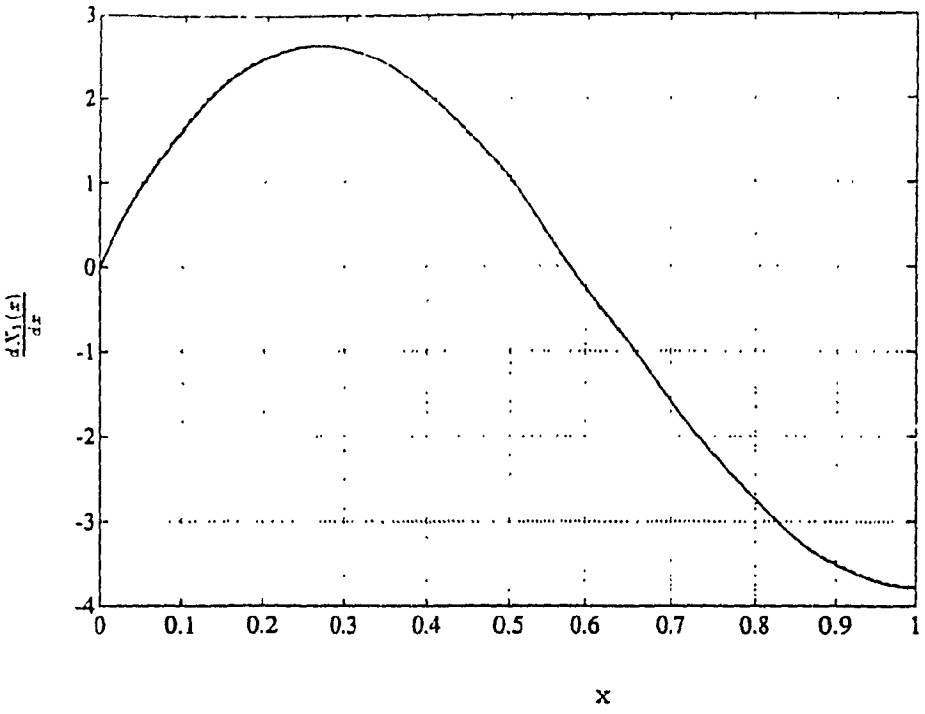

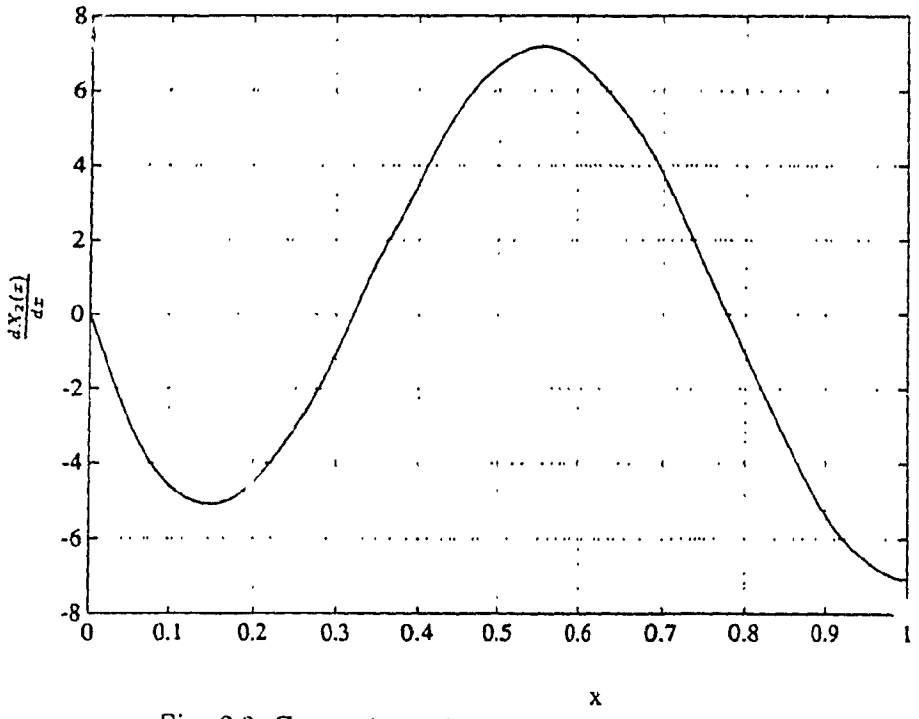

Fig. 2.9 Comparison of First Derivative of First and Second Functions of CCSF plate along x direction (— Beam Characteristic Function, and - - - Approximate Plate Function)

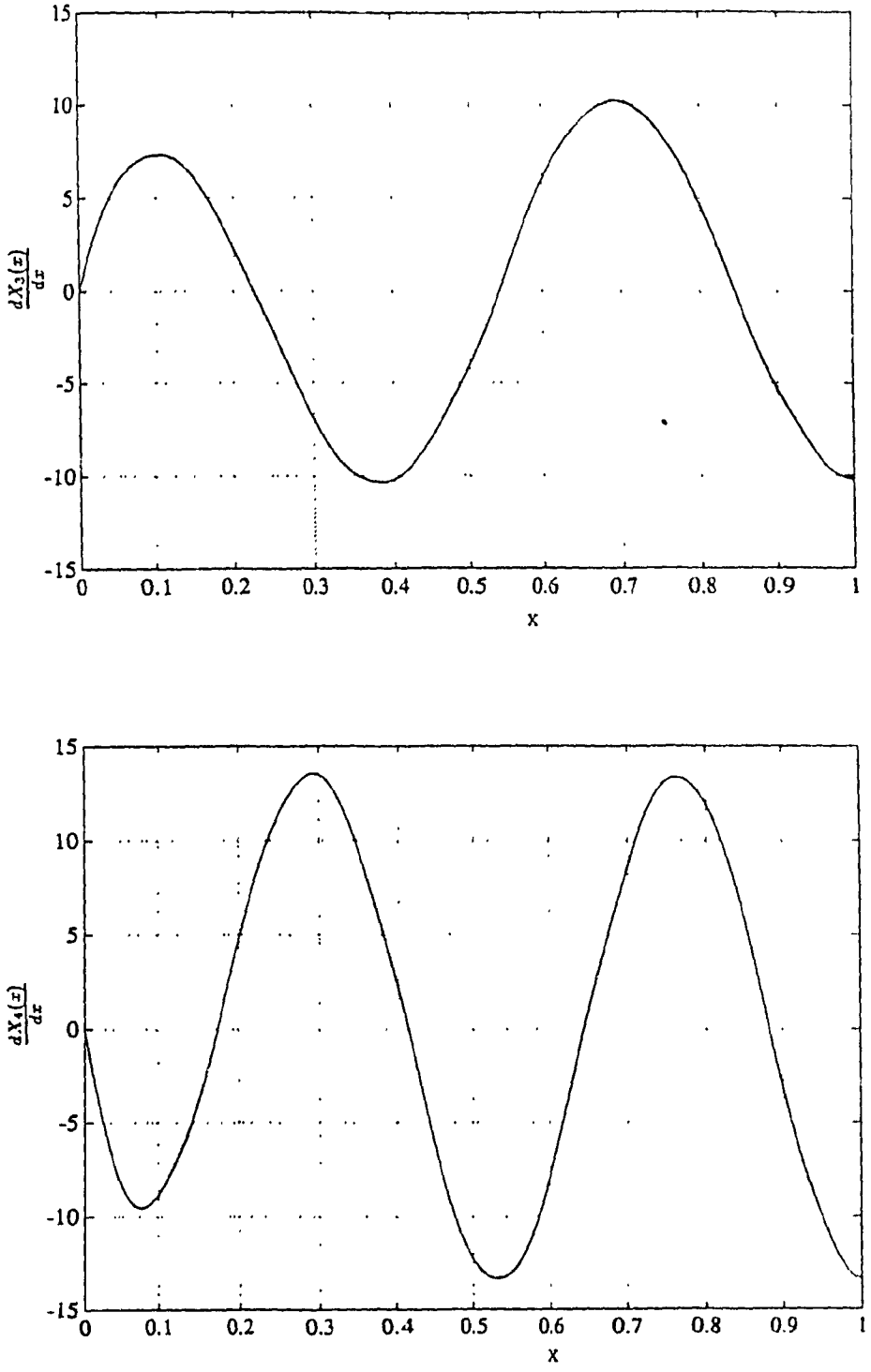

Fig. 2.10 Comparison of First Derivative of Third and Fourth Functions of CCSF plate along x direction (— Beam Characteristic Function, and - - - Approximate Plate Function)

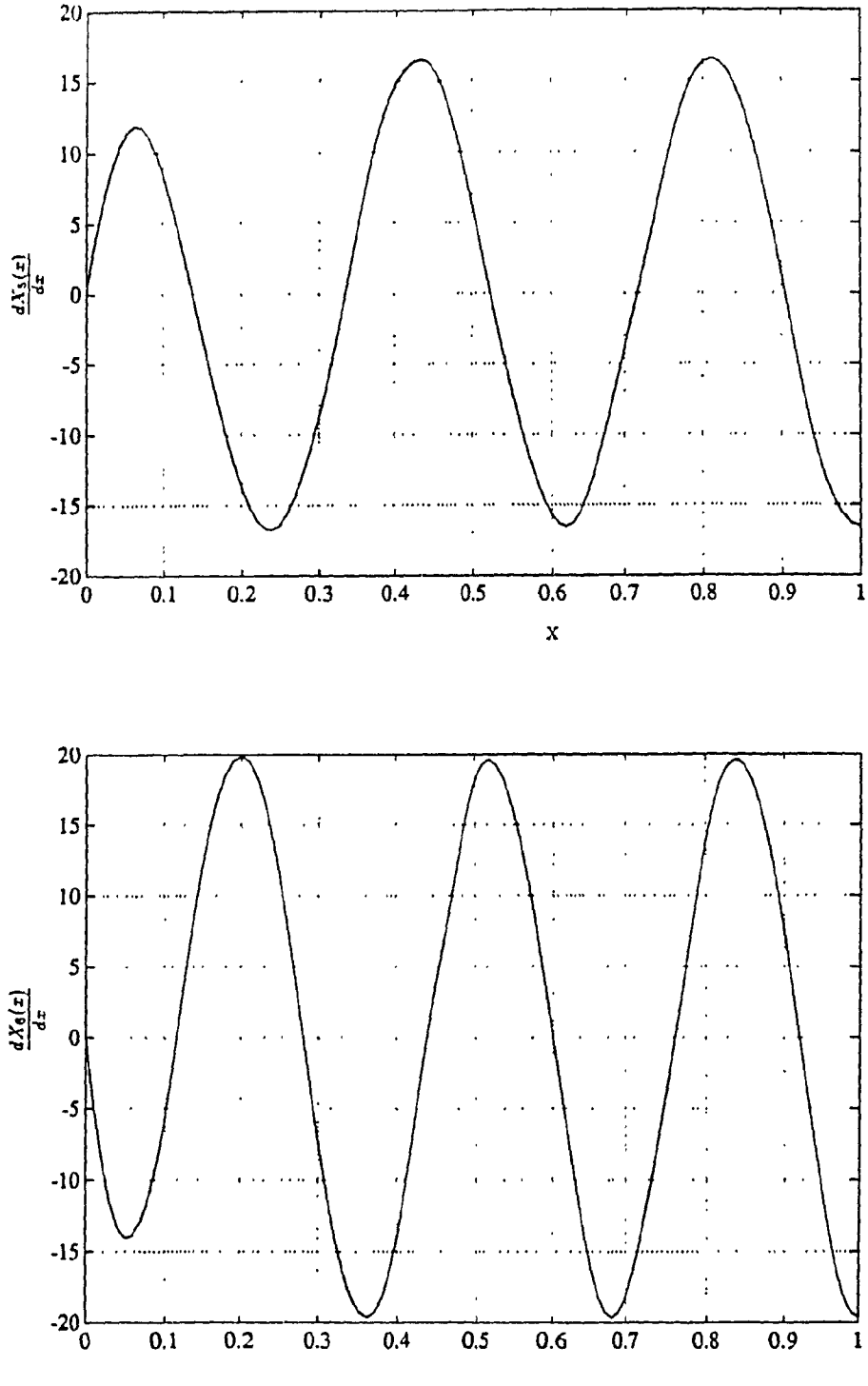

Fig. 2.11 Comparison of First Derivative of Fifth and Sixth Functions of CCSF plate along x direction (— Beam Characteristic Function, and - - - Approximate Plate Function)

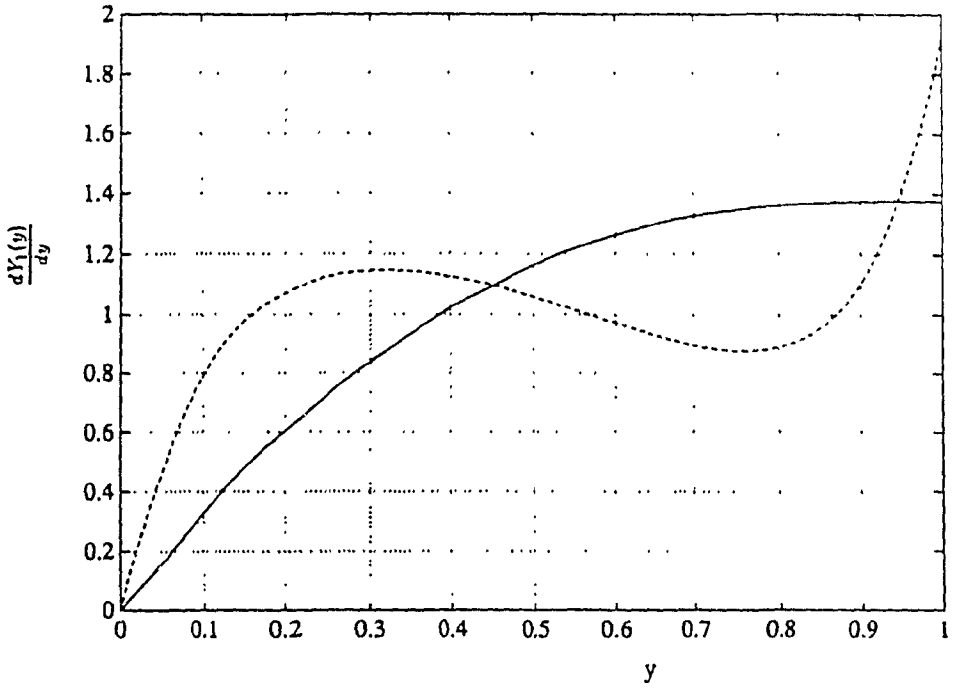

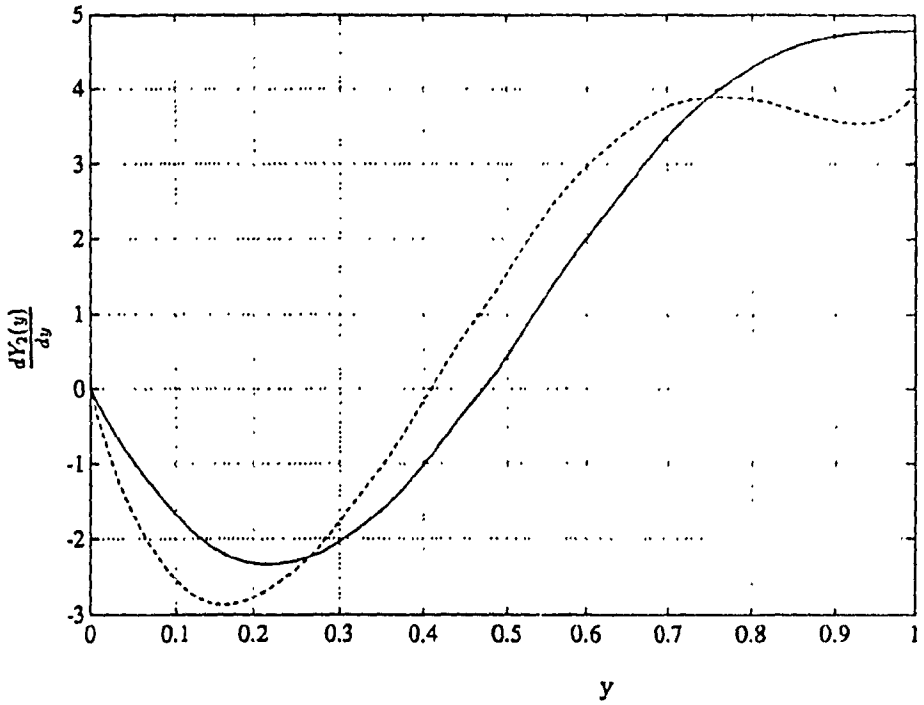

Fig. 2.12 Comparison of First Derivative of First and Second Functions of CCSF plate along y direction (— Beam Characteristic Function, and - - - Approximate Plate Function)

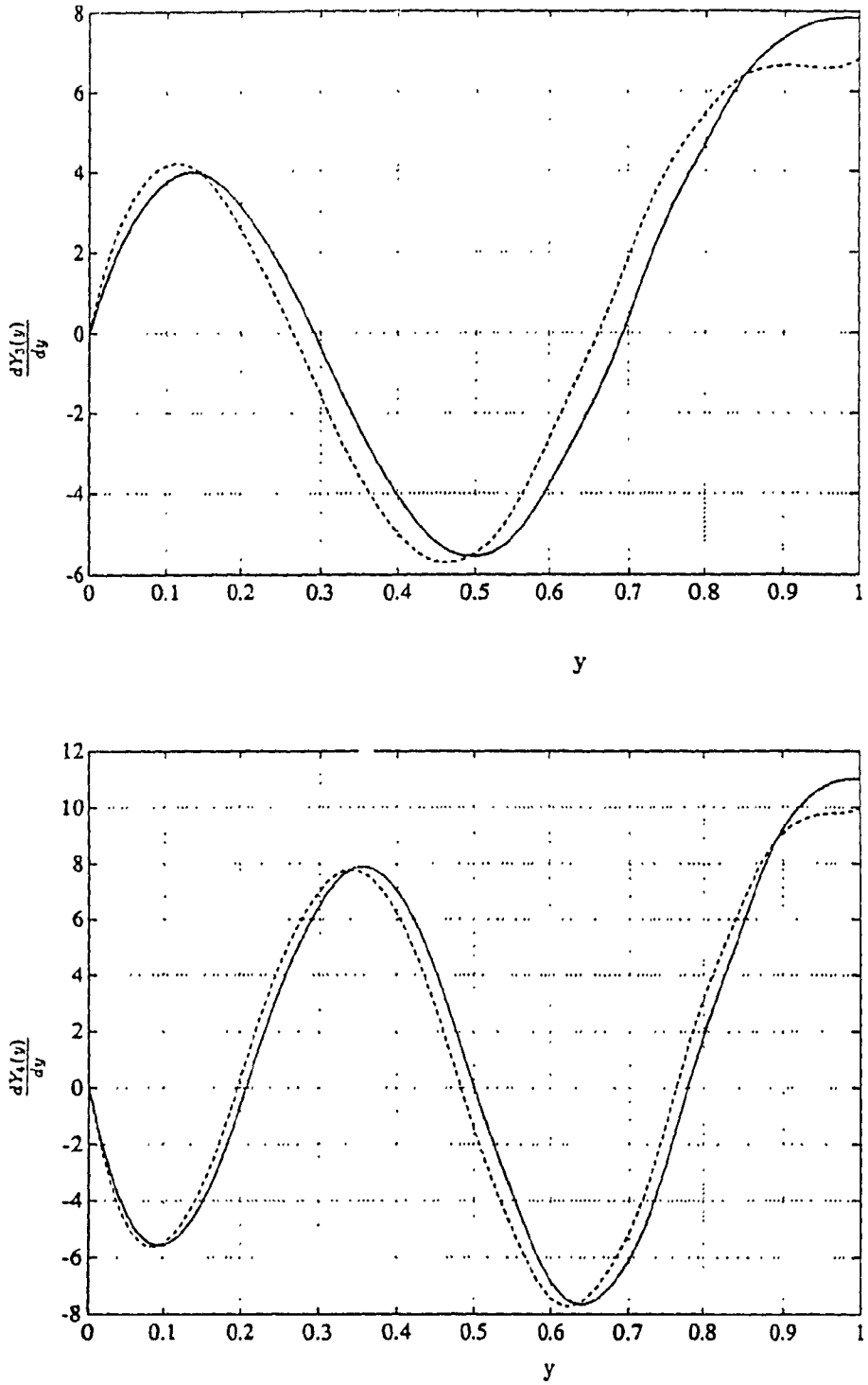

Fig. 2.13 Comparison of First Derivative of Third and Fourth Functions of CCSF plate along y direction (— Beam Characteristic Function, and - - - Approximate Plate Function)

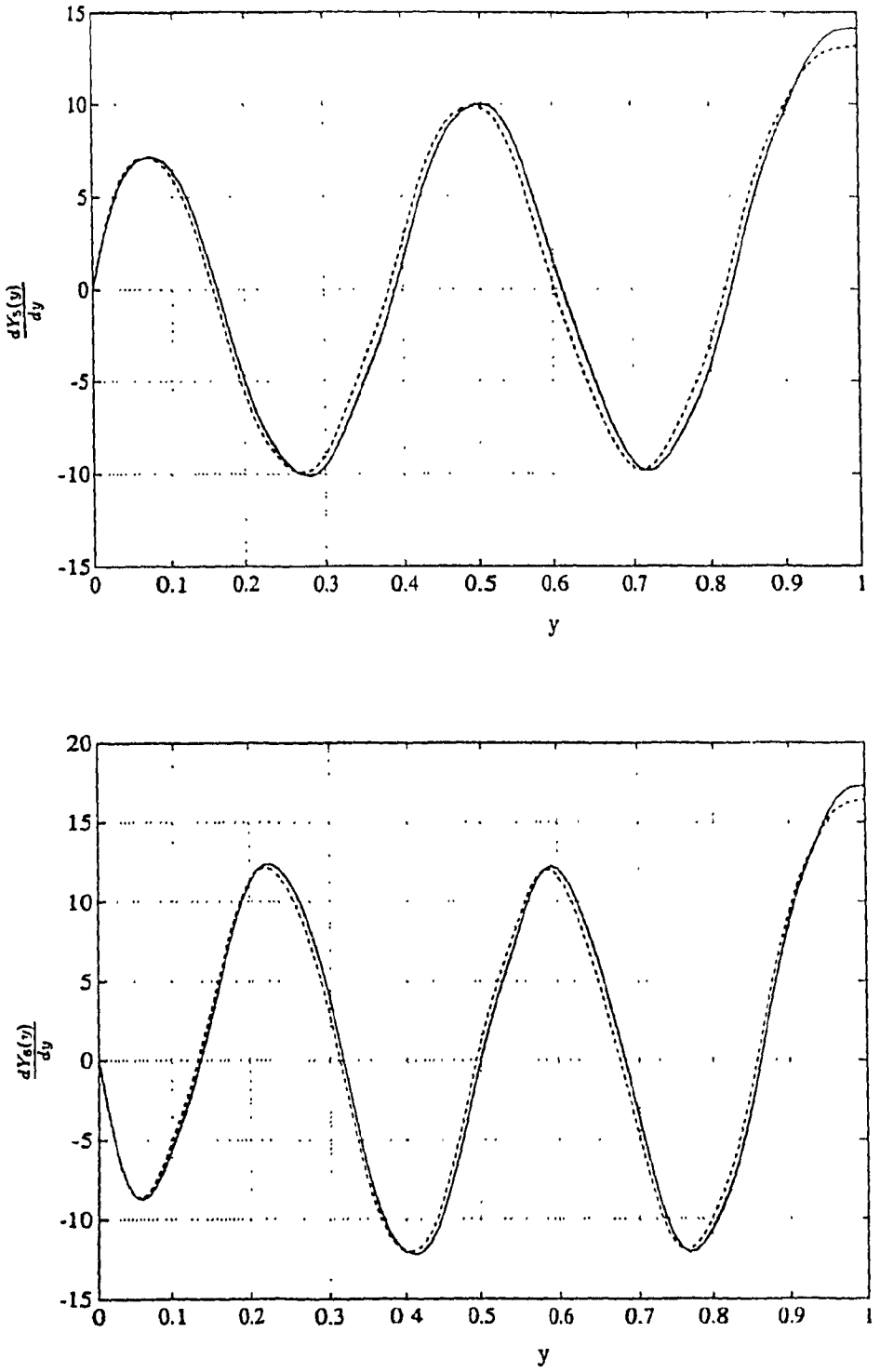

Fig. 2.14 Comparison of First Derivative of Fifth and Sixth Functions of CCSF plate along y direction (— Beam Characteristic Function, and - - - Approximate Plate Function)

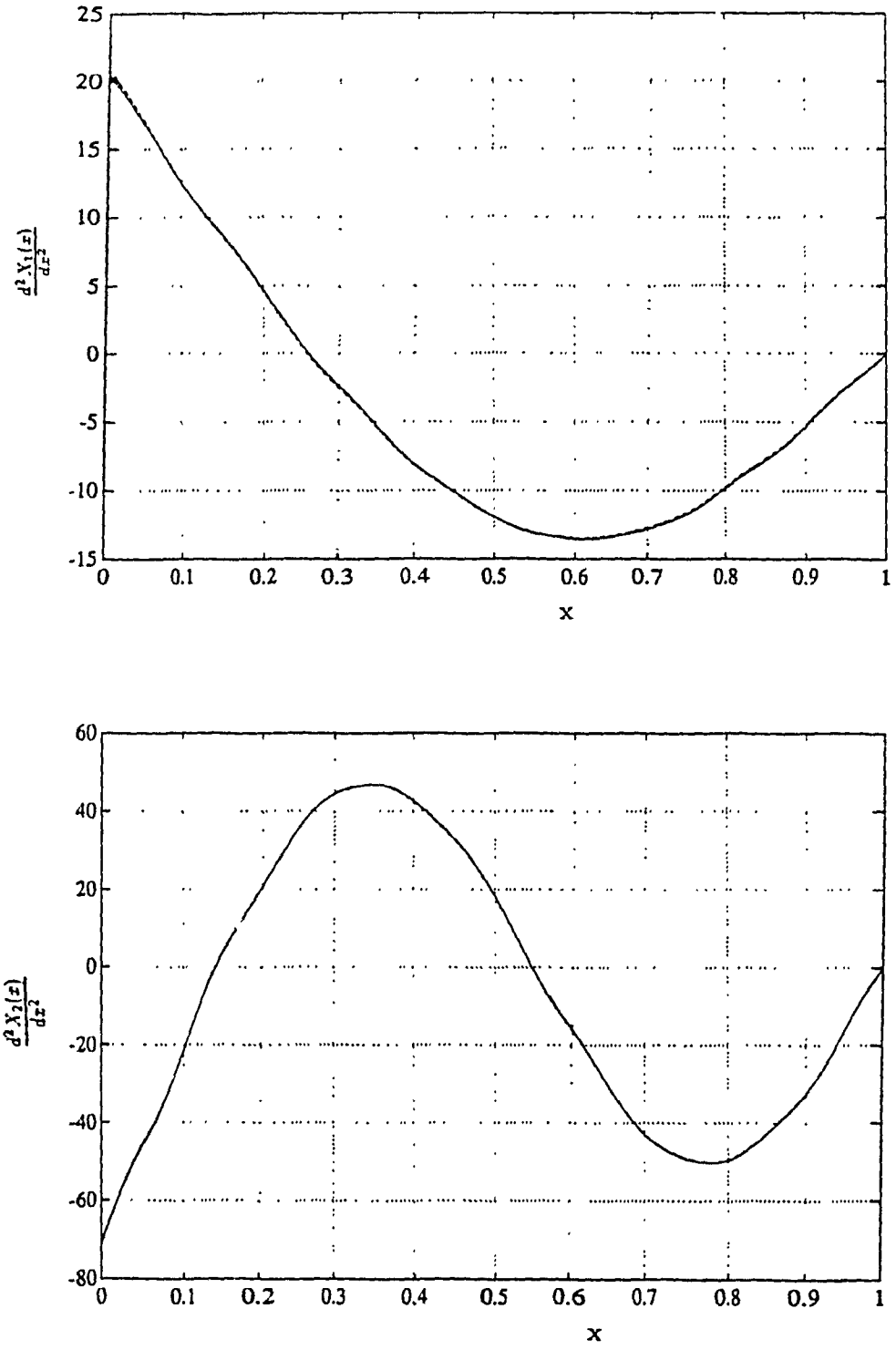

Fig. 2.15 Comparison of Second Derivative of First and Second Functions of CCSF plate along x direction (— Beam Characteristic Function, and - - - Approximate Plate Function)

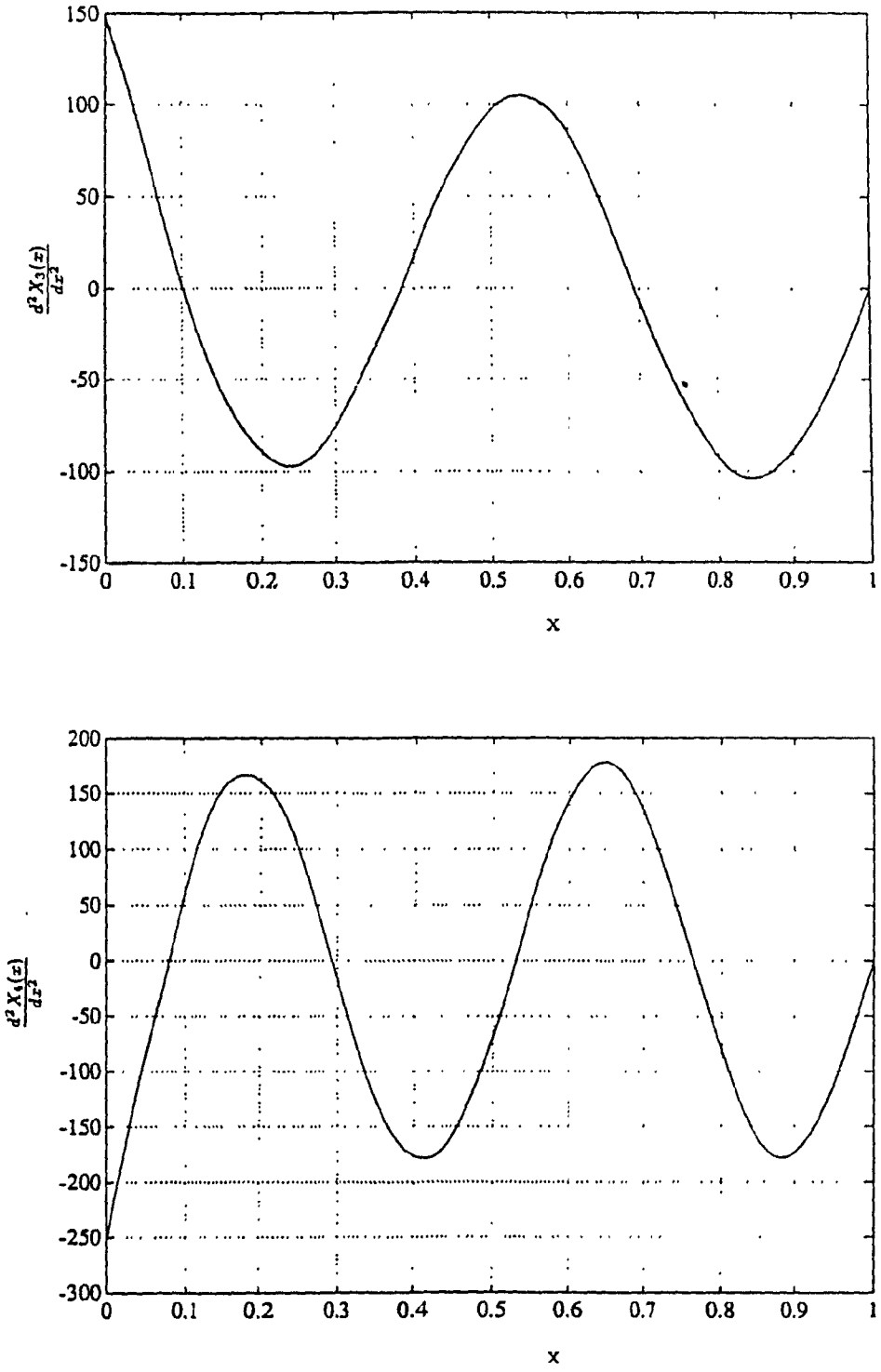

Fig. 2.16 Comparison of Second Derivative of Third and Fourth Functions of CCSF plate along x direction (— Beam Characteristic Function, and - - - Approximate Plate Function)

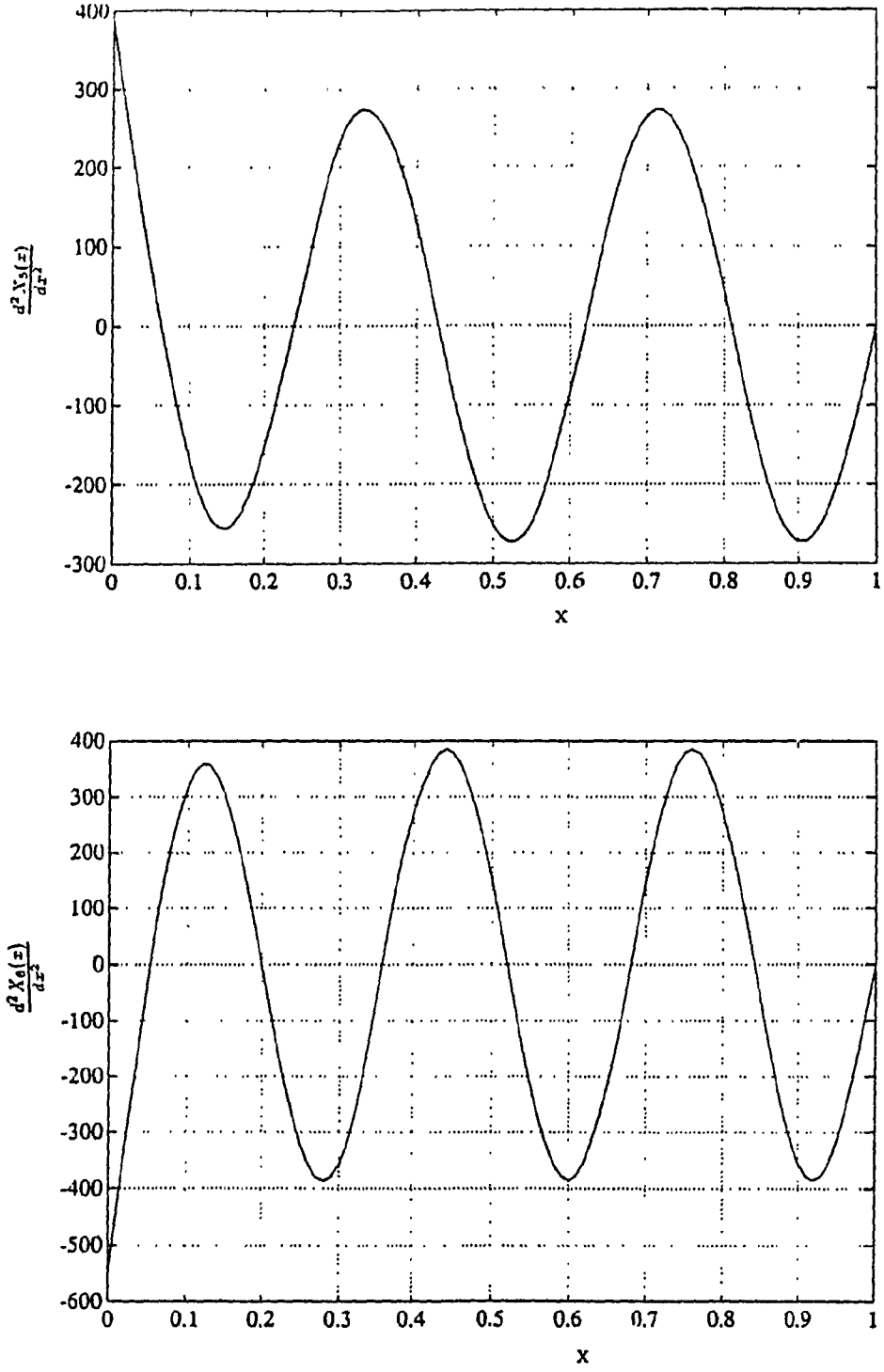

Fig. 2.17 Comparison of Second Derivative of Fifth and Sixth Functions of CCSF plate along x direction (— Beam Characteristic Function, and - - - Approximate Plate Function)

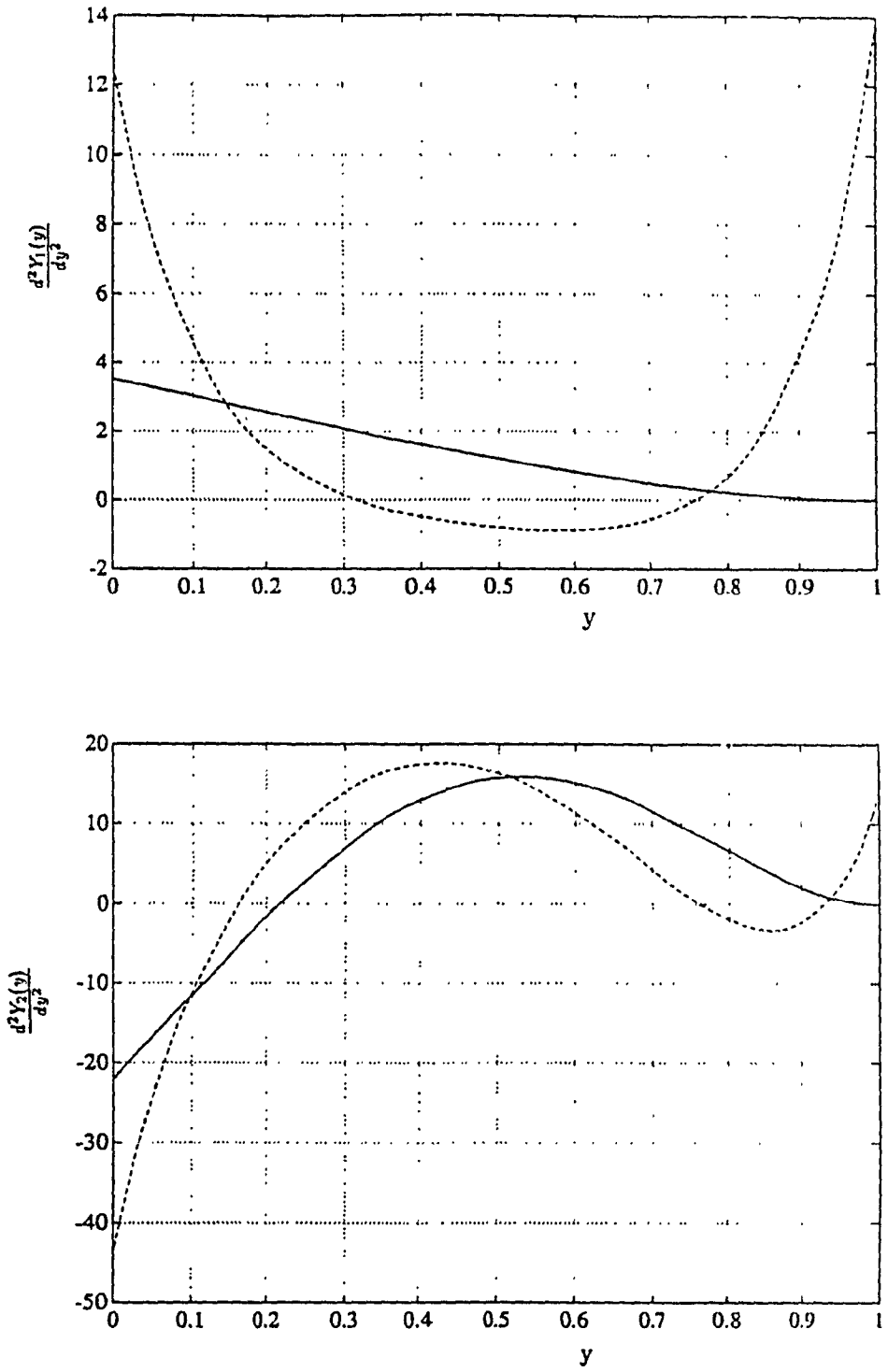

Fig. 2.18 Comparison of Second Derivative of First and Second Functions of CCSF plate along y direction (— Beam Characteristic Function, and - - - Approximate Plate Function)

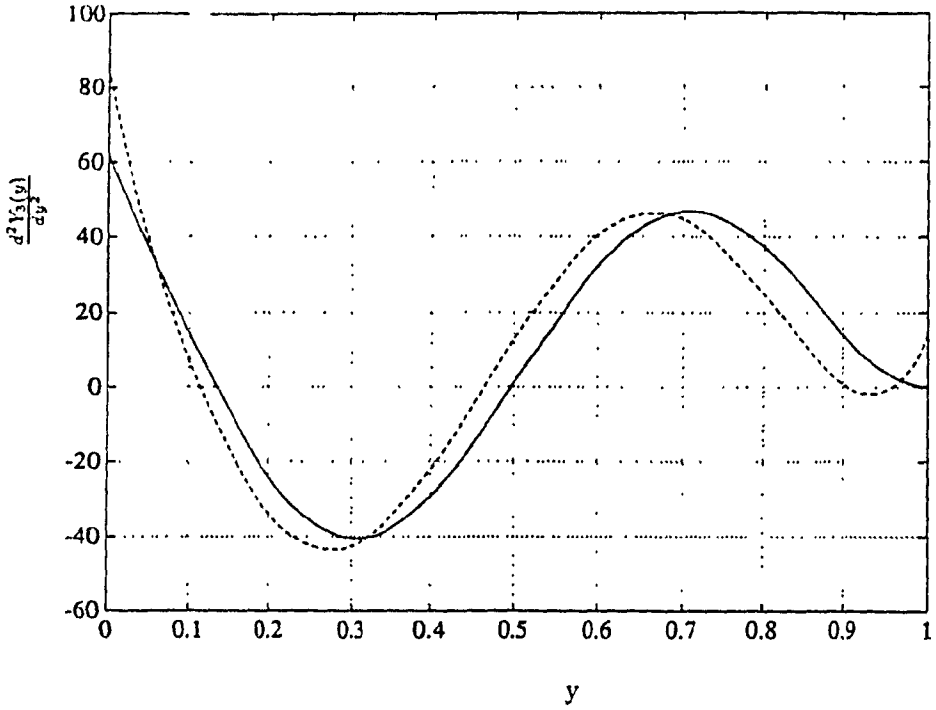

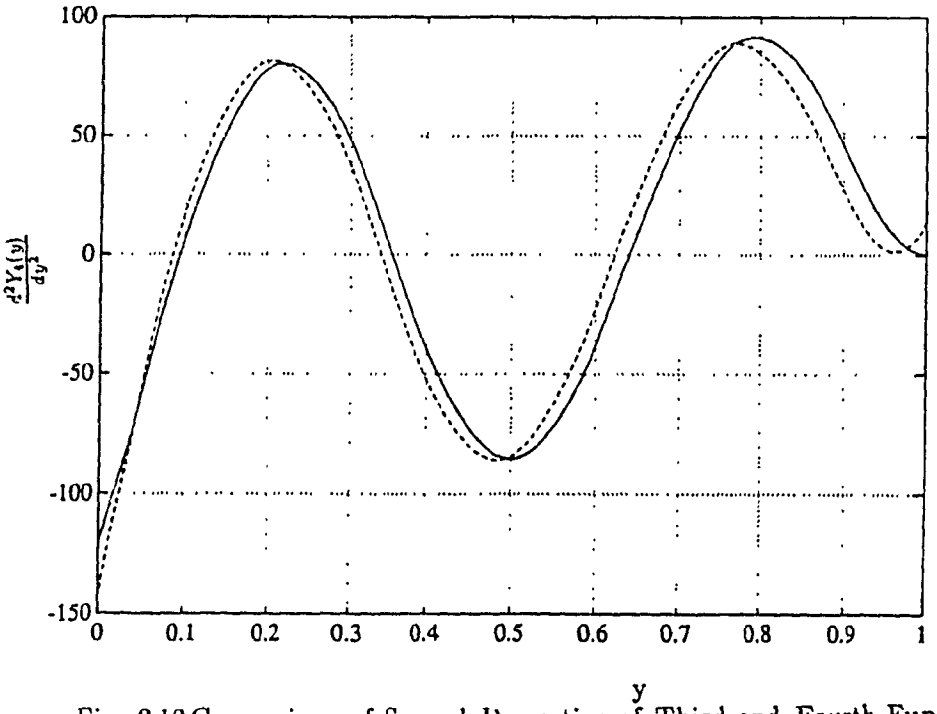

Fig. 2.19 Comparison of Second Derivative of Third and Fourth Functions of CCSF plate along y direction (— Beam Characteristic Function, and - - - Approximate Plate Function)

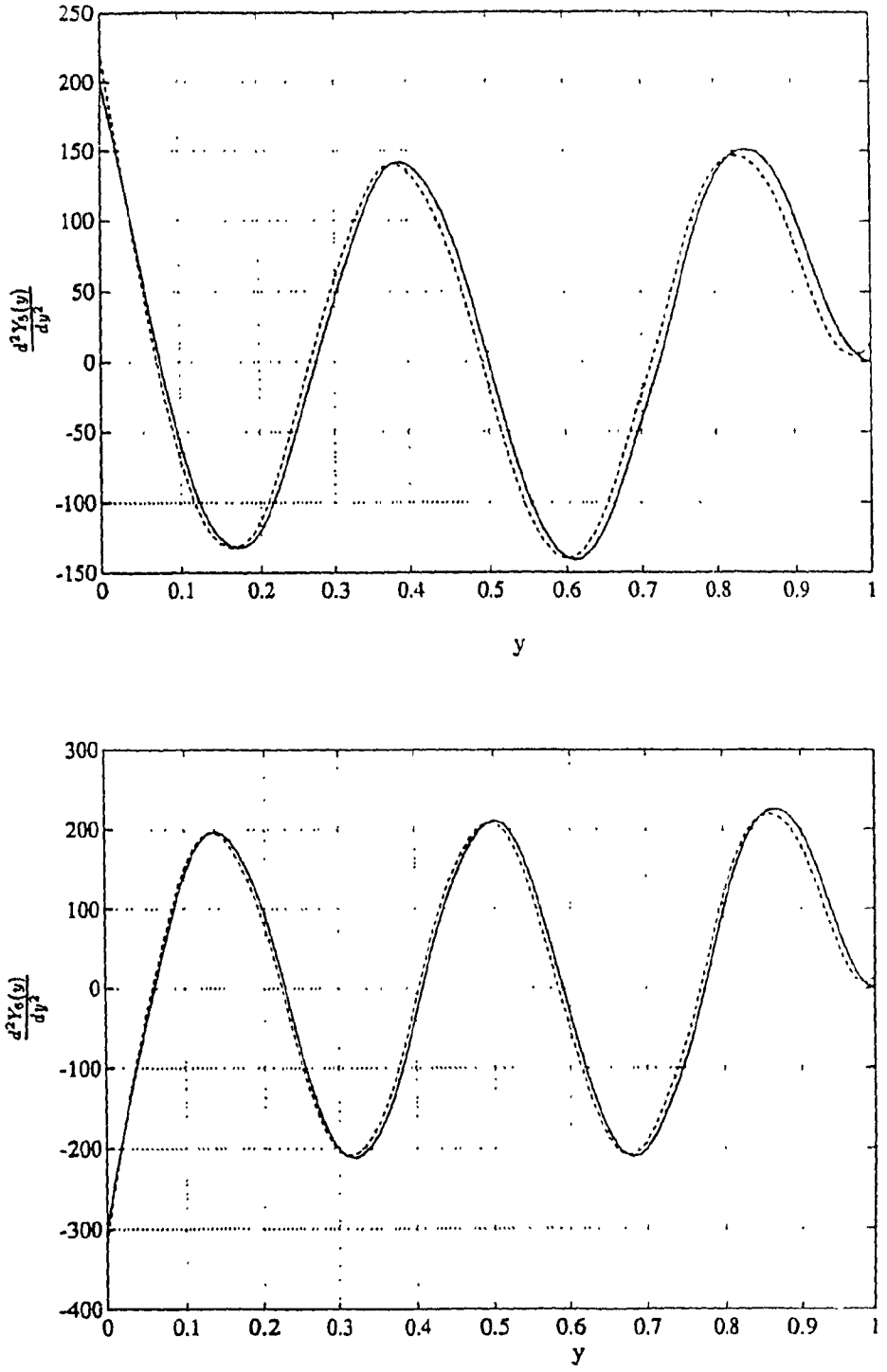

Fig. 2.20 Comparison of Second Derivative of Fifth and Sixth Functions of CCSF plate along y direction (— Beam Characteristic Function, and - - - Approximate Plate Function)

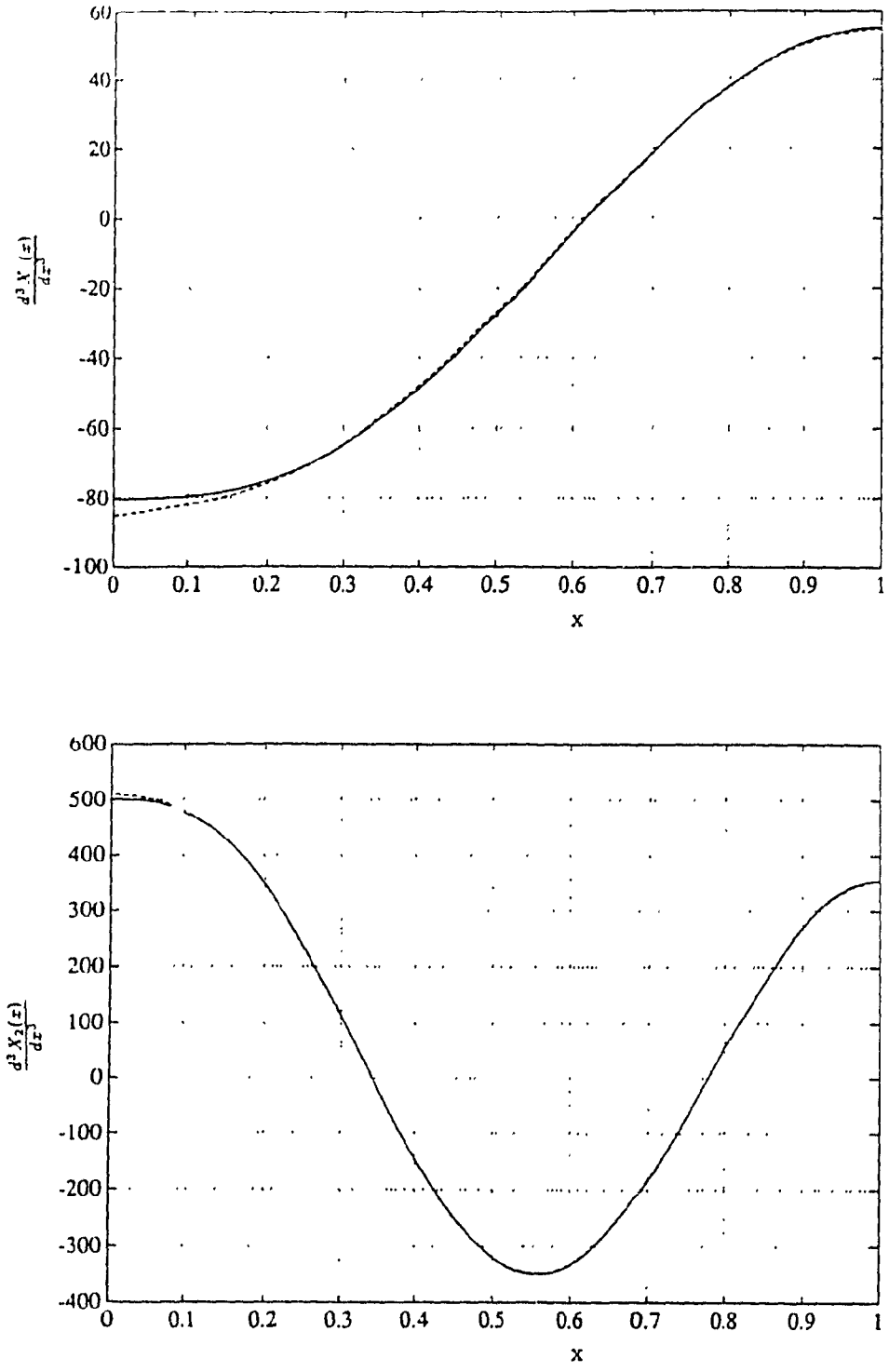

Fig. 2.21 Comparison of Third Derivative of First and Second Functions of CCSF plate along x direction (— Beam Characteristic Function, and - - - Approximate Plate Function)

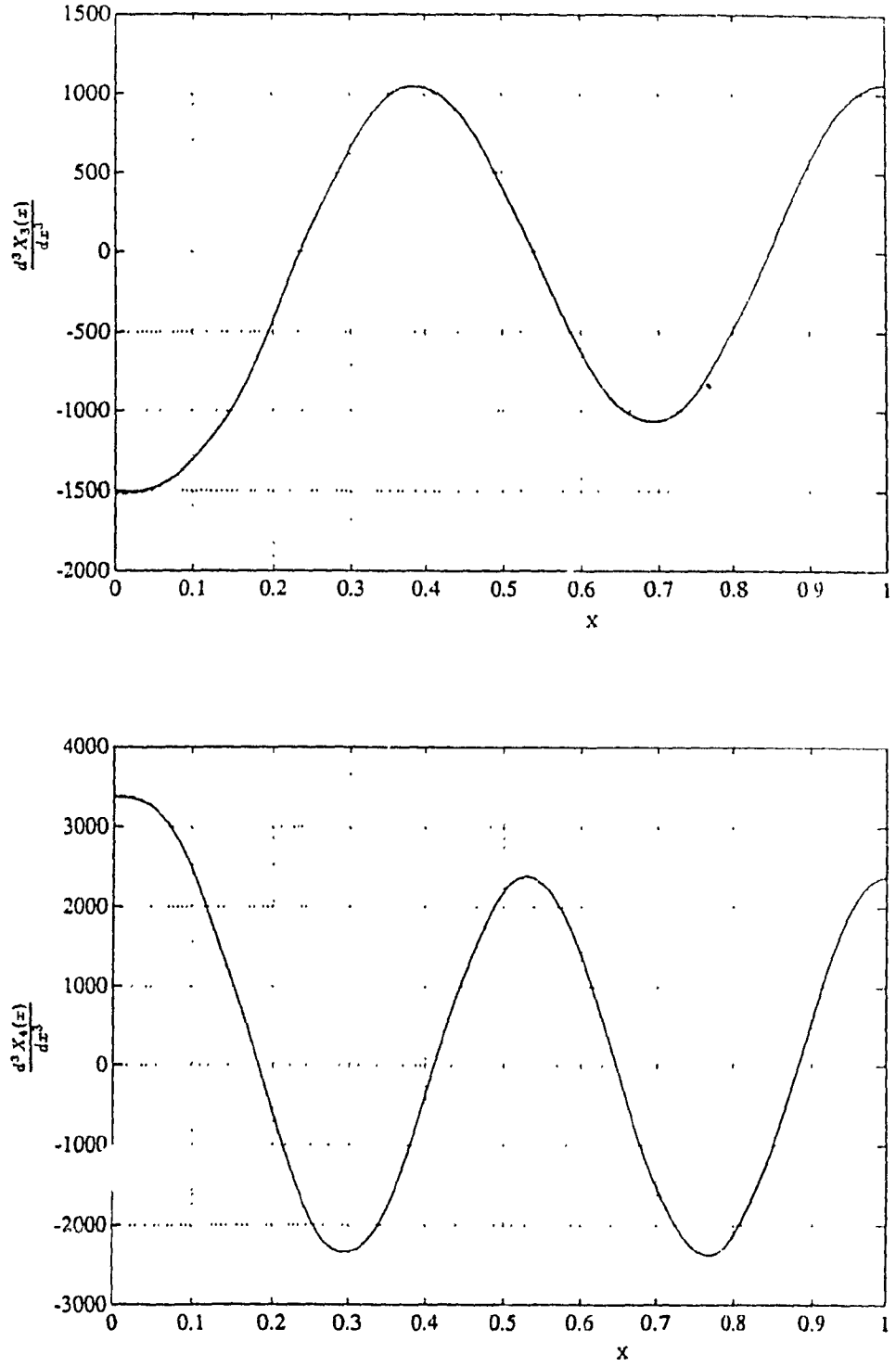

Fig. 2.22 Comparison of Third Derivative of Third and Fourth Functions of CCSF plate along x direction (— Beam Characteristic Function, and - - - Approximate Plate Function)

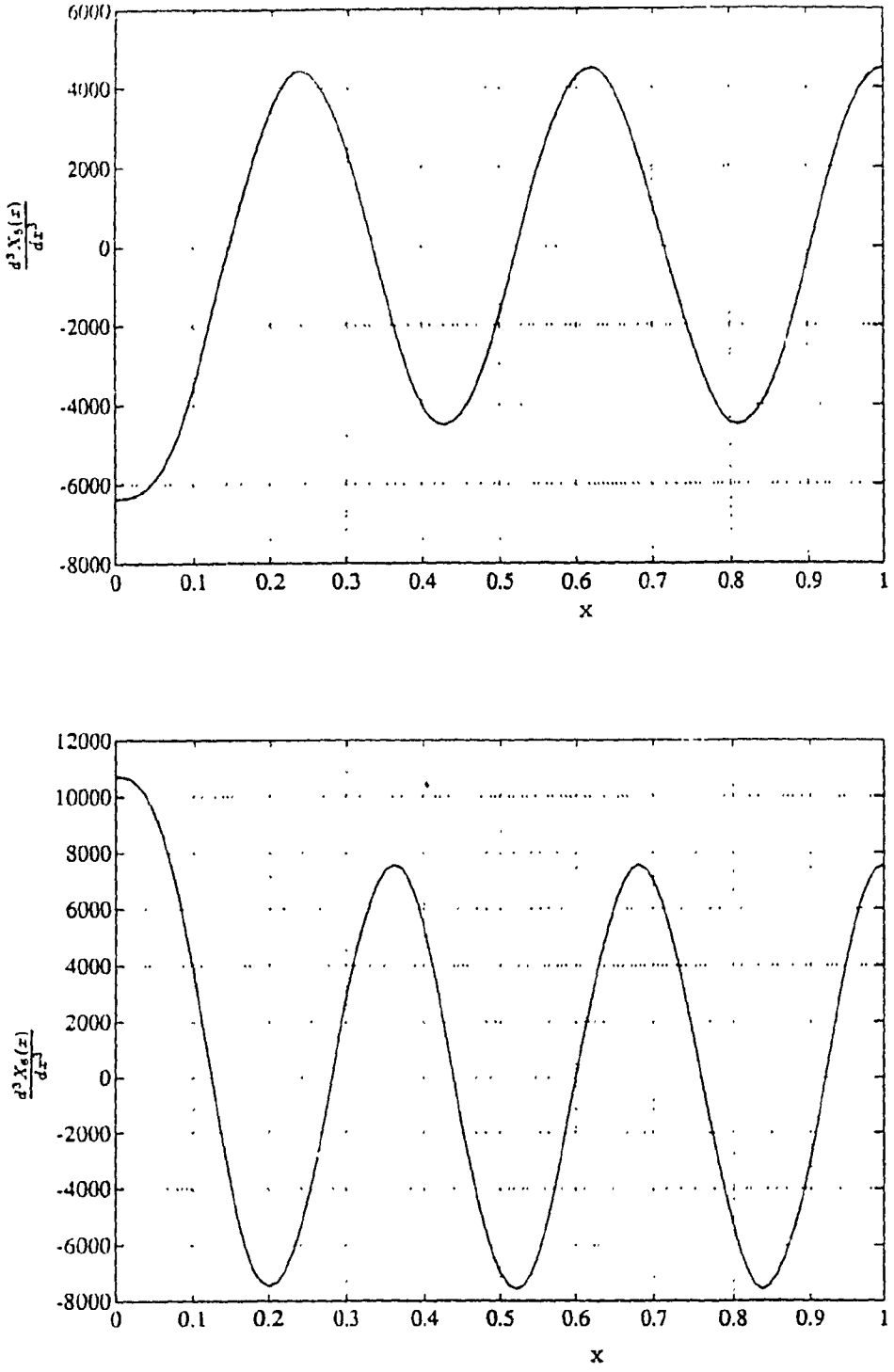

Fig. 2.23 Comparison of Third Derivative of Fifth and Sixth Functions of CCSF plate along x direction (— Beam Characteristic Function, and - - - Approximate Plate Function)

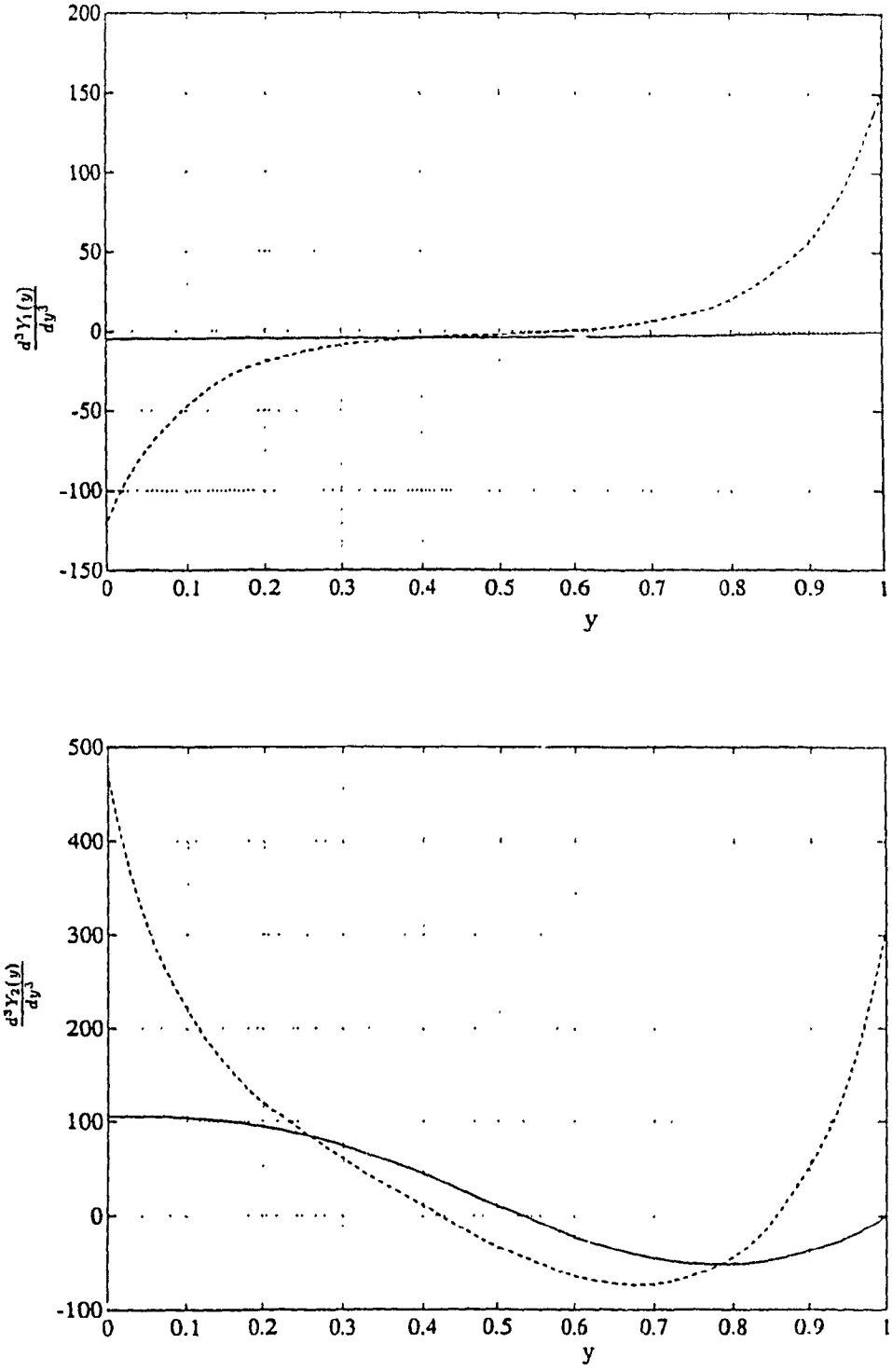

Fig. 2.24 Comparison of Third Derivative of First and Second Functions of CCSF plate along y direction (— Beam Characteristic Function, and - - - Approximate Plate Function)

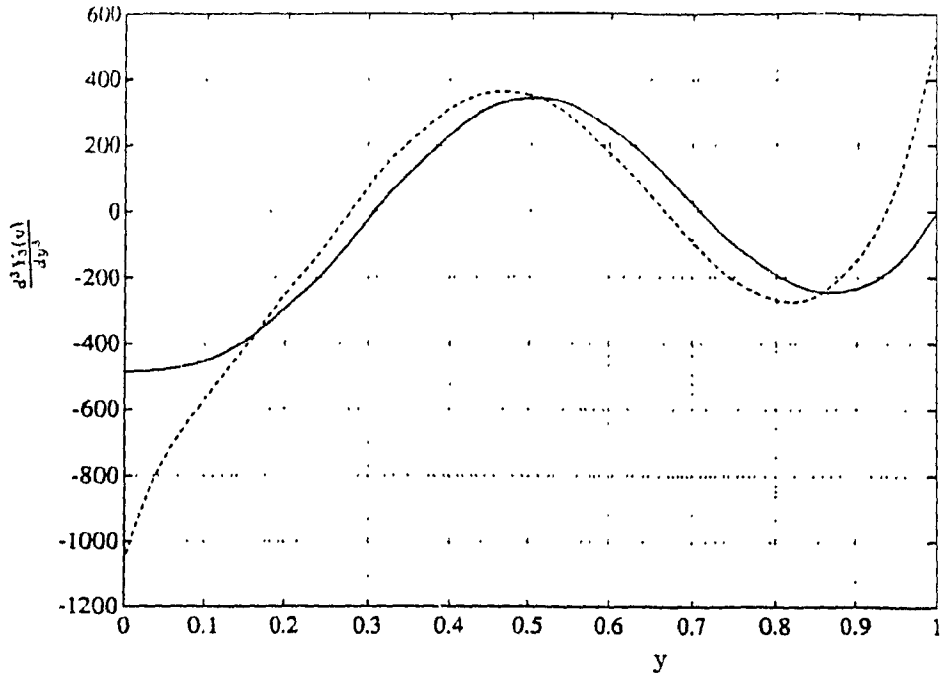

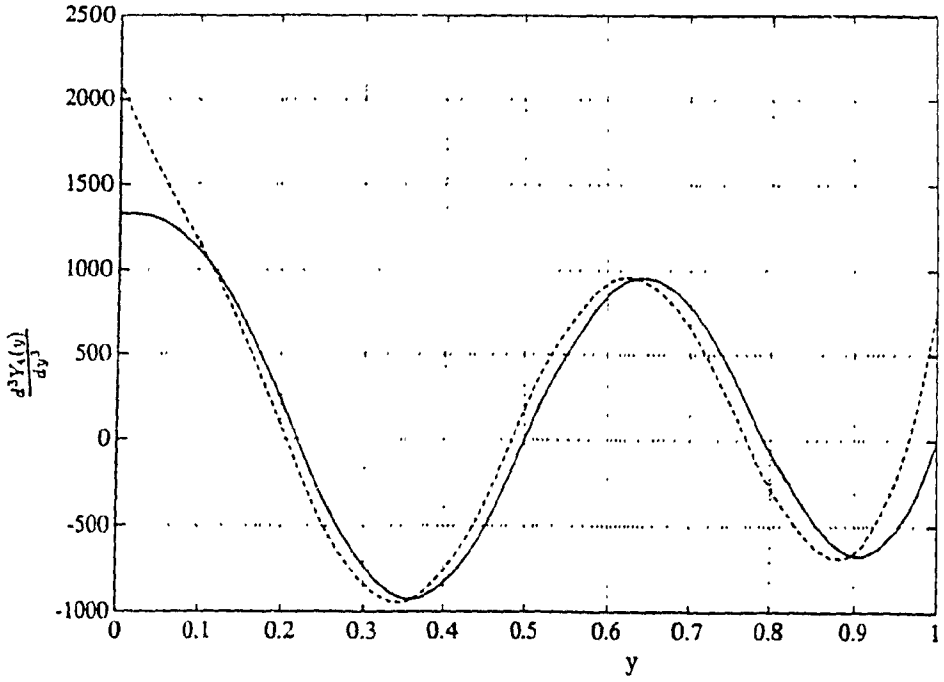

Fig. 2.25 Comparison of Third Derivative of Third and Fourth Functions of CCSF plate along y direction (— Beam Characteristic Function, and - - - Approximate Plate Function)

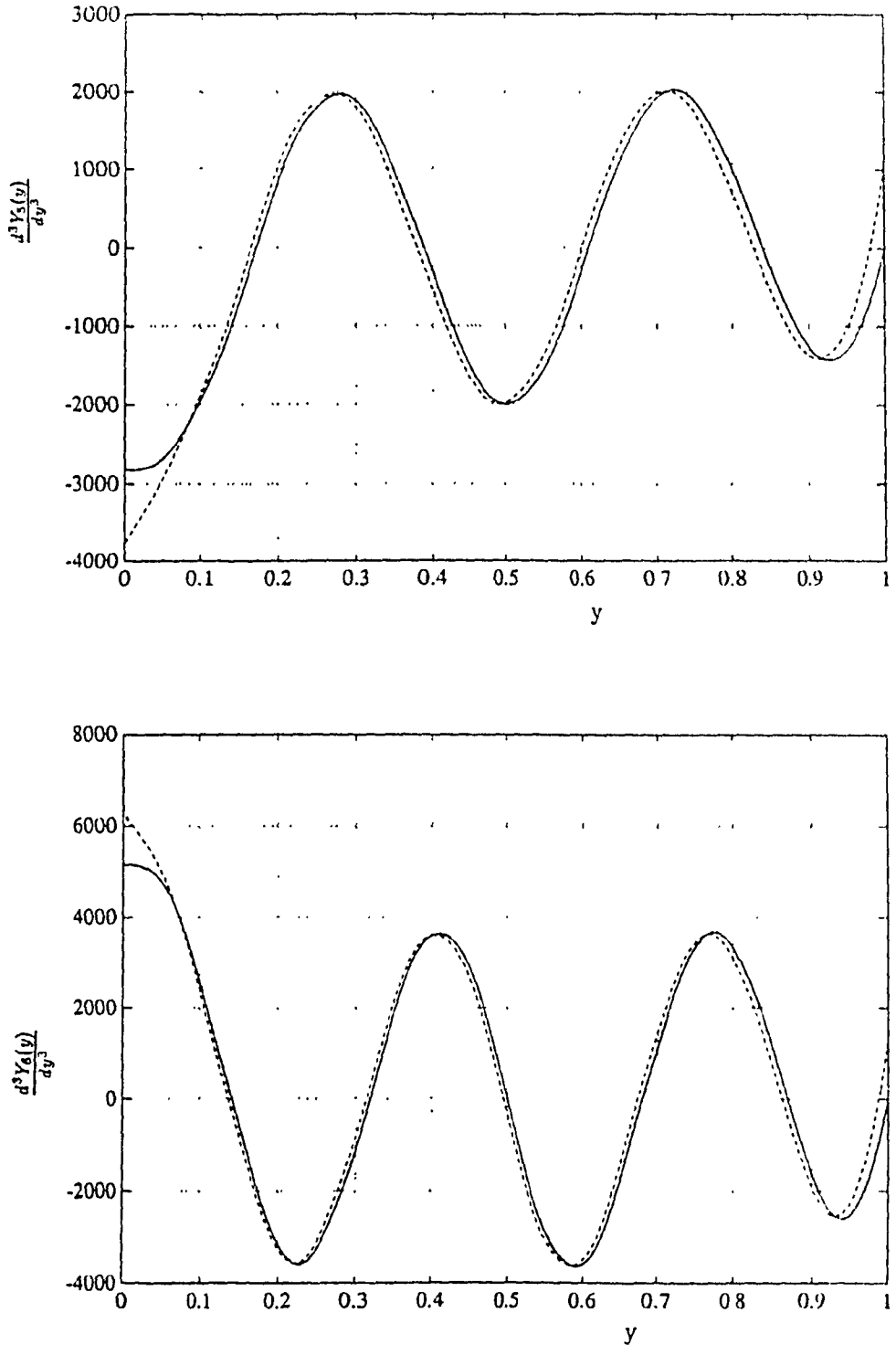

Fig. 2.26 Comparison of Third Derivative of Fifth and Sixth Functions of CCSF plate along y direction (— Beam Characteristic Function, and - - - Approximate Plate Function)

Chapter 3

ELASTIC RESPONSE OF BEAMS AND PLATES TO IMPULSIVE LOADS

In the last chapter the natural frequencies and mode shapes of beams and plates were discussed. When the response is in the linear elastic range, it can be expressed as the sum of responses from individual normal modes of the structure. The natural frequency and normal mode results of the previous chapter are used in normal mode analysis to evaluate the response of these structures to impulsive loads, in this chapter. Normal mode analysis is meaningful only if the structure is elastic. In reality, structures may have geometric or material nonlinearities, and the structural deflections may cross into plastic range depending on the intensity of the impulse loading. However, linear response analysis in the elastic range using normal mode analysis provides information that can be useful in comparing the behaviours of different structures under impulsive loading.

Impulsive loads are of short duration and are generally studied in terms of standard pulse shapes as shown in Fig. 3.1. Actual impulsive loads may have arbitrary shapes and hence response to such loads may be quite difficult to evaluate.

3.1 BEAM RESPONSE

In order to study the response of a beam to impulse loading, the equation of motion of the beam with external load $f(x,t)$ is written as,

$$EI\frac{\partial^4 y}{\partial x^4} + m\frac{\partial^2 y}{\partial t^2} = f(x,t) \tag{3.1}$$

By assuming a separable solution of the form,

$$y(x,t) = \sum_{i=0}^{\infty} Y_i(x) \cdot q_i(t) \tag{3.2}$$

where Y_i and q_i are functions of space and time respectively.

Substituting (3.2) in (3.1),

$$EI\sum_{i=0}^{\infty} q_i(t)\frac{\partial^4 Y_i(x)}{\partial x^4} + m\sum_{i=0}^{\infty} Y_i(x)\frac{\partial^2 q_i(t)}{\partial t^2} = f(x,t)$$

Multiplying by $Y_j(x)$ and integrating over the length of the beam.

$$\int_0^l EI\sum_{i=0}^{\infty} q_i(t)\frac{\partial^4 Y_i(x)}{\partial x^4}Y_j(x)dx + \int_0^l m\sum_{i=0}^{\infty} Y_i(x)\frac{\partial^2 q_i(t)}{\partial t^2}Y_j(x)dx = \int_0^l f(x,t)Y_j(x)dx$$

If $Y_i(x)$ is a normalized function, then by orthogonal property of modes [31],

$$\begin{aligned}\int_0^l EI\frac{\partial^4 Y_i(x)}{\partial x^4}Y_j(x)dx &= \omega_i^2 a_{ij} \quad and\\ \int_0^l mY_i(x)Y_j(x)dx &= a_{ij} \qquad a_{ij} = 0;\ i \neq j \end{aligned} \tag{3.3}$$

Therefore, the equation of motion can be written as,

$$\ddot{q}_i(t) + \omega_i^2 q_i(t) = \frac{Q_i(t)}{a_{ii}} \qquad i = 1,2,3,\ldots n$$

where $Q_i(t) = \int_0^l Y_j(x)f(x,t)dx$ is the generalized force associated with the generalized coordinate $q_i(t)$. The equation of motion is now expressed as n number of uncoupled equations, each corresponding to one degree of freedom.

The general response of a undamped SDOF system is given in terms of the convolution integral as [31],

$$q_i(t) = \frac{1}{a_{ii}\omega_i}\int_0^t Q_i(\tau)\sin\omega_i(t-\tau)d\tau + q_{i_0}\cos\omega_i t + \frac{\dot{q}_{i_0}}{\omega_i}\sin\omega_i t \tag{3.4}$$

where $q_{i_0} = q_i(0)$ *and* $\dot{q}_{i_0} = \dot{q}_i(0)$ are the initial conditions. Using this in equation (3.2),

$$y(x,t) = \sum_{i=0}^{\infty} Y_i(x)\left[\frac{1}{a_{ii}\omega_i}\int_0^t Q_i(\tau)\sin\omega_i(t-\tau)d\tau + q_{i_0}\cos\omega_i t + \frac{\dot{q}_{i_0}}{\omega_i}\sin\omega_i t\right] \tag{3.5}$$

Generalized load $Q_i(t)$ in the case of a half sine pulse of magnitude F_p and half period τ, acting at a distance c from the left supported end of a simply supported beam, can be obtained as

$$\begin{aligned} Q_i(t) &= \int_0^l F_p \sin\frac{\pi t}{\tau}\delta(x-c)Y_i(x)dx \\ &= F_p \sin\frac{\pi t}{\tau}Y_i(c) \qquad for\ t<\tau \end{aligned} \tag{3.6}$$

Using such an expression in (3.5) along with other expressions like ω_i and $Y_i(x)$, which depend on the beam boundary conditions, leads to the general form of beam response to various pulse forcing functions. In non-dimensional form,

$$Y^* = F\left\{\sum_{i=0}^{\infty}\frac{1}{(\beta_i l)^4}\left[Y_i(c)\right]\ \left[Y_i(x)\right]\ \left[\eta_i(T)\right]\right\} \tag{3.7}$$

where

$$Y^* = y\cdot\frac{EI}{F_p l^3};\quad T=\sqrt{\frac{EI}{ml^4}}\cdot t$$

$\Omega_i^* = \beta_i l$, and $\beta_i l$, $Y_i(x)$, and $Y_i(c)$ depend on the boundary conditions of the beam , and x is the point at which the response is to be evaluated due to a force at c. $\eta_i(t)$ is the solution of convolution integral, $\left(\sin pt - \left(\frac{T_i}{2\tau}\right)\sin\omega_i(t)\right)$ for a half sine pulse load, where $p=\pi/\tau$.

The response of a simply-supported beam and cantilever beam are studied for the pulse forcing functions shown in Fig. 3.1, and the responses at the center of the beam span with the load acting at the center are plotted as shown in Figs. 3.2–3.7. The expressions for β_i *and* $Y_i(x)$ are available in literature [13], and the response to various pulse loads in case of SDOF system is listed in [1].

It is observed that the convergence of the response for different pulse loads occurs after taking contributions from varying number of modes for a given time step as in Fig. 3.2. In case of step input the response converges to 10^{-5} accuracy after 58 modes when the time step is close to the fundamental period, $T_1 = 0.63$. Likewise there are larger number of modes contributing at time steps close to multiples of fundamental period. The percentage error plotted also shows a peak at these points.

This shows that since a large number of modes contribute to achieve the required accuracy in response, the Rayleigh-Ritz results using only six modes cannot give required accuracy at these points. However, it is observed that at maximum response the number of modes required for the same level of convergence is less. A similar study for the steady state response sinusoidal excitation also shows a similar trend, but at half period $\tau/2$ of force. The convergence of response is much faster after removal of the pulse loads. These comparisons are available in exact solution only and are not available for Rayleigh-Ritz results with beam orthogonal polynomials, as they are obtained upto the sixth frequency only.

It is hard to find reports on response evaluation using the Rayleigh Ritz method in literature . In order to establish this method, the Rayleigh-Ritz results with orthogonal polynomials for the simply-supported beam are used to evaluate the response. It can be seen that the average difference in response without considering sudden peaks at natural periods and its multiples is between 2 5% among exact solution and Rayleigh-Ritz results using orthogonal polynomials. Figs. 3.4 and 3.5 show the comparison between exact solution with convergence upto a relative error of 10^{-5} and those obtained using orthogonal polynomials. Since only six modes can be used for comparison of Rayleigh-Ritz method using orthogonal polynomials, the Figs. 3.4b and 3.5b show the comparison between the response by these and exact solution when only contributions from six modes are considered in the response.

Similar trend in results is found in response at the free end of a cantilever beam with the pulse load acting at the tip. The plots of percentage difference in exact solution and the Rayleigh-Ritz solution using orthogonal polynomials is shown in Fig. 3.7. Here also it can be seen that the error at the natural period of the beam is larger than those at other points as shown in Figs. 3.7a and 3.7c.

The reason for more modes contributing at the minimum response could be attributed to the fact that the response being minimum, even higher modes contribute considerably to the response as compared to the lower modes. But in the case of

maximum response the lower modes contribute a larger share to the total response and the higher modes very little, and hence the faster convergence. At maximum response the accuracy is good with contributions from minimum number of modes. therefore, it is sufficient if only those modes are used for response evaluation since the objective of design is to limit the maximum displacements.

For an undamped system the response does not die out even after long duration of time. However, if some amount of damping is present in the system, the response after large T will be smaller, indicating decay in response. This is due to the fact that the system falls into fundamental mode of vibration after the initial energy provided by the force is lost due to absorbtion of energy by the damping.

3.2 PLATE RESPONSE

In the case of beams, the solutions for the natural frequencies and natural modes are readily available. However, in the case of plates, the Rayleigh-Ritz method is used for obtaining the natural frequency and mode shapes as described in chapter 2. The eigenvalues and eigenvectors obtained by the Rayleigh-Ritz method are used in response calculations by normal mode summation. Since these values are estimated, the comparisons with exact solutions is carried out in the case of simply-supported plates only.

3.2.1 RESPONSE TO PULSE LOADS

The equation of motion of a rectangular plate is given by [29],

$$\rho h \frac{\partial^2 w}{\partial t^2} + D[w'''' + 2\ddot{w}'' + \ddot{w}] = f(x,y,t) \tag{3.8}$$

The solution of this equation can be assumed in separable form as,

$$w(x,y,t) = \sum_m \sum_n q_{mn}(t)\, X_m(x)\, Y_n(y) \tag{3.9}$$

As in case of beams, when the equations are reduced by orthogonal properties

of modes,

$$\ddot{q}_{mn}(t) + \omega_{mn}^2 q_{mn}(t) = \frac{Q_{mn}(t)}{a_{mnj}} \tag{3.10}$$

where

$$Q_{mn}(t) = \int_0^a \int_0^b X_i(x) Y_j(y) f(x,y,t) dx dy$$

The general response is similar to equation (3.4), and is given by,

$$\begin{aligned} q_{mn}(t) &= \frac{1}{a_{mnj}\omega_{mn}} \int_0^t Q_{mn}(\tau) \sin \omega_{mn}(t-\tau) d\tau + (q_{mn0})_0 \cos \omega_{mn} t \\ &\quad + \frac{(\dot{q}_{mn0})_0}{\omega_{mn}} \sin \omega_{mn} t \end{aligned} \tag{3.11}$$

This equation is reduced to a non - dimensional form as,

$$W^* = F \left\{ \sum_{m=0}^{\infty} \sum_{n=0}^{\infty} \frac{1}{(\Omega_{mn})^2} [X_m(c) Y_n(d)] \; [X_m(x) Y_n(y)] \; [\eta_{mn}(T)] \right\} \tag{3.12}$$

where

$$W^* = w \cdot \frac{Db}{F_p a^3}; T = \sqrt{\frac{D}{\rho h a^4}} \cdot t$$

$\Omega_{mn} = \omega_{mn} a^2 \sqrt{\rho h / D}$, and $X_m(c)Y_n(d)$ and $X_m(x)Y_n(y)$ depend on the boundary conditions of the plate, the point of loading, and the point of response evaluation respectively. The factor F is 4 for a simply-supported beam. $\eta_{mn}(T)$ is a function representing response to various pulse loads as given in Shock & Vibration Handbook[1] for a single degree of freedom system , but with the contributions from all modes as a sum.

For a simply-supported plate where there is an exact solution available for Ω_{mn} and mode shapes, the convergence of response is checked for a relative accuracy of 10^{-5}. It is seen that the response converges with varying number of modes contributing to the total response at different steps of time as shown in Fig. 3.8. The fundamental period of a simply-supported plate is 0.318 in non - dimensional unit of time. In the case of a step input the plate responds with this period and it is seen that the contribution of the modes for convergence is varying from 11 to all of 625 (25,25) modes tried. As in the case of beams, at the time steps of fundamental period and its multiples the response takes contributions from larger number of modes to converge.

At the even numbered multiples of fundamental period, the modes summed are even larger than in odd numbered periods.

In the case of pulse loads involving period $\tau = 1$ it is seen that the convergence is much faster in the transient portion of response, but in forced phase it requires maximum number of modes to achieve required convergence at certain points.

The comparisons between exact solution and the results obtained with orthogonal polynomials is compared in case of simply-supported plate. The response by orthogonal polynomials is generally higher than that obtained by exact solution. The response by using the Rayleigh-Ritz results is obtained by summing all 36 modes (6×6). This is compared with exact solution in Figs. 3.9–3.10. Figs. 3.9b and 3.10b show the percentage difference in orthogonal polynomial results and exact solutions.

Results compared between BCF and APF do not show any variations as they are almost the same, only the natural frequencies being little better than the former. This is due to the sine term dominating in the shape function, the hyperbolic sine term being negligible. However, orthogonal polynomial results show larger difference about 15%. Comparisons in other cases are not carried out except in case of CCFF plate, where the results from BCF and APF match closely.

3.2.2 RESPONSE DUE TO A FALLING MASS

In this section, a simply-supported plate is analysed for its response due to a impact force excited by a falling mass.

The potential energy of a vibrating plate due to deformations is given by,

$$U = \int_0^a \int_0^b \int_{-h/2}^{h/2} dU = \frac{D}{2} \int_0^a \int_0^b \left[\left(\frac{\partial^2 w}{\partial x^2} \right)^2 + \left(\frac{\partial^2 w}{\partial y^2} \right)^2 + 2\nu \frac{\partial^2 w}{\partial x^2} \frac{\partial^2 w}{\partial y^2} + 2(1-\nu) \left(\frac{\partial^2 w}{\partial x \partial y} \right)^2 \right] dx\, dy \qquad (3.13)$$

where $D = Eh^3/[12(1-\nu^2)]$ is the flexural rigidity of the plate.

The kinetic energy of a transversely vibrating plate will be

$$T = \rho\frac{h}{2}\iint \dot{w}^2 dxdy \tag{3.14}$$

where ρh is the mass per unit area. From the above energy expressions, it is possible to obtain the partial differential equation for the plate in the form

$$D\left[w'''' + 2\ddot{w}'' + \ddot{w}\right] + \rho h\frac{d^2w}{dt^2} = 0 \tag{3.15}$$

The deflection of a simply-supported plate can be expressed as,

$$w(x,y,t) = \sum_{m=1}^{\infty}\sum_{n=1}^{\infty} sin\frac{m\pi x}{a} sin\frac{n\pi y}{b} q_{mn}(t) \tag{3.16}$$

which satisfies the boundary conditions exactly.

Substituting this solution in the differential equation (3.15) we obtain,

$$\ddot{w} + \frac{D}{\rho h}\left[\left(\frac{m\pi}{a}\right)^2 + \left(\frac{n\pi}{b}\right)^2\right]^2 w = 0 \tag{3.17}$$

The solution of this equation can be written as,

$$q_{mn}(t) = C_{mn}^{(1)}\sin\omega_{mn}t + C_{mn}^{(2)}\cos\omega_{mn}t \tag{3.18}$$

where $\omega_{mn} = \sqrt{\frac{D}{\rho h}}\frac{\pi^2}{a^2}(m^2 + \alpha^2 n^2)$

The deflection of the plate can be written as,

$$w(x,y,t) = \sum_{m=1}^{\infty}\sum_{n=1}^{\infty}\left(C_{mn}^{(1)}\sin\omega_{mn}t + C_{mn}^{(2)}\cos\omega_{mn}t\right)\sin\frac{m\pi x}{a}\sin\frac{n\pi y}{b} \tag{3.19}$$

At $t = 0$,

$$w(x,y,0) = \sum_{m=1}^{\infty}\sum_{n=1}^{\infty} C_{mn}^{(2)}\sin\frac{m\pi x}{a}\sin\frac{n\pi y}{b} \tag{3.20}$$

The response of a plate due to impact of an object of known mass falling from a height is obtained by using the principles of relative velocity and conservation of momentum, before and after impact.

The coefficient $C_{mn}^{(2)}$ is evaluated for a case with initial conditions for the plate at a distance $C = c/a$ and $D = d/b$ using delta function as,

$$C_{mn}^{(2)} = \frac{1}{\omega_{mn}} \left(\frac{2MV}{M + \rho hab} \right) \sin m\pi C \sin n\pi D \tag{3.21}$$

The response equation (3.19) reduces to,

$$w(x, y, t) = \sum_{m=1}^{\infty} \sum_{n=1}^{\infty} \frac{8MV_1}{\omega_{mn}(M + \rho hab)} \sin m\pi C \sin n\pi D \sin \frac{m\pi x}{a} \sin \frac{n\pi y}{b} \tag{3.22}$$

where M = Mass of the falling object, V_1 = velocity of the object (calculated from the known height from which it falls). C and D are the coordinates of location of the fall of a mass on the plate.

In non - dimensional form,

$$\overline{w} = \frac{w\pi^2}{8V_1 a^2} \sqrt{\frac{D}{\rho h}} = \sum_{m=1}^{\infty} \sum_{n=1}^{\infty} \frac{1}{\mu_{mn}(1 + \beta)} \sin m\pi C \sin n\pi D \sin \frac{m\pi x}{a} \sin \frac{n\pi y}{b} \sin \omega_{mn} t \tag{3.23}$$

where $\beta = \rho hab/M$.

$$\mu_{mn} = \omega_{mn} \frac{a^2}{\pi^2} \sqrt{\frac{\rho h}{D}} = \left(m^2 + \alpha^2 n^2 \right)$$

It can be written in the form,

$$w^* = \frac{w}{a} = \sum_{m=1}^{\infty} \sum_{n=1}^{\infty} \frac{8H^*}{\mu_{mn1} \left(1 + \frac{\rho hab}{M} \right)} \sin m\pi C \sin n\pi D \sin \frac{m\pi x}{a} \sin \frac{n\pi y}{b} \sin \omega_{mn} t \tag{3.24}$$

where $\mu_{mn1} = \frac{\mu_{mn}}{\mu_{11}}$ and $H^* = \frac{V_1}{a\omega_{11}}$

This is the non-dimensionalized plate response due to a falling mass which is plotted against C for different values of D and mass ratio as in Fig 3.11. The total response of the plate is calculated upto $m = n = 25$. Fig. 3.12 gives the plot of plate response for different values of location and velocity factors. It can be seen that the response at the center ($C = 0.5, D = 0.5$) is maximum. The response varies

linearly with velocity, V_1 and mass ratio, β. There is sudden increase in response at the vicinity of impact point. The response is also found to be directly proportional to the velocity (height of fall) and mass ratio.

In this chapter, response evaluation of beams and plates is carried out by normal mode analysis using the natural frequencies and modes estimated by Rayleigh-Ritz method. The response of a simply-supported plate due to a mass falling on the plate is also studied. The next chapter deals with rigid plastic analysis of a cantilever beam due to impact load.

Rectangular.

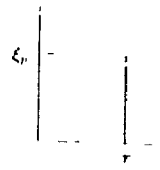

$$\left.\begin{aligned} \xi(t) &= \xi_p \\ \nu &= \xi_p(1 - \cos \omega_n t) \end{aligned}\right\} \quad [0 \le t \le \tau]$$

$$\left.\begin{aligned} \xi(t) &= 0 \\ \nu &= \xi_p \left[2 \sin \frac{\pi\tau}{T}\right] \sin \omega_n \left(t - \frac{\tau}{2}\right) \end{aligned}\right\} \quad [\tau \le t]$$

Half-cycle sine:

$$\left.\begin{aligned} \xi(t) &= \xi_p \sin \frac{\pi t}{\tau} \\ \nu &= \frac{\xi_p}{1 - T^2/4\tau^2} \left(\sin \frac{\pi t}{\tau} - \frac{T}{2\tau} \sin \omega_n t\right) \end{aligned}\right\} \quad [0 \le t \le \tau]$$

$$\left.\begin{aligned} \xi(t) &= 0 \\ \nu &= \xi_p \left[\frac{(T/\tau) \cos (\pi\tau/T)}{(T^2/4\tau^2) - 1}\right] \sin \omega_n \left(t - \frac{\tau}{2}\right) \end{aligned}\right| \quad [\tau \le t]$$

Versed-sine

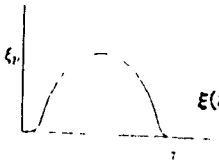

$$\left.\begin{aligned} \xi(t) &= \frac{\xi_p}{2}\left(1 - \cos \frac{2\pi t}{\tau}\right) \\ \nu &= \frac{\xi_p/2}{1 - \tau^2/T^2} \left(1 - \frac{\tau^2}{T^2} - \frac{\tau^2}{T^2} \cos \frac{2\pi t}{\tau} - \cos \omega_n t\right) \end{aligned}\right\} \quad [0 \le t \le \tau]$$

$$\left.\begin{aligned} \xi(t) &= 0 \\ \nu &= \xi_p \left[\frac{\sin \pi\tau/T}{1 - \tau^2/T^2}\right] \sin \omega_n \left(t - \frac{\tau}{2}\right) \end{aligned}\right| \quad [\tau \le t]$$

Triangular:

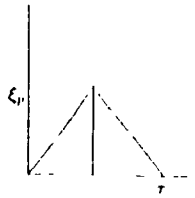

$$\left.\begin{aligned} \xi(t) &= 2\xi_p \frac{t}{\tau} \\ \nu &= 2\xi_p \left(\frac{t}{\tau} - \frac{T}{\tau} \frac{\sin \omega_n t}{2\pi}\right) \end{aligned}\right| \quad \left[0 \le t \le \frac{\tau}{2}\right]$$

$$\left.\begin{aligned} \xi(t) &= 2\xi_p \left(1 - \frac{t}{\tau}\right) \\ \nu &= 2\xi_p \left(1 - \frac{t}{\tau} - \frac{T}{\tau} \frac{\sin \omega_n t}{2\pi} - \frac{T}{\tau} \frac{\sin \omega_n (t - \tau/2}{\pi}\right) \end{aligned}\right\} \quad \left[\frac{\tau}{2} \le t \le \tau\right]$$

$$\left.\begin{aligned} \xi(t) &= 0 \\ \nu &= \xi_p \left[2 \frac{\sin^2 (\pi\tau/2T}{\pi\tau/2T}\right] \sin \omega_n (t - \tau/2 \end{aligned}\right| \quad [\tau \le t]$$

Fig. 3.1 Pulse Load Shapes and their Response expressions for SDOF systems [1]
(ξ = Force, ξ_p = Magnitude of force , ν = response, T = period)

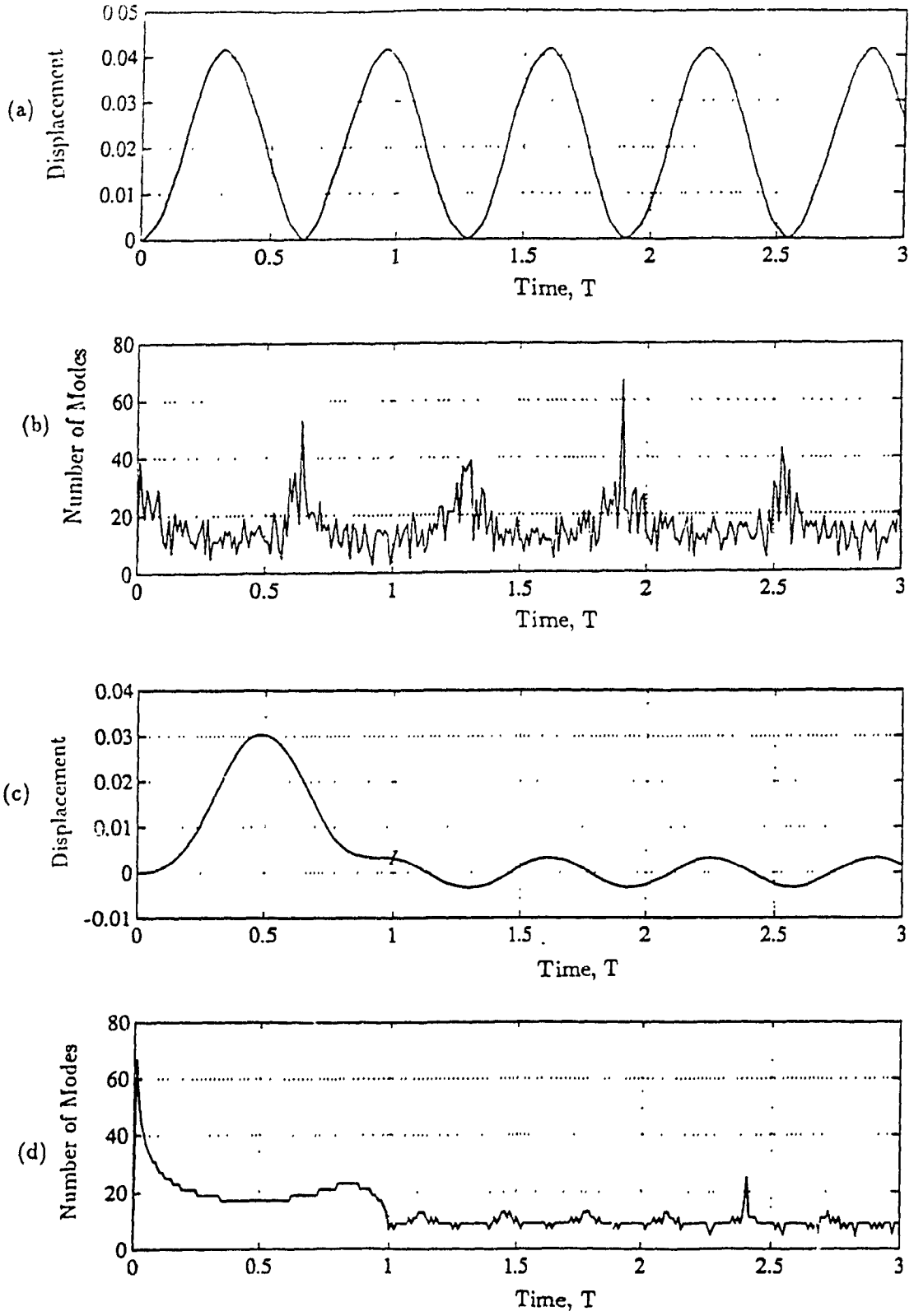

Fig. 3.2 Simply-supported beam response to (a) step input, (b) mode contributions for convergence, (c) half sine pulse, and (d) mode contributions for its convergence

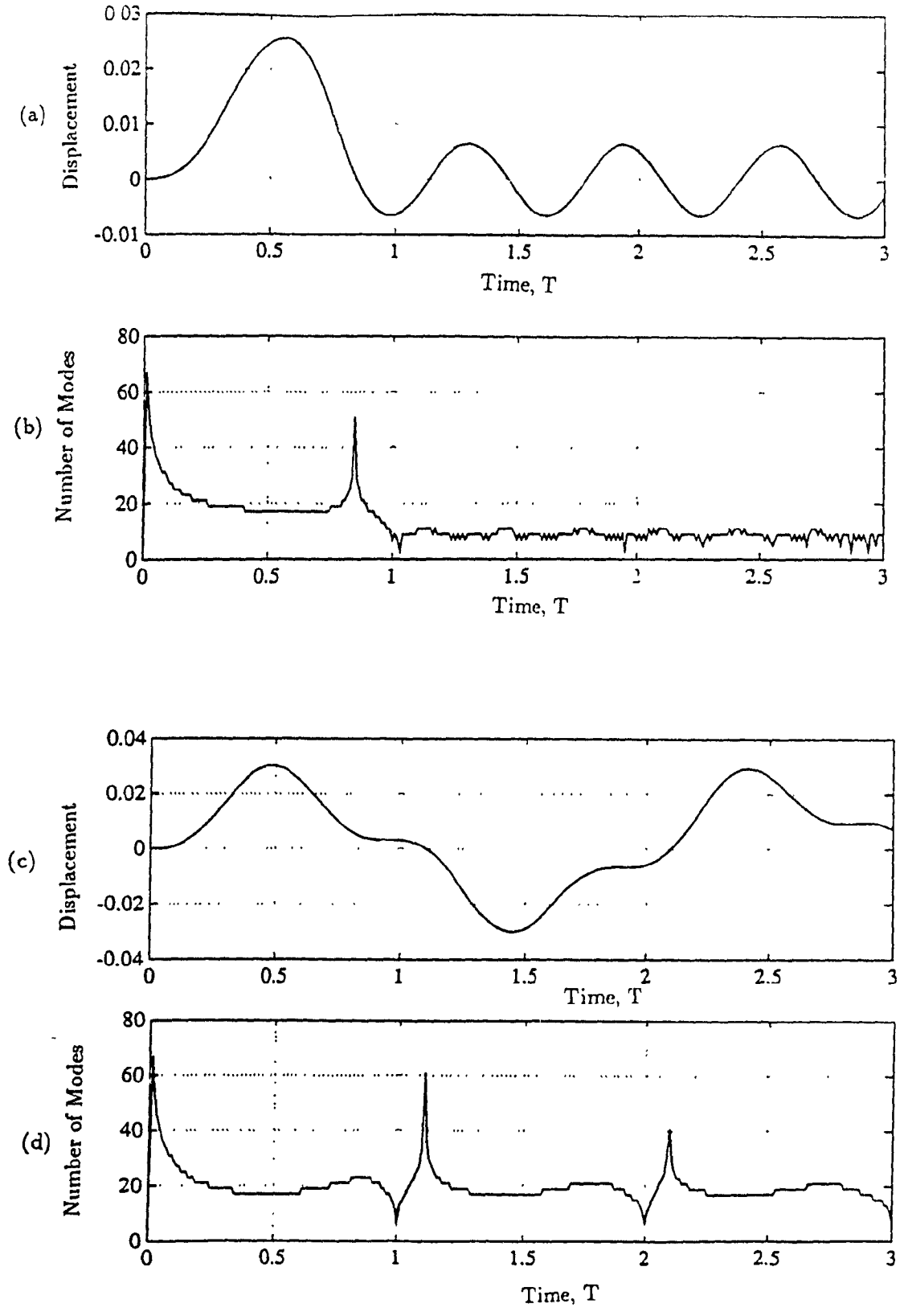

Fig. 3.3 Simply-supported beam response to (a) triangular pulse, (b) mode contributions for convergence, (c) steady state sine loading, and (d) mode contributions for its convergence

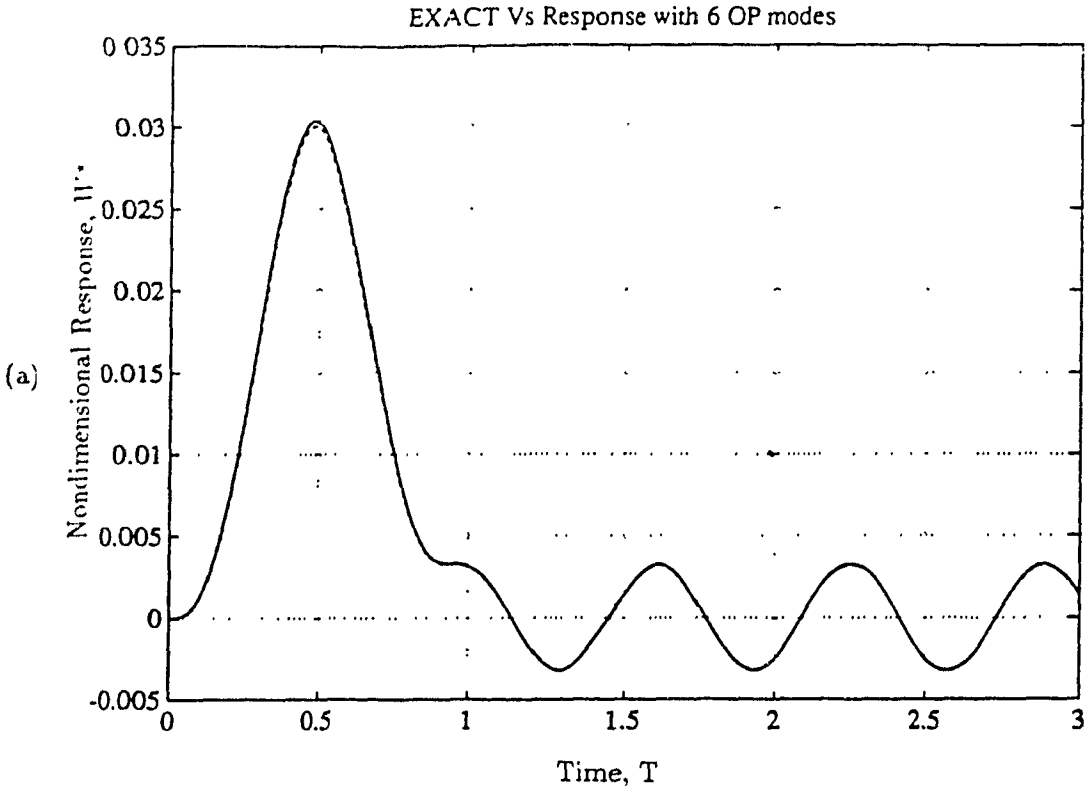

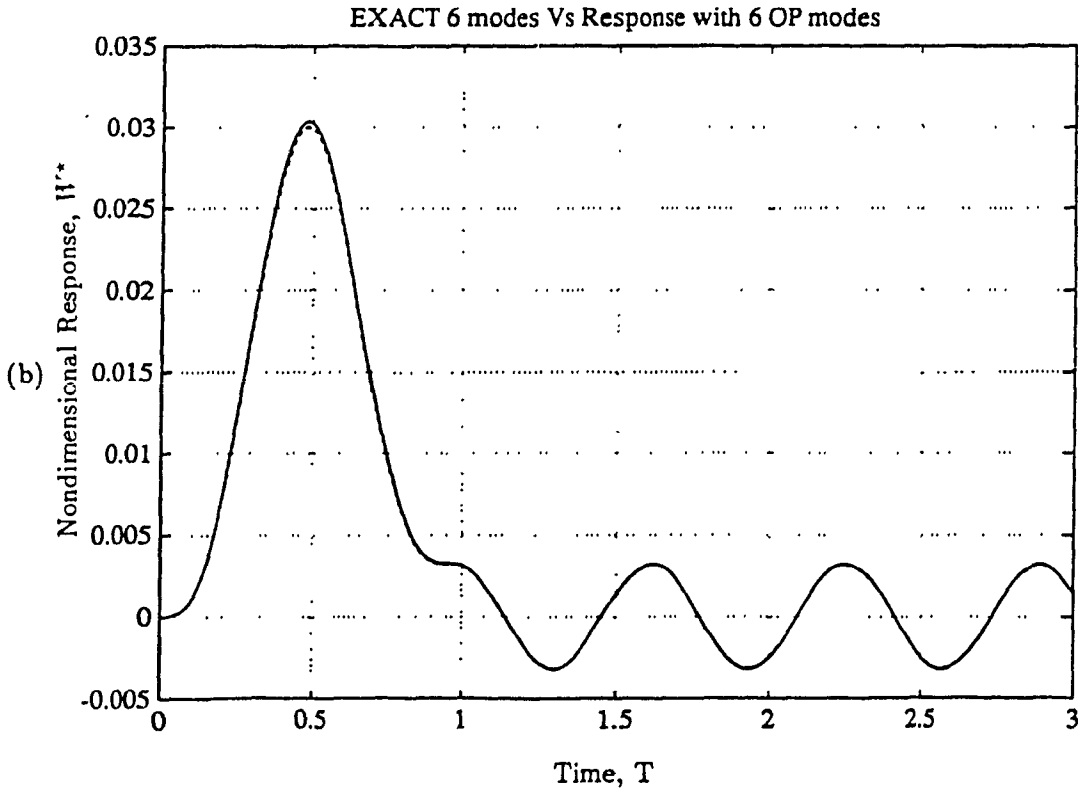

Fig. 3.4 Simply-supported beam response to half sine pulse, (a) Comparison between Exact solution (—) and orthogonal polynomial results (- - -), (b) Six modes of exact solution and six orthogonal polynomial modes

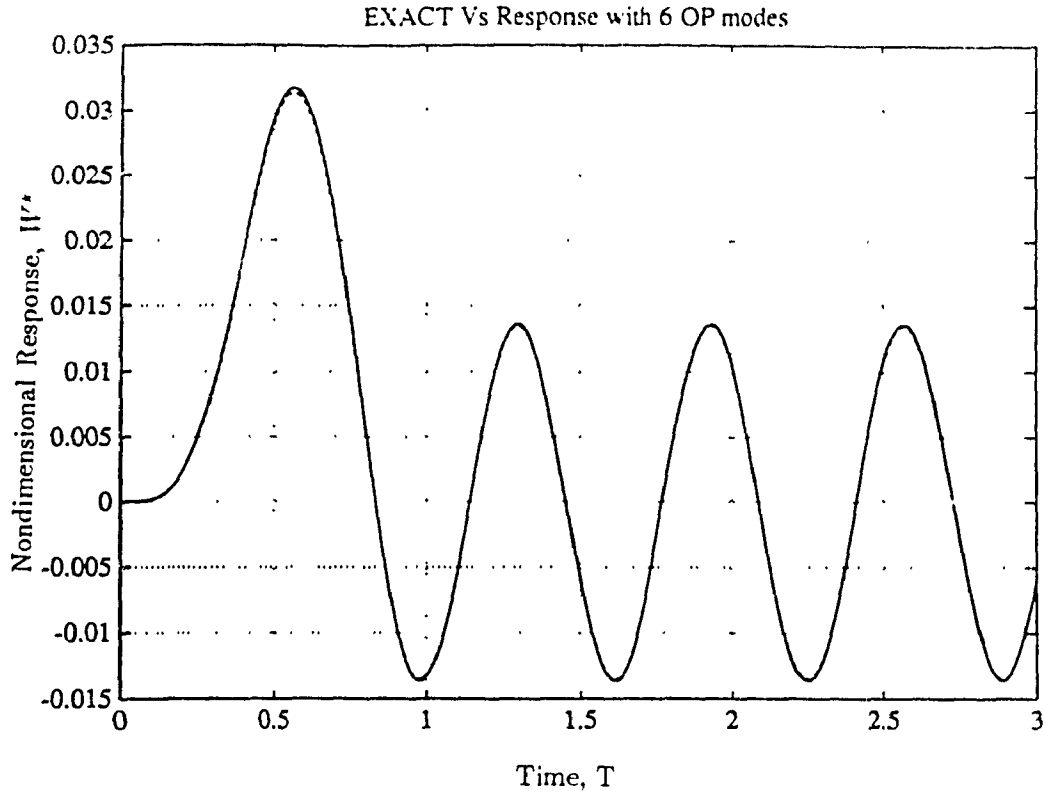

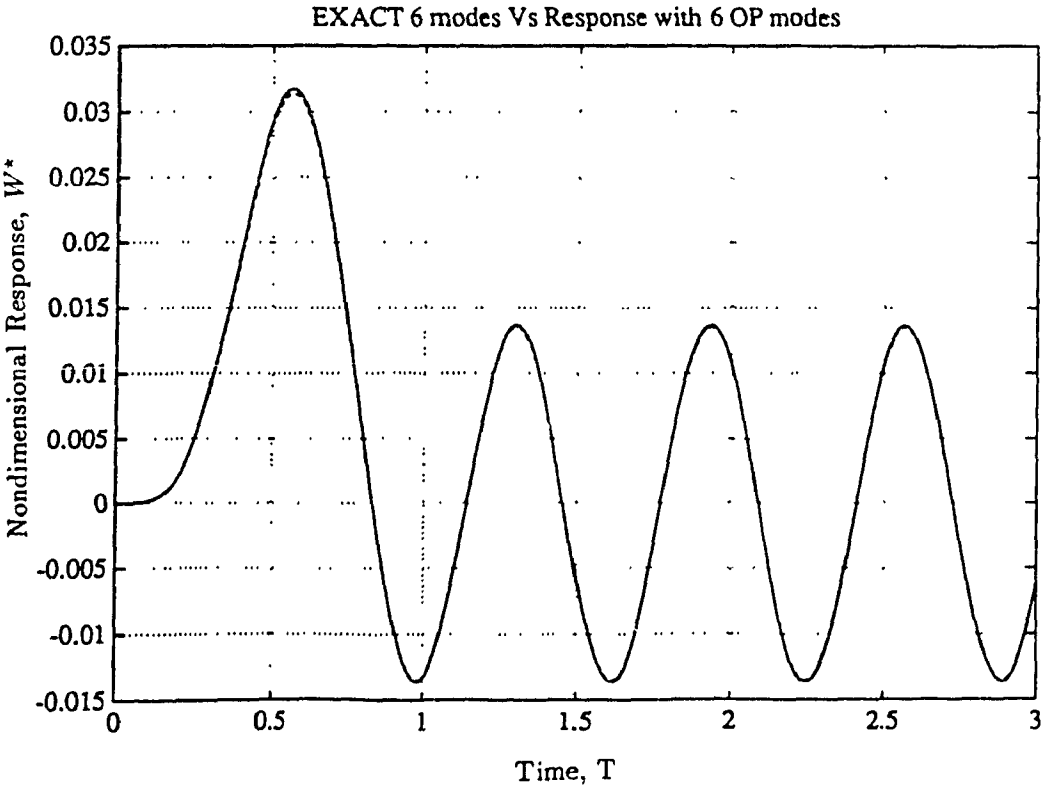

Fig. 3.5 Simply-supported beam response to triangular pulse, (a) Comparison between Exact solution (—) and orthogonal polynomial results (- - -), (b) Six modes of exact solution and six orthogonal polynomials modes

(a)

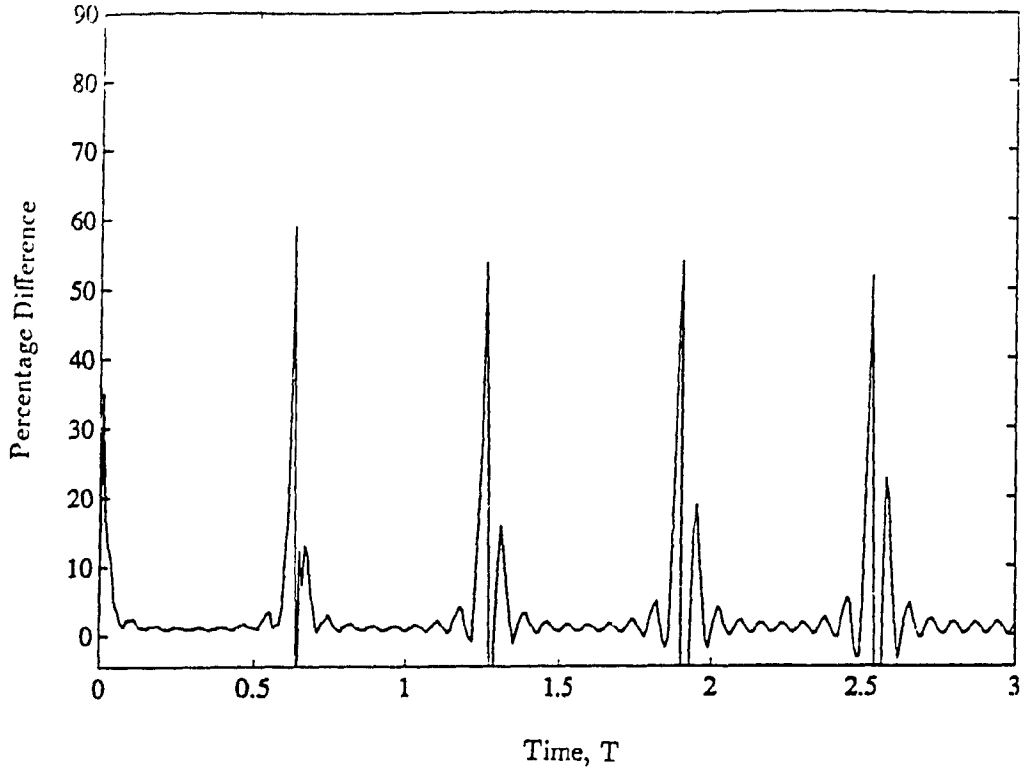

(b)

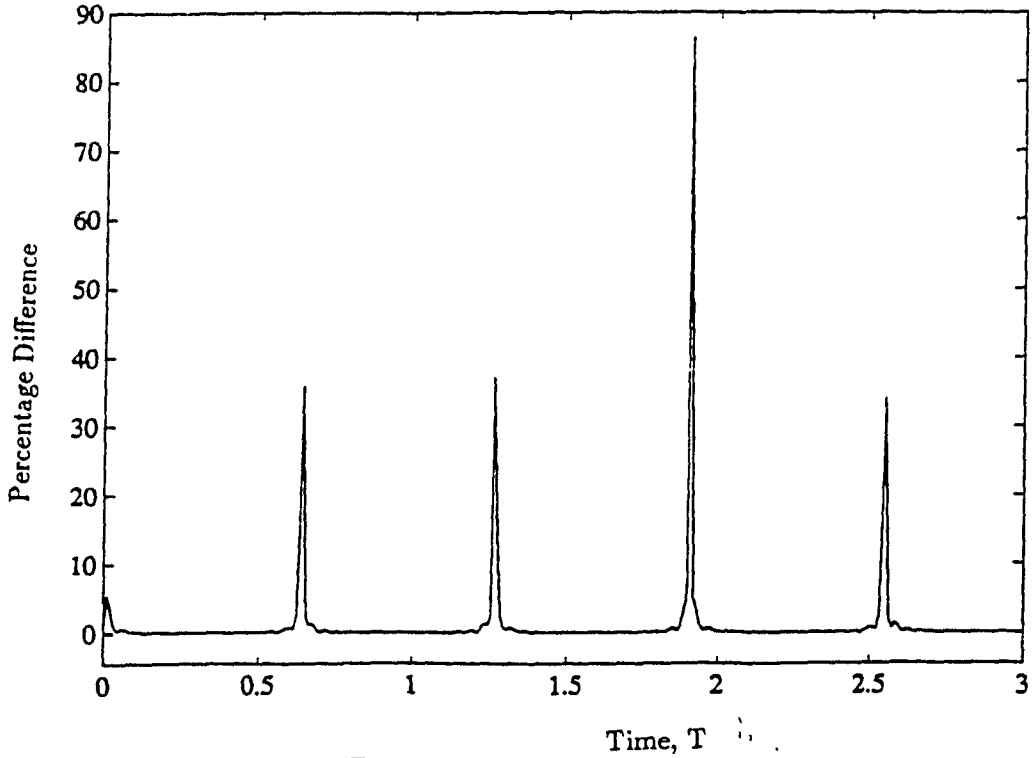

Fig. 3.6 Relative Difference (%) between (a) exact solution (1.E-5 rel. error) response and by use of six modes of orthogonal polynomial results, and (b) exact solution and six exact modes in case of Simply-supported beam

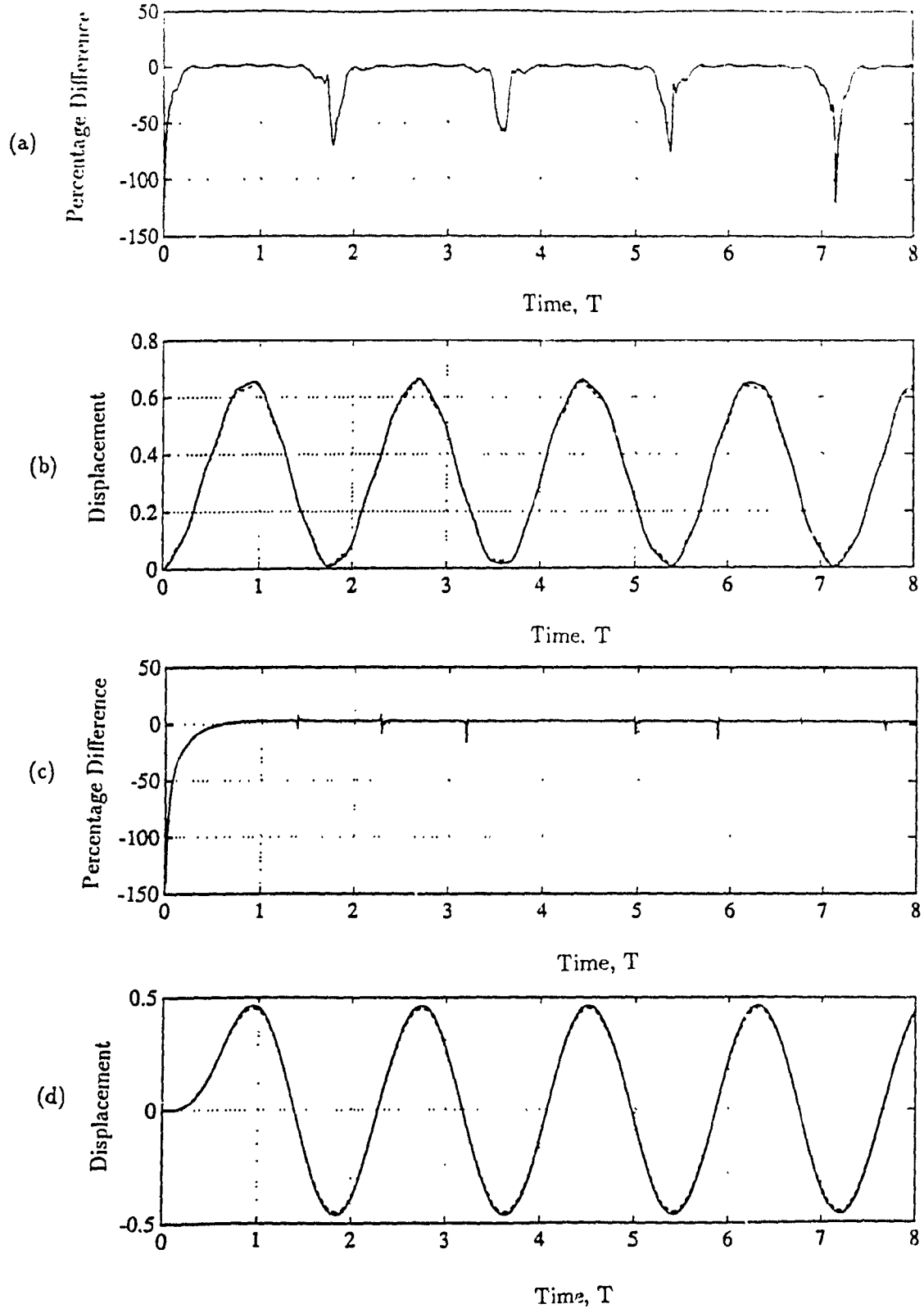

Fig. 3.7 Cantilever beam response to step input, (a) Difference between Exact solution and orthogonal polynomials result, (b) response , and (c & d) Difference and response in versed sine pulse

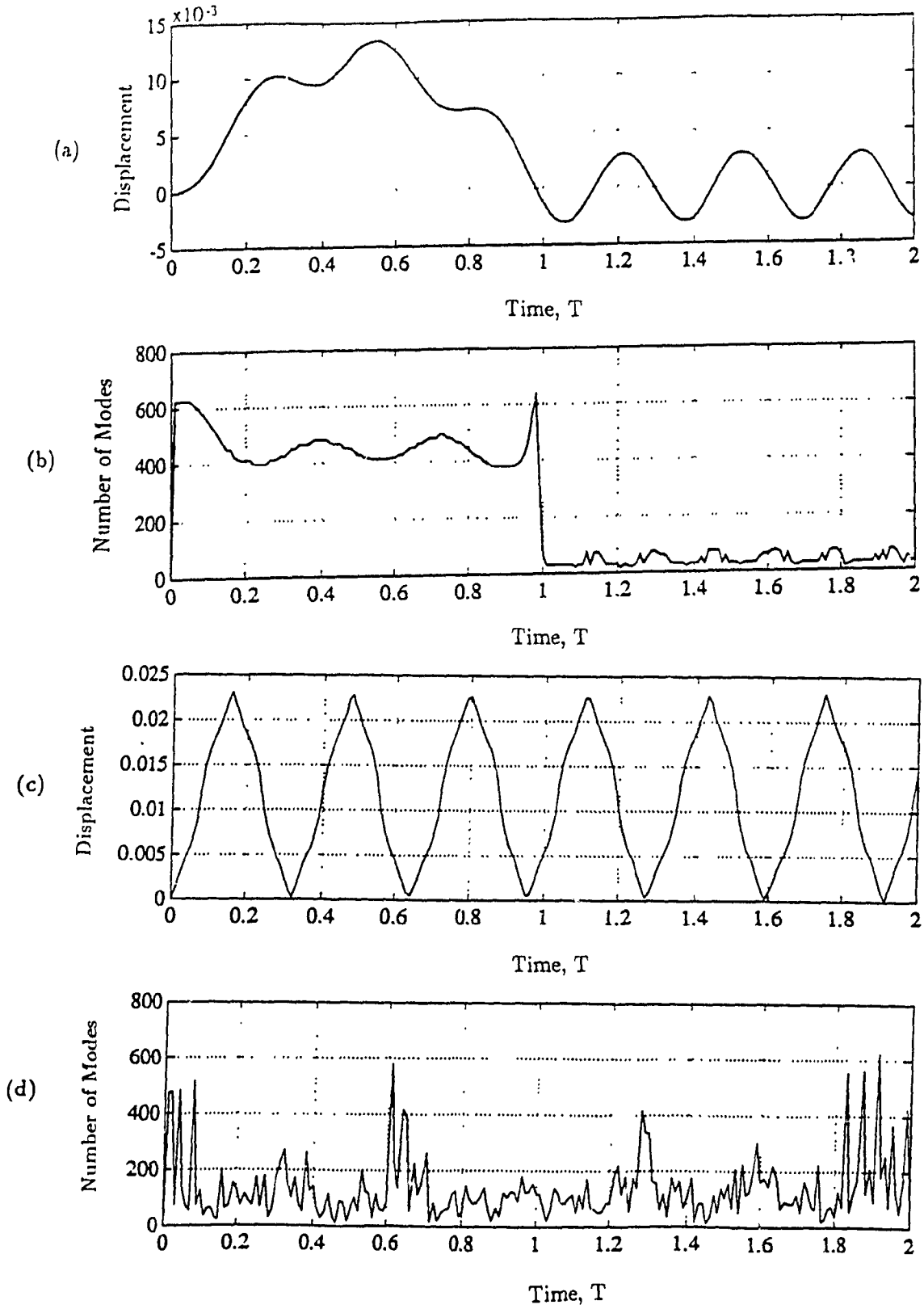

Fig. 3.8 Simply-supported plate (a) response to triangular pulse, and (b) number of modes contributing (c) response due to step input, and (d) number of modes.

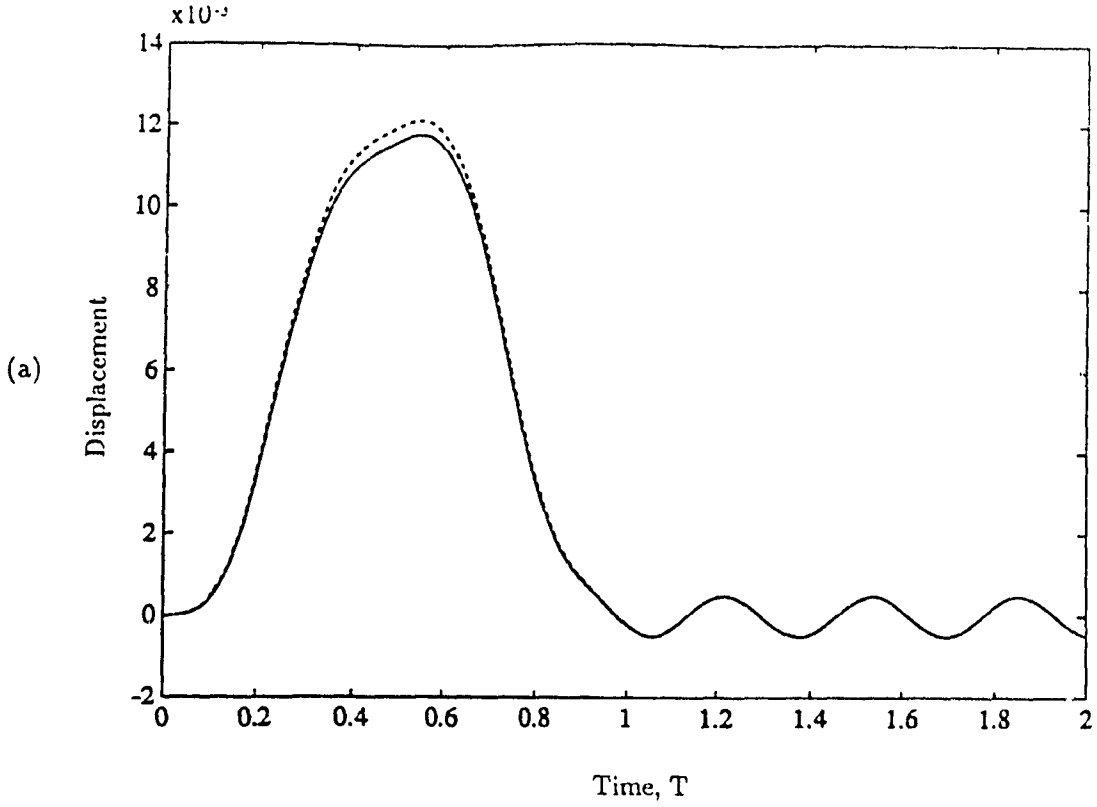

(a)

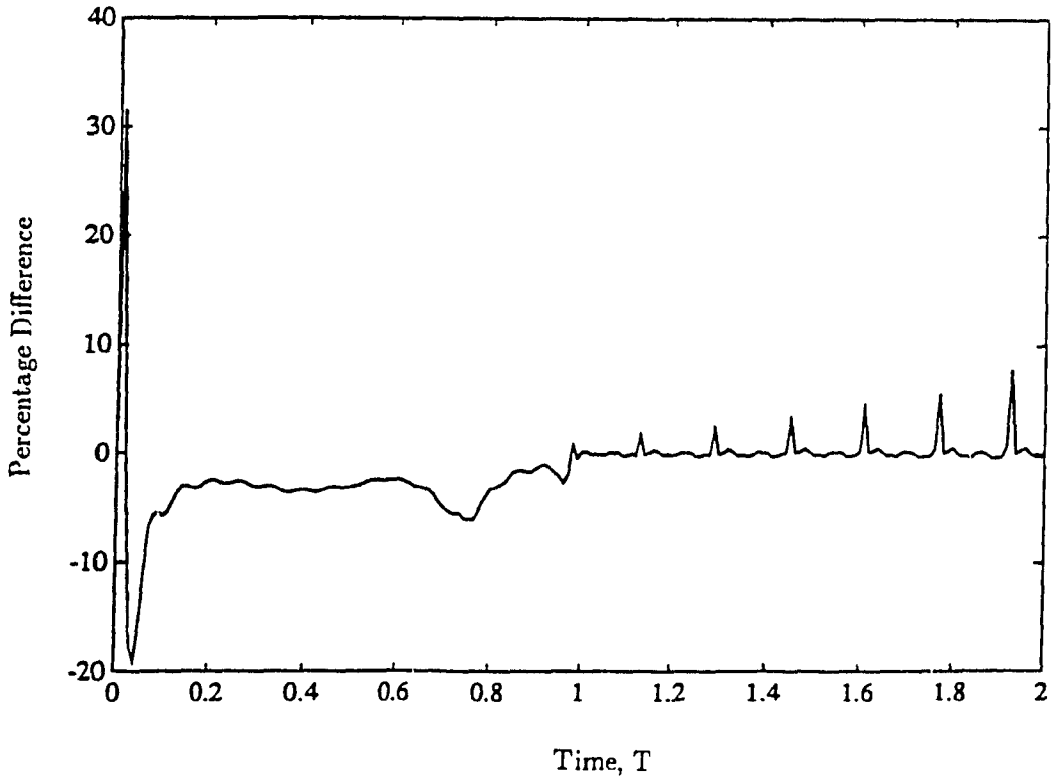

(b)

Fig. 3.9 Simply-supported plate response to versed sine pulse, (a) Comparison of response between orthogonal polynomials (- - -) and exact solution (—), (b) Relative difference in percent

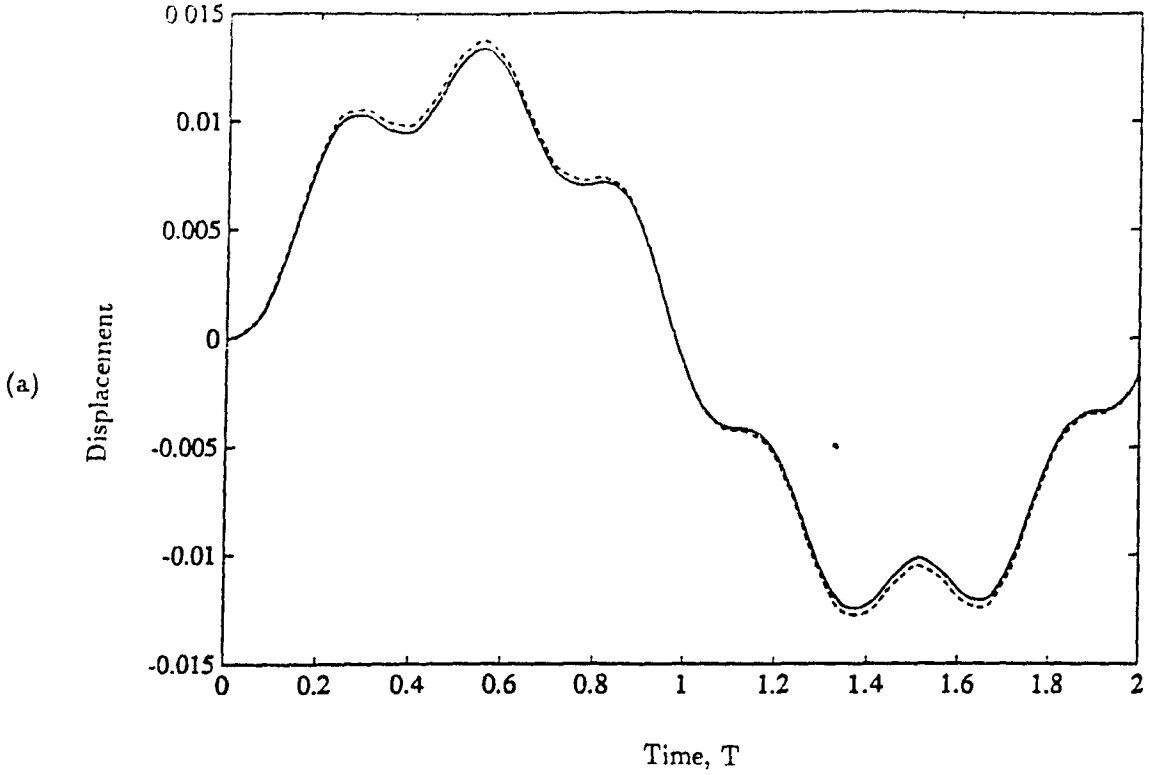

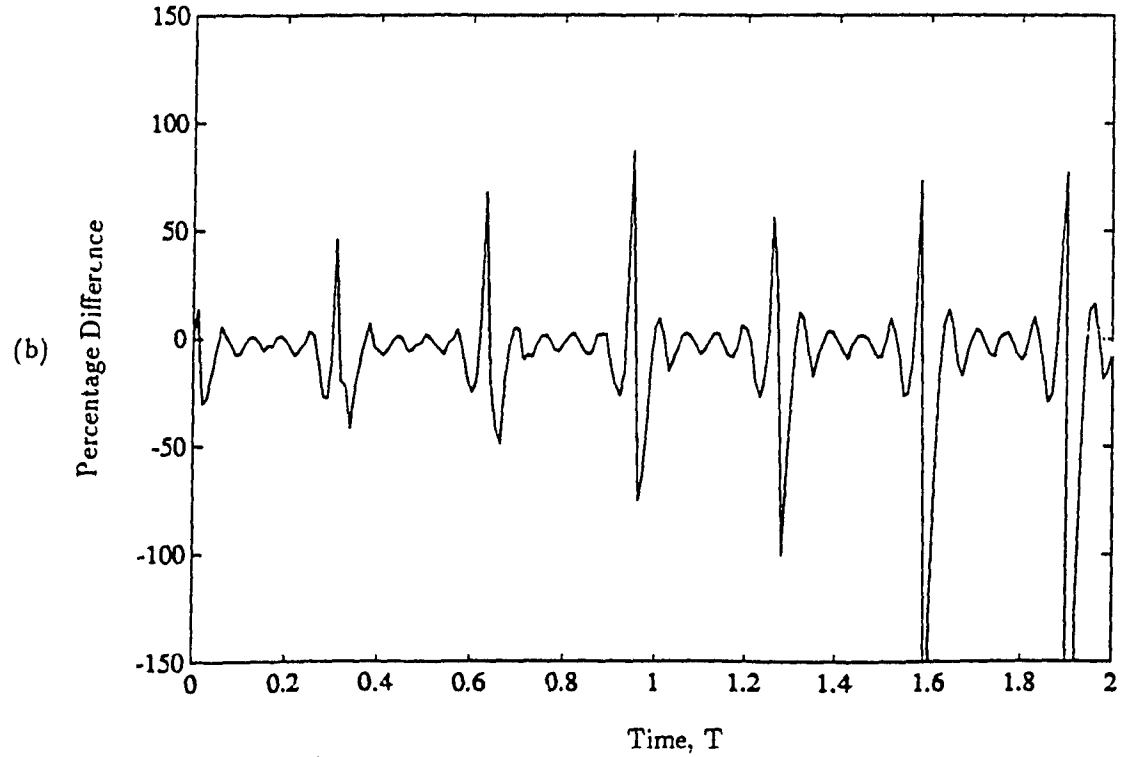

Fig. 3.10 Simply-supported plate response to steady state sine loading, (a) Comparison of response between orthogonal polynomials (- - -) and exact solution (—) (b) Relative difference in percent

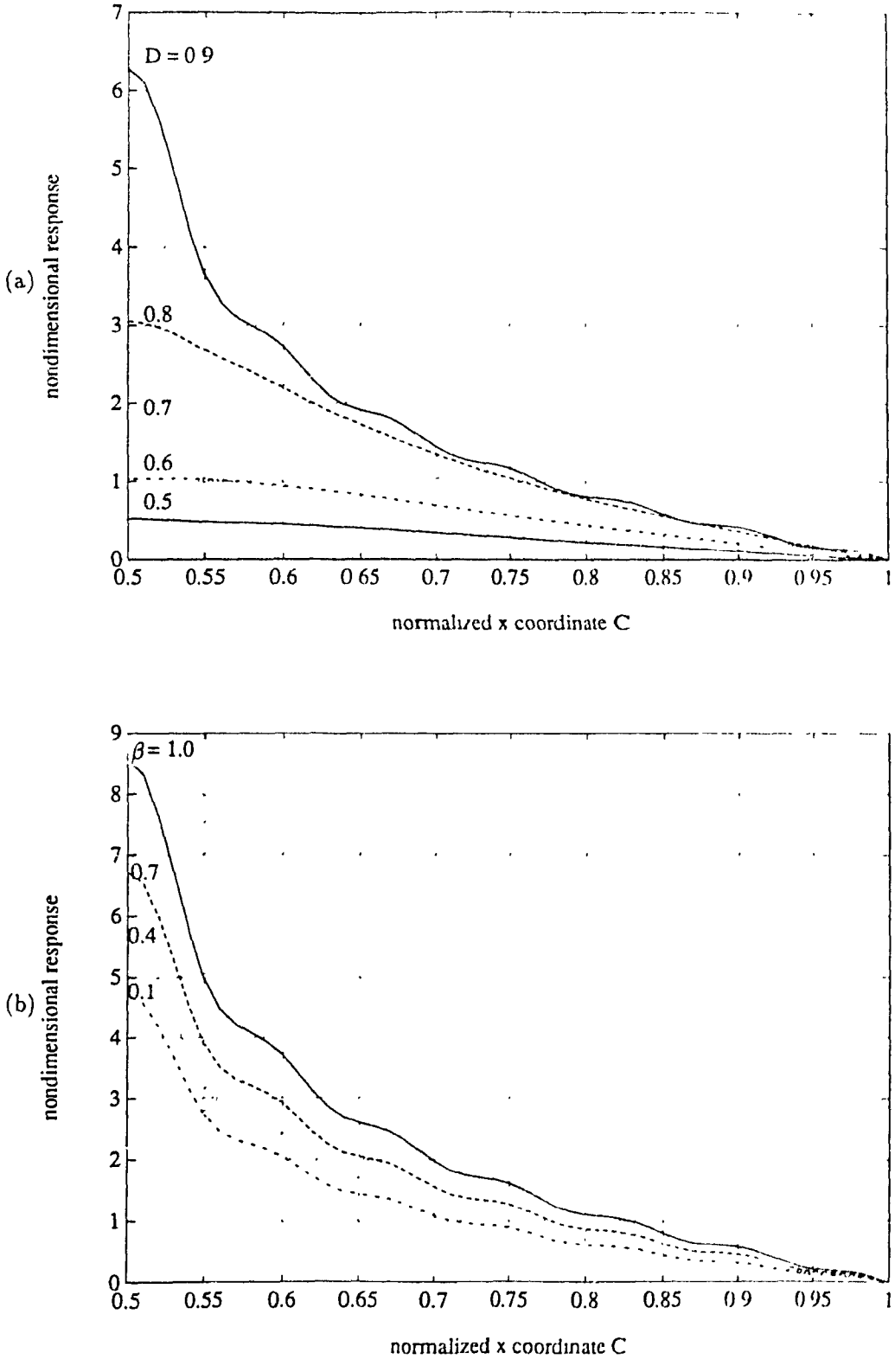

Fig. 3.11 Displacement response of a Simply-supported plate to a falling mass: (a) $\beta = 0.5$, $H^* = 0.5$; (b) $H^* = 0.5$, $D = 0.5$

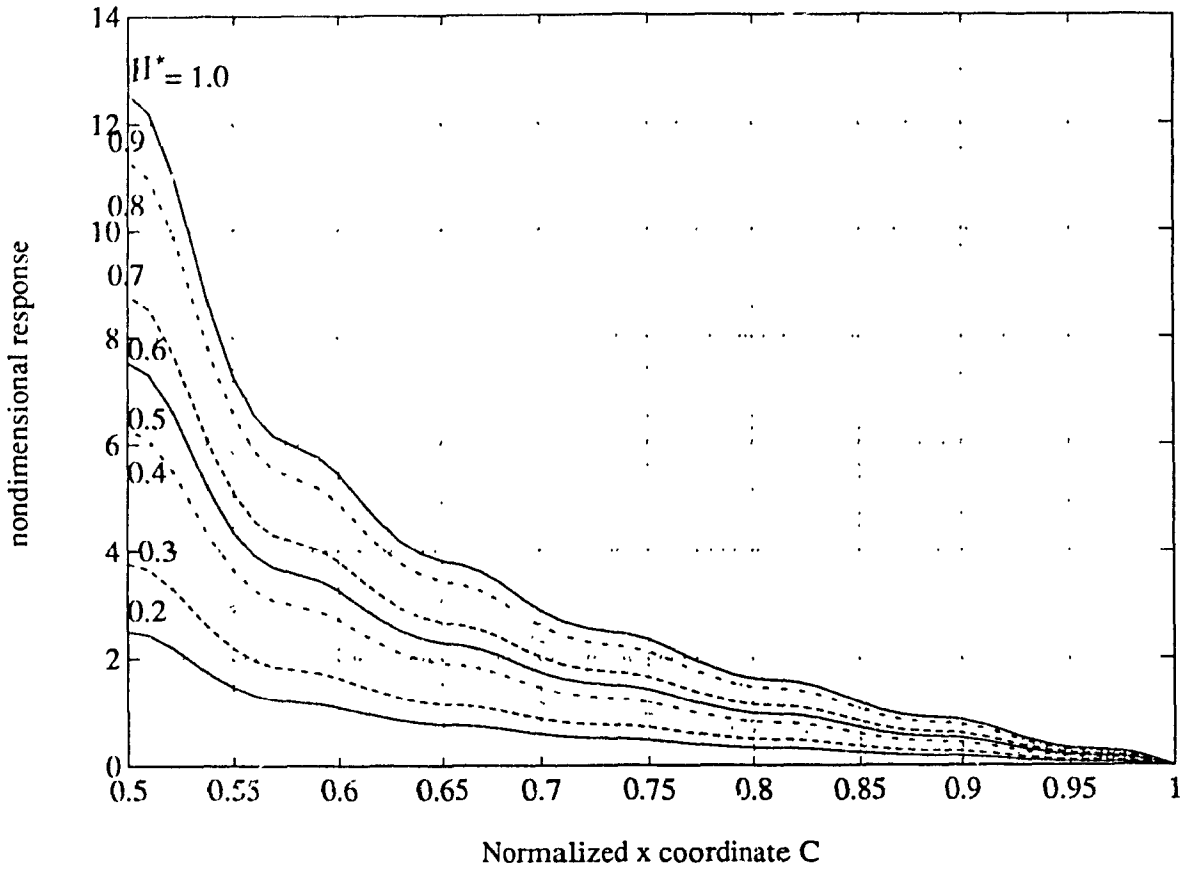

Fig. 3.12 Displacement response of a Simply-supported plate to a falling mass; $\beta = 0.5$, $D = 0.5$

Chapter 4

PLASTIC ANALYSIS OF STRUCTURES TO IMPACT LOADING

In the previous chapter the elastic response of beams and plates using normal mode analysis was presented. When the impact is of a larger magnitude the response of these structures will exceed the elastic limit. Plastic analysis is needed to analyse structures due to high velocity impacts, and for steel on steel this limit is 0.3 meters per second. Under impact loads plastic deformations within certain limits is allowed to dissipate the energy imparted. In this chapter a rigid plastic analysis of a beam is carried out to find the response due to a rectangular pulse forcing function. Design of structures for impact loads generally involve allowance for plastic deformations within certain limits. The total impulse response involves three stages, first the early time response by theory of wave propagation, secondly the long term response causing the permanent deformations, and third, the failure of the structure.

Theory of plasticity has to be applied to study the behavior of any structure subjected to impact loads when the stresses and strains generated by such loads cause deformations which either partly or fully yield the structure. This is done by establishing equations of equilibrium and upper and lower bound theorems. The idealized stress strain diagram shown in Fig. 4.1 gives different cases of material behavior.

a) Perfectly Elastic.

b) Rigid, perfectly plastic.

c) Rigid, linear work-hardening.

d) Elastic, perfectly plastic.

e) Elastic, linear work-hardening.

The analysis of a rigid-plastic fan blade modeled as a cantilever shown in Fig. 4.2 subjected to transverse force at the tip along with centrifugal forces due to rotation is carried out. When a transverse impact acts at the tip of the cantilever, a rigid plastic cantilever will bend at a discrete plastic hinge once the energy imparted by the force is dissipated by the work done at the plastic hinge , that moves towards the root. The permanent deformation of the beam develops at the plastic hinge. Due to rotation of the cantilever it is subjected to continuous acceleration in the radial direction.

Small and Large deformation formulations are outlined in this chapter, and the results for tip deflection against time are plotted for various parameters.

4.1 LARGE DEFLECTION FORMULATION

The uniform beam of mass per unit length m is subjected to a transverse force $f(t)$ at the tip. The body force due to rotation of the blade is gm per unit length that acts in the initial axial direction, being positive toward the tip. Rigid-plastic beam deforms due to the bending moment exceeding the yield moment M_0 at the hinge where the deformation is concentrated.

Coordinate s is intrinsic and measured along the neutral axis from the tip. As shown in Fig. 4.2, due to impact at the tip the hinge is formed at a distance λ from the tip. The deflection is made of two coordinates $w(s,t)$ and $u(s,t)$ measured from the hinge in x and z directions respectively. $\theta(s,t)$ is the angle of inclination of the beam at s when the hinge is at λ.

The kinematics of the beam are:

$$\frac{du}{ds} = -\cos\theta(s,t)$$

$$u = u_0 - \int_0^s \cos\theta(\xi,t)d\xi; \quad u_0 \text{ is } u \text{ at the tip.}$$

When $s = \lambda$, u = 0. therefore

$$\begin{aligned} u_0 &= \int_0^{\lambda} \cos\theta(\xi,t)d\xi \\ u &= \int_s^{\lambda} \cos\theta(\xi,t)d\xi \end{aligned} \tag{4.1}$$

Similarly.

$$w = \int_s^{\lambda} \sin\theta(\xi,t)d\xi \tag{4.2}$$

$$\theta = \int_s^{\lambda} \kappa(\xi)d\xi \tag{4.3}$$

where κ is the curvature of the neutral axis.

The velocity of any point on the neutral axis in terms of the coordinates is,

$$\dot{\theta} = \kappa(\lambda)\cdot\dot{\lambda}$$

where θ is small and independent of s; defining $\dot{\psi} \equiv \dot{\theta}$

$$\dot{\psi} = \kappa(\lambda)\cdot\dot{\lambda} \tag{4.4}$$

$$\begin{aligned} \dot{u} &= \cos\theta(\lambda,t)\dot{\lambda} - \int_s^{\lambda} \sin\theta(\xi,t)\,\dot{\theta}\,d\xi \\ &= \dot{\lambda} - \dot{\psi}w \\ \dot{w} &= \sin\theta(\lambda,t)\dot{\lambda} + \int_s^{\lambda} \cos\theta(\xi,t)\,\dot{\theta}\,d\xi \\ &= \dot{\psi}u \end{aligned} \tag{4.5}$$

The acceleration of the point on the neutral axis is,

$$\begin{aligned} \ddot{u} &= \ddot{\lambda} - \ddot{\psi}w - \dot{w}\dot{\psi} \\ &= \ddot{\lambda} - \ddot{\psi}w - \dot{\psi}^2 u \\ \ddot{w} &= \dot{\psi}\dot{u} + u\ddot{\psi} \\ &= -\dot{\psi}^2 w + \dot{\psi}\dot{\lambda} + u\ddot{\psi} \end{aligned} \tag{4.6}$$

Initially when u = 0 and w = 0, $\ddot{w} = \dot{\psi}\dot{\lambda}$, which indicates an initial jump in acceleration and the velocity, $\dot{w} = 0$.

The equations of motion are written by equating impulse due to force *f(t)* and the momentum at any time, and the change of Kinetic Energy to the work done by the impact force - energy dissipated by the hinge. The following notations are defined for use in further analysis.

The second moment of the deformed part of the beam about the plastic hinge is,

$$i_0 = \int_0^\lambda \left[u^2(s,t) + w^2(s,t)\right] ds \tag{4.7}$$

The first moment of the deformed part of the beam about the z axis is,

$$i_1 = \int_0^\lambda u(s,t) ds \tag{4.8}$$

The first moment of the deformed part of the beam about the x axis is,

$$i_2 = \int_0^\lambda w(s,t) ds \tag{4.9}$$

and subsequently after simplification.

$$\begin{aligned} \frac{di_0}{d\lambda} &= 2i_1(\lambda) \\ \frac{di_1}{d\lambda} &= \lambda - i_2(\lambda)\kappa(\lambda) \end{aligned} \tag{4.10}$$

$$\begin{aligned} \int_0^t f(t)dt &= m\int_0^\lambda \dot{w}(s,t)ds \\ f(t)u(0,t) - mgi_2(\lambda) - M_0 &= m\left[i_0\ddot{\psi} + i_1\dot{\lambda}\dot{\psi}\right] \end{aligned} \tag{4.11}$$

Assuming the impact force to be constant F during duration τ and zero thereafter, the non-dimensionalized parameters are,

$$S = \frac{sF}{M_0};\quad \Lambda = \frac{\lambda F}{M_0};\quad K = \frac{\kappa M_0}{F};\quad T = \frac{tF^{3/2}}{M_0 m^{1/2}};\quad \dot{\Psi} = \frac{\dot{\psi} M_0 m^{1/2}}{F^{3/2}};\quad G = \frac{gmM_0}{F^2}$$

the equations of motion can be reduced to

$$\begin{aligned} 1 &= \ddot{\Psi} I_1 + \dot{\Psi}\dot{\Lambda}\left[\Lambda - I_2 K\right] \\ U(0,T) - GI_2 - 1 &= \ddot{\Psi} I_0 + \dot{\Psi}\dot{\Lambda} I_1 \qquad T < \tau \end{aligned} \tag{4.12}$$

After removal of the impact force,

$$\begin{aligned} 0 &= \ddot{\Psi} I_1 + \dot{\Psi}\dot{\Lambda}\left[\Lambda - I_2 K\right] \\ -GI_2 - 1 &= \ddot{\Psi} I_0 + \dot{\Psi}\dot{\Lambda} I_1 \qquad\qquad T > \tau \end{aligned} \tag{4.13}$$

4.2 SMALL DEFLECTION APPROXIMATION:

When θ is assumed to be small, and by defining the tip deflection W_0 = $W(0,T)$, from equations (4.5) and (4.6) the tip velocity and acceleration is given by substituting $U = \Lambda$,

$$\begin{aligned} \dot{W}_0 &= \dot{\Psi}\Lambda \\ \ddot{W}_0 &= \dot{\Lambda}\dot{\Psi} + \ddot{\Psi}\Lambda \end{aligned}$$

Initially the beam being at rest $W_0 = 0$ and therefore,

$$I_0 = U^3/3 = \Lambda^3/3; \qquad I_1 = U^2/2 = \Lambda^2/2$$

and since $U(S,\Lambda) = (\Lambda - S)$ for small θ, $\dot{W}(S,T) = \dot{W}_0(1 - S/\Lambda)$

Therefore by integrating,

$$W(S,\Lambda) = \int_0^T \dot{W}_0(1 - S/\Lambda)dT$$

Using this in (4.9) we get,

$$I_2 = \frac{W_0\Lambda}{2}$$

The equations of motion for small deflection is obtained by substituting I_0, I_1, I_2 in (4.12) and (4.13) as,

$$\begin{aligned} \dot{\Lambda}\dot{W}_0 &= (6 + 6GI_2 - 2\Lambda,)/\Lambda \\ \ddot{W}_0 &= (4\Lambda - 6GI_2 - 6)/\Lambda^2 \qquad\qquad T < \tau \end{aligned} \tag{4.14}$$

$$\begin{aligned} \dot{\Lambda}\dot{W}_0 &= (6+6GI_2)/\Lambda \\ \ddot{W}_0 &= -(6+6GI_2)/\Lambda^2 \qquad T>\tau \end{aligned} \tag{4.15}$$

If $\dot{W}_0 = V$, from (4.14) and (4.15),

$$\begin{aligned} \dot{\Lambda}V &= (6+6GI_2-2\Lambda)/\Lambda \\ \dot{V} &= (4\Lambda-6GI_2-6)/\Lambda^2 \qquad T<\tau \end{aligned} \tag{4.16}$$

$$\begin{aligned} \dot{\Lambda}V &= (6+6GI_2)/\Lambda \\ \dot{V} &= -(6+6GI_2)/\Lambda^2 \qquad T>\tau \end{aligned} \tag{4.17}$$

Since $\frac{d}{dt}(\Lambda V) = \Lambda\dot{V} + \dot{\Lambda}V$, substituting from (4.16) and (4.17),

$$\begin{aligned} \frac{d}{dt}(\Lambda V) &= 2 \qquad T<\tau \\ &= 0 \qquad T>\tau \end{aligned}$$

Integrating,

$$\begin{aligned} \Lambda V &= 2T \qquad T<\tau \\ &= 2\tau \qquad T>\tau \end{aligned} \tag{4.18}$$

Therefore,

$$\begin{aligned} \dot{I}_2 &= \Lambda V/2 \\ &= T \qquad T<\tau \\ &= \tau \qquad T>\tau \end{aligned}$$

$$\begin{aligned} I_2 &= T^2/2 \qquad T<\tau \\ &= \tau T - \tau^2/2 \qquad T>\tau \end{aligned} \tag{4.19}$$

Substituting (4.18) and (4.19) in equations (4.16) and (4.17) and simplifying, the hinge position in terms of time is,

$$\dot{\Lambda} = (6+6GI_2-2\Lambda)/\Lambda V$$

$$
\begin{aligned}
&= \left(6 + 6GT^2/2 - 2\Lambda\right)/\Lambda V \\
&= \left(3 + 3GT^2/2 - \Lambda\right)/T \\
i.e.\ T\dot{\Lambda} + \Lambda &= 3 + 3GT^2/2 \\
\frac{d}{dt}(T\Lambda) &= 3 + 3GT^2/2 \\
T\Lambda &= 3T + GT^3/2 \\
\Lambda &= 3 + GT^2/2 \qquad T < \tau \qquad (4.20)
\end{aligned}
$$

$$
\begin{aligned}
\dot{\Lambda} &= (6 + 6GI_2)/\Lambda V \\
&= (6 + 6GI_2)/2\tau \\
&= \frac{[3 + 3G(\tau T - \tau^2/2)]}{\tau} \\
i.e.\ \Lambda &= 3T/\tau + 3GT/2(T - \tau) + G\tau^2/2 \\
&= G\tau^2/2 + 3T/\tau(1 - G\tau^2/2) + 3GT^2/2 \qquad T > \tau \qquad (4.21)
\end{aligned}
$$

Substituting for Λ in equation (4.18),

$$
\begin{aligned}
V &= \frac{2T}{3 + GT^2/2} \qquad T < \tau \\
&= \frac{2\tau}{G\tau^2/2 + 3T/\tau(1 - G\tau^2/2) + 3GT^2/2} \qquad T > \tau
\end{aligned}
$$

The tip deflection,

$$
\begin{aligned}
W_0 &= \int V \\
&= \int_0^T \frac{2T}{3 + GT^2/2} dT \\
&= \frac{2}{G}\left[\ln\left(3 + GT^2/2\right) - \ln(3)\right]_0^T \\
&= \frac{2}{G}\left[\ln\left(\frac{3 + GT^2/2}{3}\right)\right] \qquad T < \tau \qquad (4.22)
\end{aligned}
$$

For $T > \tau$ the tip deflection is,

$$
W = W_\tau + \int_\tau^T \frac{2\tau}{G\tau^2/2 + 3T/\tau(1 - G\tau^2/2) + 3GT^2/2}\, dT
$$

Dividing both the numerator and denominator by $G\tau^2/2$,

$$
W = W_\tau + \int_\tau^T \frac{4/G}{1 + 3T/\tau\left(\frac{2 - G\tau^2}{G\tau^2}\right) + 3\left(\frac{T}{\tau}\right)^2}\, dT
$$

By defining $Z = \frac{T}{\tau}$ and $\alpha = \frac{2-G\tau^2}{G\tau^2}$,

$$W_0 = W_\tau + \frac{4}{3G}\int_1^Z \frac{dZ}{(Z+\alpha)^2 + \frac{1}{3} - \alpha^2}$$

If $p^2 = \frac{1}{3} - \alpha^2$ and when p^2 is negative ($\alpha > \sqrt{1/3}$).

$$\begin{aligned} W_0 &= W_\tau + \frac{4}{3G}\left[\frac{1}{2p}\ln\left(\frac{Z+\alpha-p}{Z+\alpha+p}\right) + C\right]_1^Z \\ &= W_\tau + \frac{2}{3Gp}\left[\ln\left(\frac{(Z+\alpha-p)(1+\alpha+p)}{(Z+\alpha+p)(1+\alpha-p)}\right)\right] \end{aligned} \tag{4.23}$$

When p^2 is positive ($\alpha < \sqrt{1/3}$).

$$\begin{aligned} W_0 &= W_\tau + \frac{4}{3Gp}\left[\arctan\left(\frac{Z+\alpha}{p}\right) + C\right]_1^Z \\ &= W_\tau + \frac{4}{3Gp}\left[\arctan\left(\frac{Z+\alpha}{p}\right) - \arctan\left(\frac{1+\alpha}{p}\right)\right] \end{aligned} \tag{4.24}$$

In this analysis an exact solution is obtained for hinge position and tip deflection unlike in [43], where the numerical solution process was used.

It is seen from equation (4.20) that the hinge is initially (T = 0) at $\Lambda = 3$ irrespective of G. When the fan blade is not rotating (body force,G= 0) the hinge position is constantly at $\Lambda = 3$ till the impulse is acting, and moves away from the tip linearly once the force is removed (3 *times* T/τ). When $G > 0$ the hinge moves away from the tip, as T increases, when the impulse is acting on the blade and even after the force is removed. This is due to the momentum acquired by the segment near the hinge during the action of the force. The curvature decreases as the speed of the moving hinge increases as we see from equation (4.4).

The hinge position and tip deflection for different values of G and τ are shown in Figs. 4.3 4.5. For a larger impulsive force (longer duration, $\tau = 10$) the hinge position is affected to a greater extent by the centrifugal force due to rotation (G).

From the plots it is seen that when the impulse is larger the hinge velocity is small, which is true even when G= 0 . The general trend of the tip deflections and hinge positions are same except that increased value of G causes tip deflections to flatten as time elapses after the force is removed. When G= 0 the tip deflection follows the same trend except that they are linearly affected by square of the τ value

4.3 LARGE DEFLECTION:

The exact solution is not possible in the case of large deflection assumptions as in the previous section, and therefore numerical methods are to be used.

From equations (4.10) and (4.5),

$$\begin{aligned} \frac{dh_0}{d\Lambda} &= 2\,I_1 \\ i.e.\ \dot{I}_0 &= 2\,I_1\dot{\Lambda} \\ \dot{I}_1 &= \dot{\Lambda}\,(\Lambda - I_2 K) \\ \dot{I}_2 &= \dot{\Lambda}\,(I_1 K) \\ \dot{U}_0 &= \dot{\Lambda}\,(1 - W_0 K) \\ \dot{W}_0 &= \dot{\Lambda}\,(U_0 K) \end{aligned} \tag{4.25}$$

If $\dot{\Psi} = Z$, $\ddot{\Psi} = \dot{Z}$, and by using these in equation (4.12) and equating for $\dot{Z}$ from both to obtain K, we get

$$\begin{aligned} \dot{\Lambda} &= \frac{Z}{K} \\ \dot{Z} &= \frac{\left[1 - \frac{Z^2}{K}(\Lambda - I_2 K)\right]}{I_1} \\ K &= \frac{Z^2(I_0\Lambda - I_1^2)}{I_0(1 + I_2 Z^2) - I_1(U_0 - GI_2 - 1)} \qquad T < \tau \\ &= \frac{Z^2(I_0\Lambda - I_1^2)}{I_0 I_2 Z^2 + I_1 I_2 G + I_1} \qquad T > \tau \end{aligned} \tag{4.26}$$

Equations (4.25) and (4.26) are solved as seven simultaneous ordinary differential equations by using Runge-Kutta sixth order method along with respective value of K for $T > \tau$ *or* $T < \tau$.

The difference between large deflection and small deflection assumptions is negligible and therefore the small deflection assumptions are sufficient for this analysis. Fig. 4.3 gives the tip deflection for different values of G and for $\tau = 1.0$ $and \tau = 10.0$. Similar plot for the hinge position is given in Fig. 4.4.

When the blade is considered to be not rotating, the beam deflection and the hinge positions vary with time in a linear fashion as shown in Fig. 4.5. The numerical solution gives very accurate results when compared to exact solution.

4.4 FINITE BLADE RADIUS:

In previous sections the blade was considered to be of infinite length but in practice the length of the blade is finite therefore an analysis to take this into account has been incorporated in the formulations. The centrifugal forces (body forces) are considered to be constant in the previous formulation, which is not a realistic approximation. The centrifugal stiffening effects are not considered here but effect of varying speed on the blade displacements are taken.

The centrifugal force due to rotation has a moment,

$$m \int_0^{\lambda} [(r - \lambda) + u(s,t)] \omega^2 w(s,t) ds$$

where r is the radius of the fan blade.

$$i.e.\ m\omega^2 \left[(r - \lambda) \int_0^{\lambda} w(s,t)\, ds + \int_0^{\lambda} u(s,t) w(s,t)\, ds \right]$$

The equation of motion (4.11) reduces to,

$$f(t)u(0,t) - m\omega^2 [(r - \lambda)\, i_2 + i_3] - M_0 = m \left[i_0 \ddot{\psi} + i_1 \dot{\lambda} \dot{\psi} \right]$$

where

$$\begin{aligned} i_3 &= \int_0^{\lambda} u(s,t) w(s,t)\, ds \\ \frac{di_3}{dt} &= \int_0^{\lambda} \left[u \left(\dot{\psi} u \right) + w \left(-\dot{\psi} w + \dot{\lambda} \right) \right] ds \\ &= \int_0^{\lambda} \left[\dot{\iota} \left(u^2 - w^2 \right) + \dot{\lambda} w \right] ds \end{aligned}$$

Defining

$$\begin{aligned} \iota_4 &= \int_0^{\lambda} (u^2 - w^2)\, ds, \\ \frac{d\iota_3}{dt} &= \iota_1 \dot{v} + \dot{\lambda}\iota_2 \\ \frac{d\iota_4}{dt} &= 2\int_0^{\lambda} \left[u\left(-\dot{v}w + \dot{\lambda}\right) \quad w\left(\dot{v}u\right)\right] ds \\ &= -4\iota_3\dot{v} + 2\dot{\lambda}\iota_1 \end{aligned}$$

In non-dimensional terms,

$$\begin{aligned} \dot{I}_3 &= \dot{\Psi} I_4 + \dot{\Lambda} I_2 \\ \dot{I}_4 &= -4\dot{\Psi} I_3 + 2\dot{\Lambda} I_1 \end{aligned} \tag{4.27}$$

By non-dimensionalizing $R = \frac{\iota_F}{M_0}$ and $\Omega^2 = \frac{m\omega^2 M_0^2}{F^3}$ the equation of motion is written as,

$$U_0 - \Omega\left[I_2\left(R - \Lambda\right) + I_3\right] - 1 = I_0\dot{Z} + I_1\dot{\Lambda}Z$$

$$\begin{aligned} \dot{\Lambda} &= \frac{Z}{K} \\ \dot{Z} &= \frac{\left[1 - \frac{Z^2}{K}\left(\Lambda - I_2 K\right)\right]}{I_1} \\ K &= \frac{Z^2\left(I_0\Lambda - I_1^2\right)}{I_0\left(1 + I_2 Z^2\right) - I_1\left[U_0 - \Omega\left(\left(R - \Lambda\right)I_2 + \iota_3\right) - 1\right]} \qquad T < \tau \\ &= \frac{Z^2\left(I_0\Lambda - I_1^2\right)}{I_0 I_2 Z^2 + I_1\Omega\left[\left(R - \Lambda\right)I_2 + I_3\right] + 1} \qquad T > \tau \end{aligned} \tag{4.28}$$

Equations (4.27), (4.25) and (4.28) are used to solve the simultaneous system of equations as in previous section.

When Λ reaches R, a permanent kink is formed at the root of the cantilever and it rotates as a rigid body about this point. This final rotation is obtained by equating the residual kinetic energy to the energy absorbed due to M_0 and the centrifugal force. As G is proportional to the radius of the blade and rotational speed, it is seen that increase in G considerably changes the hinge formation along the length of the

blade from the tip. Thus for large body force (G), considering finite blade radius is of no use whereas it can be very useful if the radius of the blade has a constraint.

Energy absorbed by the centrifugal force due to rotation is $M \times \theta$:

$$\int_0^{\lambda} m\omega^2 ds\,[(r - \lambda) + (u\cos\theta - w\sin\theta)]\,(u\sin\theta + w\cos\theta)\,\Delta\theta$$

$$m\omega^2(r-\lambda)\left[\int_0^{\lambda} u\,ds\sin\theta + \int_0^{\lambda} w\,ds\cos\theta\right]\Delta\theta$$

$$+ m\omega^2\sin\theta\cos\theta\Delta\theta\int_0^{\lambda}\left(u^2 - w^2\right)ds + m\omega^2\left(\cos^2\theta - \sin^2\theta\right)\cdot\Delta\theta\int_0^{\lambda} uw\,ds$$

$$m\omega^2\left\{(r-\lambda)\left[i_1\sin\theta + i_2\cos\theta\right] + i_4\sin\theta\cos\theta + i_3\left(\cos^2\theta - \sin^2\theta\right)\right\}\cdot\Delta\theta$$

Energy absorbed during final rotation is obtained by integrating this expression

$$m\omega^2\left\{(r-\lambda)\left[-i_1\cos\theta + i_2\sin\theta\right]_0^{\theta_f} + \frac{1}{2}i_4\left(-\frac{\cos 2\theta}{2}\right)_0^{\theta_f} + i_3\left(\frac{\sin 2\theta}{2}\right)_0^{\theta_f}\right\}$$

$$i.e.\ m\omega^2\left\{(r-\lambda)\left[i_1(1-\cos\theta_f) + i_2\sin\theta_f\right] + \frac{1}{4}i_4(1-\cos 2\theta_f) + \frac{1}{2}i_3\sin 2\theta_f\right\} \quad (4.29)$$

By equating energy absorbed by M_0 and centrifugal force to residual kinetic energy,

$$M_0\theta_f + m\omega^2\left\{(r-\lambda)\left[i_1(1-\cos\theta_f) + i_2\sin\theta_f\right] + \frac{i_4}{4}(1-\cos 2\theta_f) + \frac{i_3}{2}\sin 2\theta_f\right\} = \frac{1}{2}mi_0\dot{\psi}^2 \quad (4.30)$$

Dividing throughout by M_0 and non-dimensionalizing,

$$2\theta_f + \frac{\Omega}{2}\left\{1(R-\lambda)\left[I_1(1-\cos\theta_f) + I_2\sin\theta_f\right] + I_4(1-\cos 2\theta_f) + 2I_3\sin 2\theta_f\right\} = I_0\dot{\psi}^2$$

In the case of large deflection approximations it is not possible to evaluate the kink angle as described here due to computational difficulties.

This is a transcendental equation and its solution is obtained iteratively by using the initial value of θ_f, but neglecting the centrifugal force

θ_f = Kinetic Energy − Energy absorbed due to centrifugal force

It is possible to calculate the angle of the kink that is formed after the hinge hits the base of the cantilever when the radius of the fan blade is finite and small.

Rigid plastic analysis of structural response to pulse loading has been presented in this chapter. The next chapter deals with the validation of results by experimental investigation.

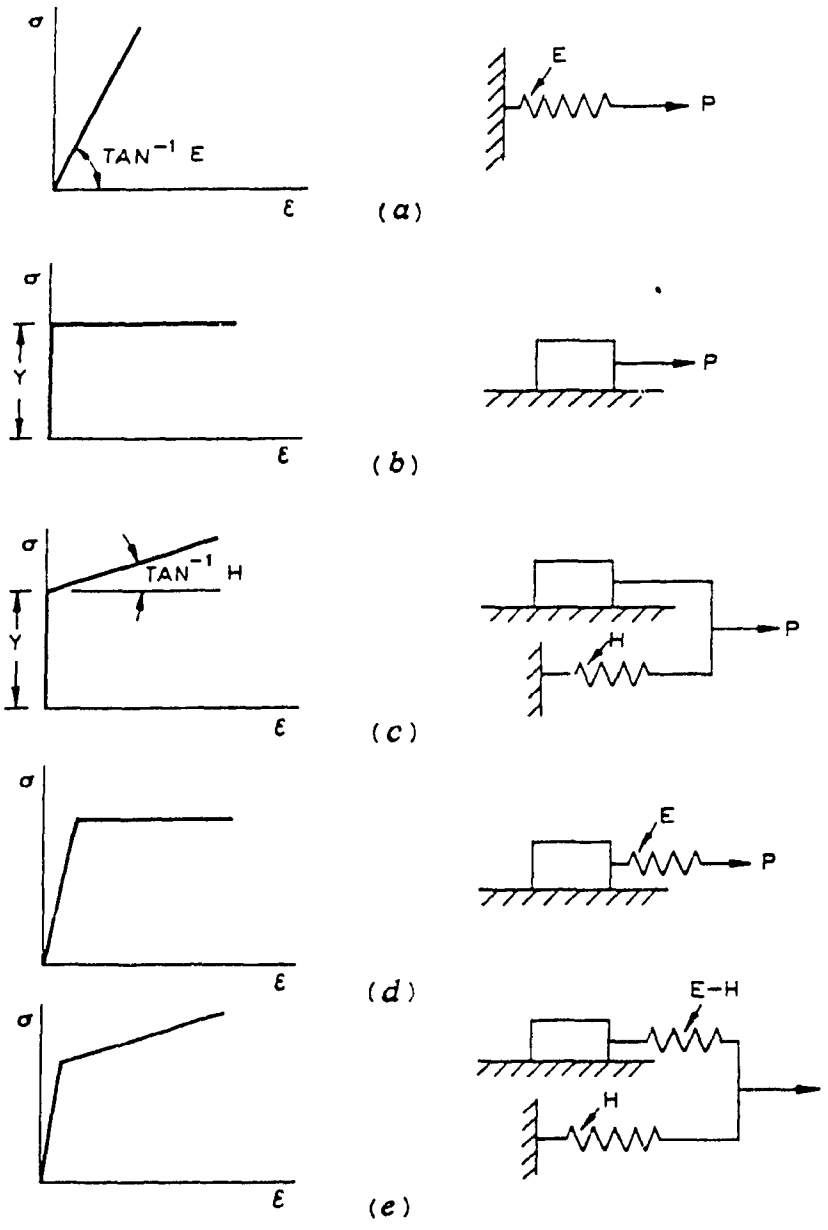

Fig. 4.1 Stress- Strain Diagram showing Material Behavior [37]

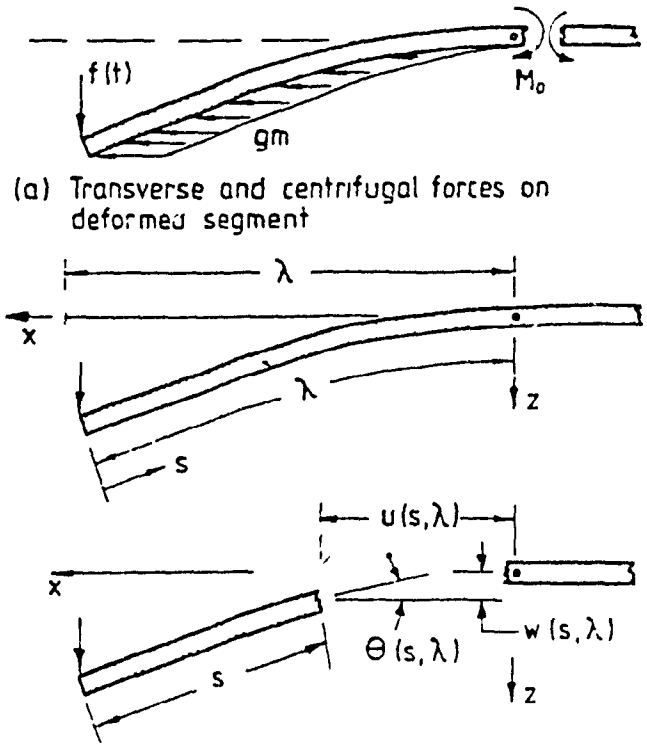

Fig. 4.2 Schematic Diagram showing Cantilever Beam with load at the tip [43]

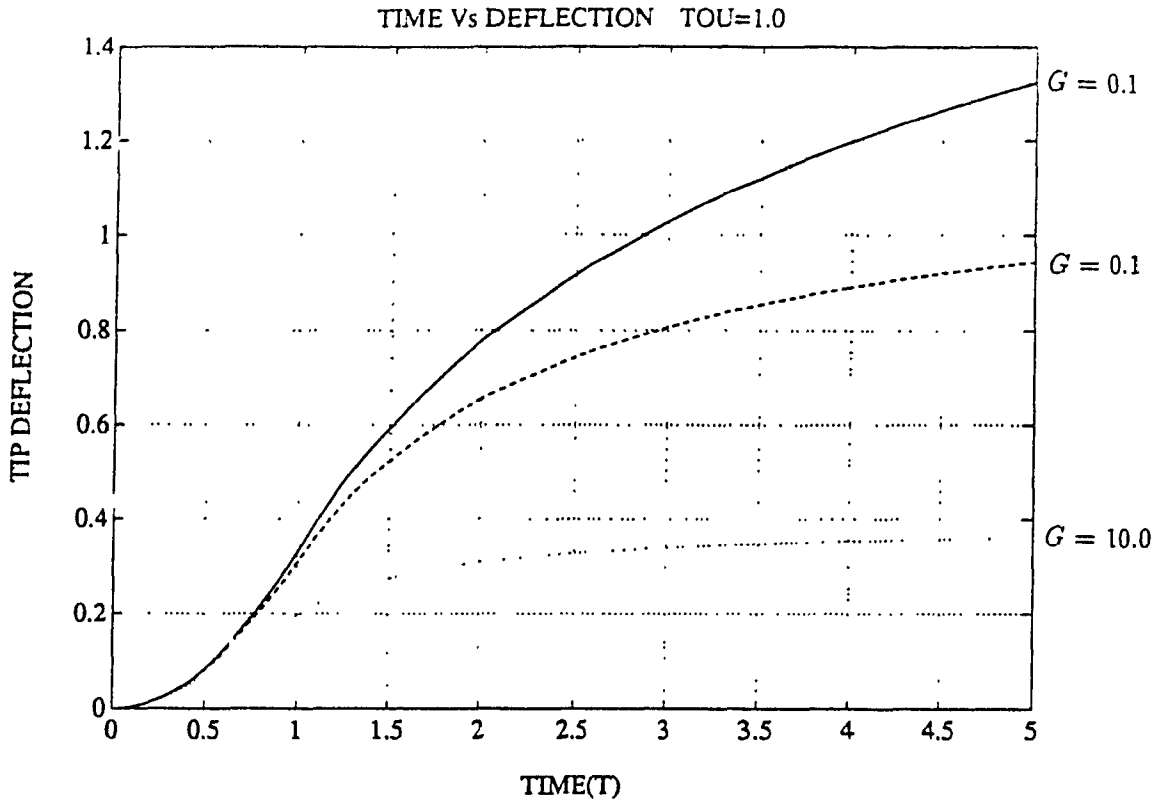

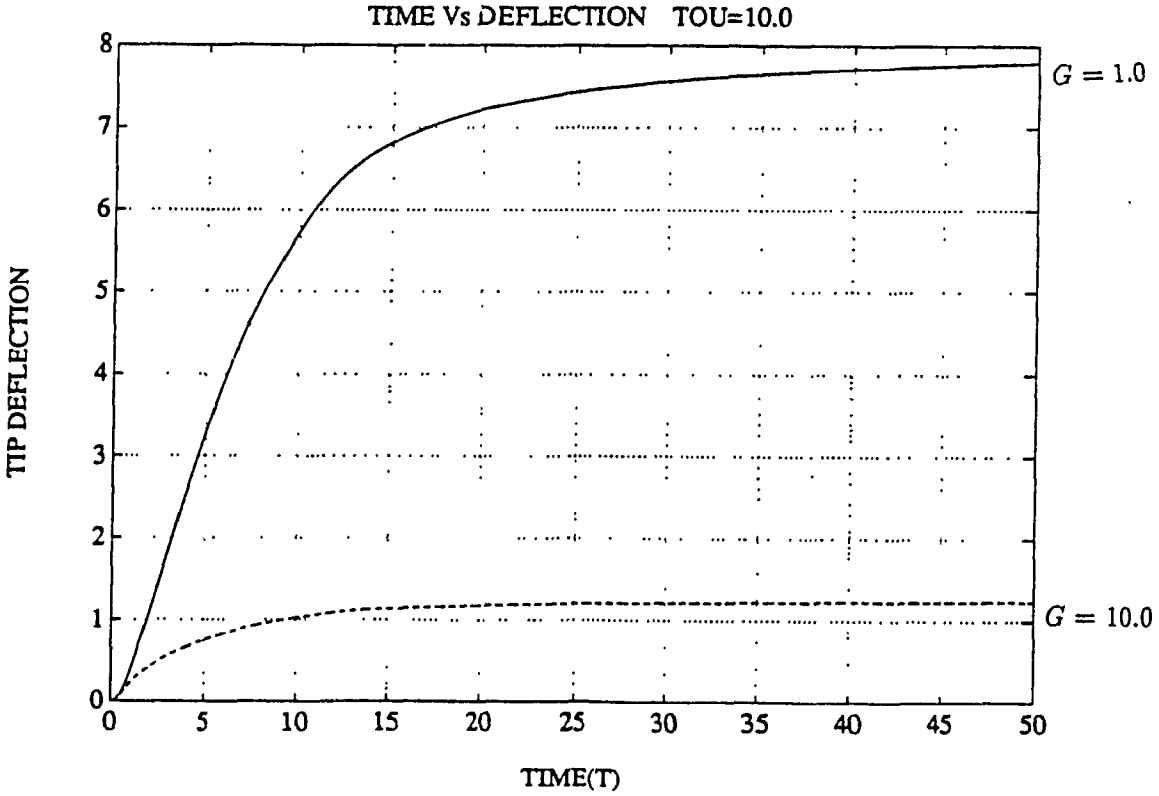

Fig 4.3 Tip Deflection for various G and τ values

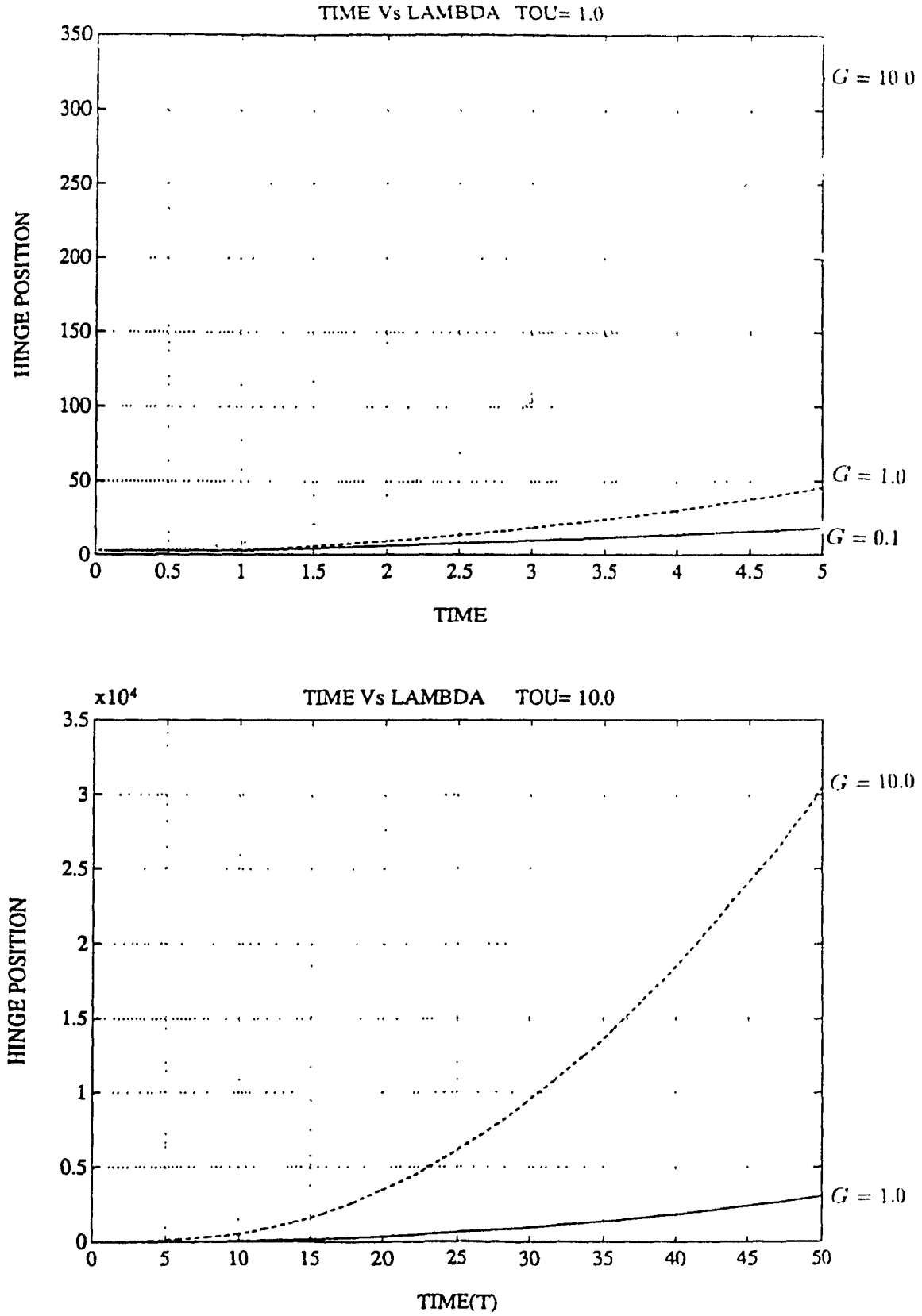

Fig. 4.4 Hinge Position for various G and τ values

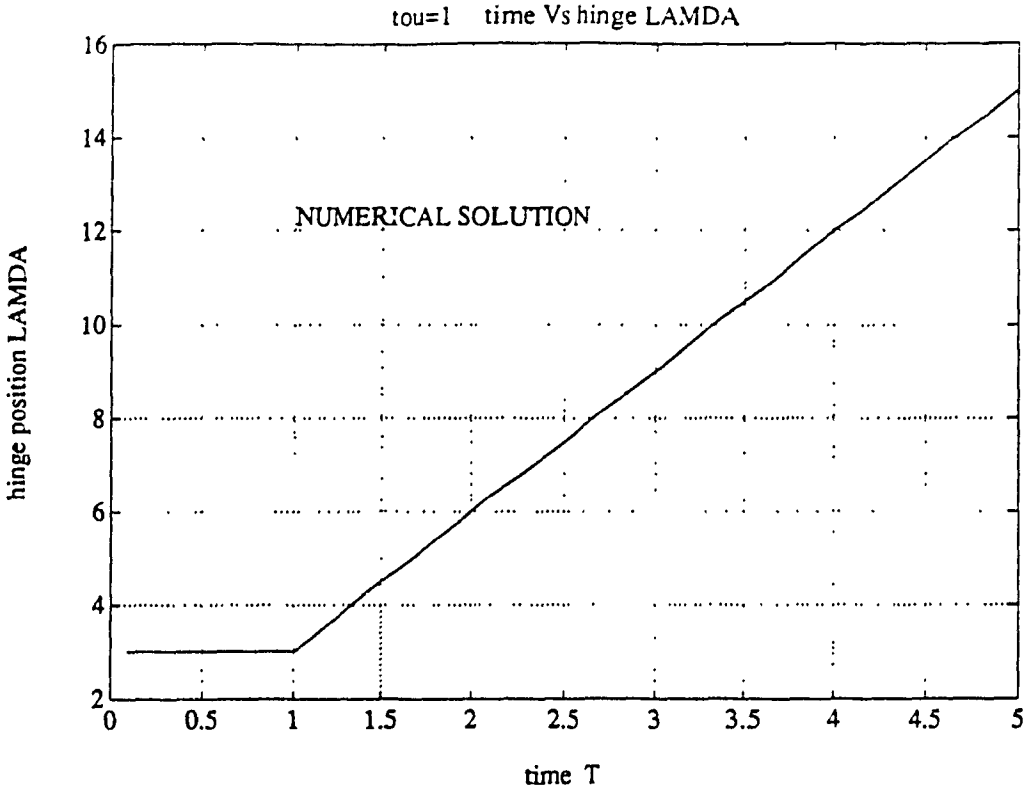

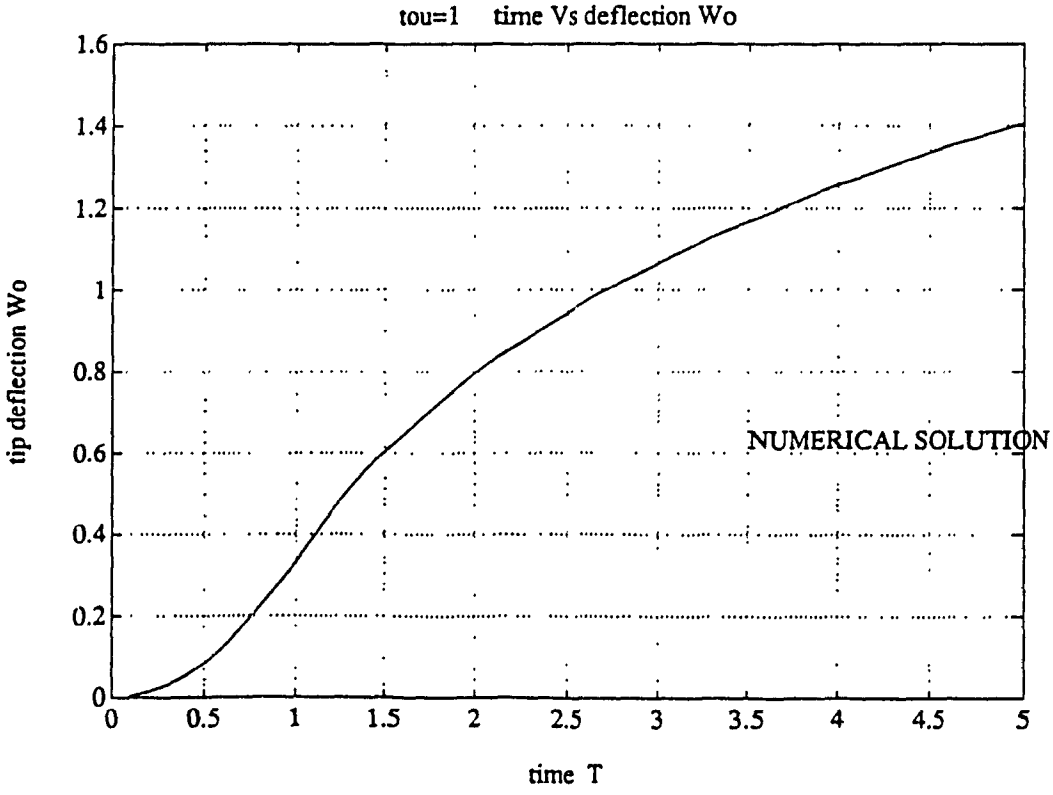

Fig. 4.5 (a) Hinge Position and (b) Tip Deflection for $G = 0$ and $\tau = 1$

Chapter 5

EXPERIMENTAL INVESTIGATIONS

The last three chapters have dealt with the methods of obtaining the elastic and plastic response of beam and plate structures. In this chapter, the experimental investigations carried out to evaluate the response of a plate is presented.

The experimental response of a plate to an impact load due to a falling mass and for the permanent deformation of a cantilever beam is studied. The experimental set-up is as shown in Fig. 5.1. A mass is held by an electro magnet and the plate or beam is clamped onto the steel structure grouted to the floor. The mass is released by breaking the power supply to the magnet.

5.1 MATHEMATICAL MODEL FOR THE TEST STRUCTURE:

A CCFF plate was used to measure the response to an impact load. The 2mm aluminum plate was clamped to a support structure with eight bolts on two adjacent sides. The schematic sketch in Fig. 5.2 shows the overall instrumentation and data acquisition system.

An initial check showed that the natural frequencies of the test structure fell in between that of a SSFF and a CCFF plate. In view of this the test structure was modeled as a plate with two adjacent edges simply-supported with rotational constraints and the other two free. The rotational stiffnesses at the edges was determined by matching the fundamental frequency of the test structure with that of the mathematical model.

The Rayleigh-Ritz analysis with the adjacent edges rotationally constrained and the other two edges free is as follows:

The boundary conditions are,

$$X(0) = 0,\ \beta_q X'(0) = D[X''(0) + \nu Y''(0)]$$

$$D(X''(1) + \nu Y''(1)) = 0,\ D[X'''(1) + (\nu - 1)Y'''(1)] = 0$$

$$Y(0) = 0,\ \beta_q Y'(0) = D[Y''(0) + \nu X''(0)]$$

$$D(Y''(1) + \nu X''(1)) = 0,\ D[Y'''(1) + (\nu - 1)X'''(1)] = 0$$

It is not possible to construct the shape functions satisfying all these conditions. Hence polynomial shape functions for simply-supported end conditions are constructed. The first member of this set of polynomials is $x - 2x^3 + x^4$. The higher polynomials are obtained by Gram-Schmidt process as explained in section 2.2.1.

The energy expressions for the plate with edge restraints is written as,

$$\begin{aligned} T_{max} &= \frac{1}{2}\rho hab\omega^2 \int_0^1 \int_0^1 w^2(x,y)dxdy \\ U_{max} &= \frac{1}{2}Dab \int_0^1 \int_0^1 \left[\left(\frac{\partial^2 w}{\partial x^2}\right)^2 + \left(\frac{\partial^2 w}{\partial y^2}\right)^2 + 2\nu \frac{\partial^2 w}{\partial x^2}\frac{\partial^2 w}{\partial y^2} + 2(1-\nu)\left(\frac{\partial^2 w}{\partial x \partial y}\right)^2 \right] dxdy \\ &\quad + \frac{1}{2}\sum_{q=1}^{Q} \left[\beta_q \int_0^l \left(\frac{\partial w}{\partial s}\right)^2 dl \right] \end{aligned} \tag{5.1}$$

where the term with rotational edge supports with stiffnesses β_q per unit rotation is given as a sum along each edge.

The terms in strain energy expression remain same as that in previous case discussed in section 2.2 but with an additional term due to the rotational constraint. This term can be expanded as,

$$\beta_1 \int_0^b \left(\frac{\partial w}{\partial x}\right)^2 dy + \beta_2 \int_0^a \left(\frac{\partial w}{\partial y}\right)^2 dx \tag{5.2}$$

$$\frac{\beta_1}{a^2} \int_0^1 (X'_m Y_n)^2 dy + \frac{\beta_2}{b^2} \left(X_m Y'_n\right)^2 dx \tag{5.3}$$

If both the coefficients of edge restraint are same then the above expression can be written as,

$$\frac{\beta_q}{a^2} \left[\int_0^1 (X'_m X'_i Y_n Y_j)\, dy + \alpha^2 \int_0^1 \left(X_m X_i Y'_n Y'_j\right) dx \right] \tag{5.4}$$

$$\frac{\beta_q}{a^2} \left[H^{1,1,0,0}_{minj} + \alpha^2 H^{0,0,1,1}_{minj} \right] \tag{5.5}$$

where

$$H^{(1,1,0,0)}_{minj} = \int_0^1 X'_m(x) X'_i(x) Y_n(y) Y_j(y) dy \tag{5.6}$$

and similar expression along y is $H^{0,0,1,1}_{minj}$

The eigenvalue problem similar to expression in equation (2.8) can be written as,

$$\sum_{mn} A_{mn} \left[C_{minj} + \beta_q \left(H^{(1,1,0,0)}_{minj} + \alpha^2 H^{(0,0,1,1)}_{minj} \right) - \Omega E^{(0,0)}_{mi} F^{(0,0)}_{nj} \right] \tag{5.7}$$

where $\beta_q = \frac{\beta_q a^2}{D}$ is the rotational stiffness coefficient, and $\Omega = \frac{\rho h \omega^2 a^4}{D}$.

The natural frequencies by varying the rotational stiffness parameter is obtained by solving the eigenvalue problem as explained in Chapter 2.

The stiffness parameter, β_q chosen for obtaining the fundamental frequency same as that of the experimentally observed value is 2.72. The frequencies and mode

shapes thus obtained are used in the acceleration response evaluation of a plate which has boundary conditions in between SSFF and CCFF.

In order to obtain the acceleration response plot of a CCFF plate for impact, the equation (3.12) is rewritten in terms of the acceleration as,

$$\ddot{W}^* = F\left\{\sum_{m=0}^{\infty}\sum_{n=0}^{\infty}[X_m(c)Y_n(d)]\ [X_m(x)Y_n(y)]\ [\gamma_{mn}(T)]\right\} \tag{5.8}$$

where

$$\ddot{W}^* = \ddot{w}\cdot\frac{\rho hab}{F_p}; T = \sqrt{\frac{D}{\rho h a^4}}\cdot t; \gamma_{mn} = \frac{T_i}{2\tau}\sin\omega_i t - \frac{p^2}{\omega_i}\sin pt$$

The acceleration response by using this expression in analysis is presented in Fig. 5.3 along with corresponding experimental results after converting into dimensional values. The trend in the case of both test structure and mathematical model are reasonably matching.

A study is also conducted to find a reasonable damping parameter and the load pulse duration that gives comparable acceleration magnitude and the trend. It is seen that the rectangular pulse period, τ is 0.25 seconds and the damping parameter, ζ to be between 0.5–1.5%. Plots for different damping ratios are presented in case of mathematical models in Figs. 5.3 and 5.4.

Fig. 5.1 Pictures showing Experimental set up and the [illegible]on

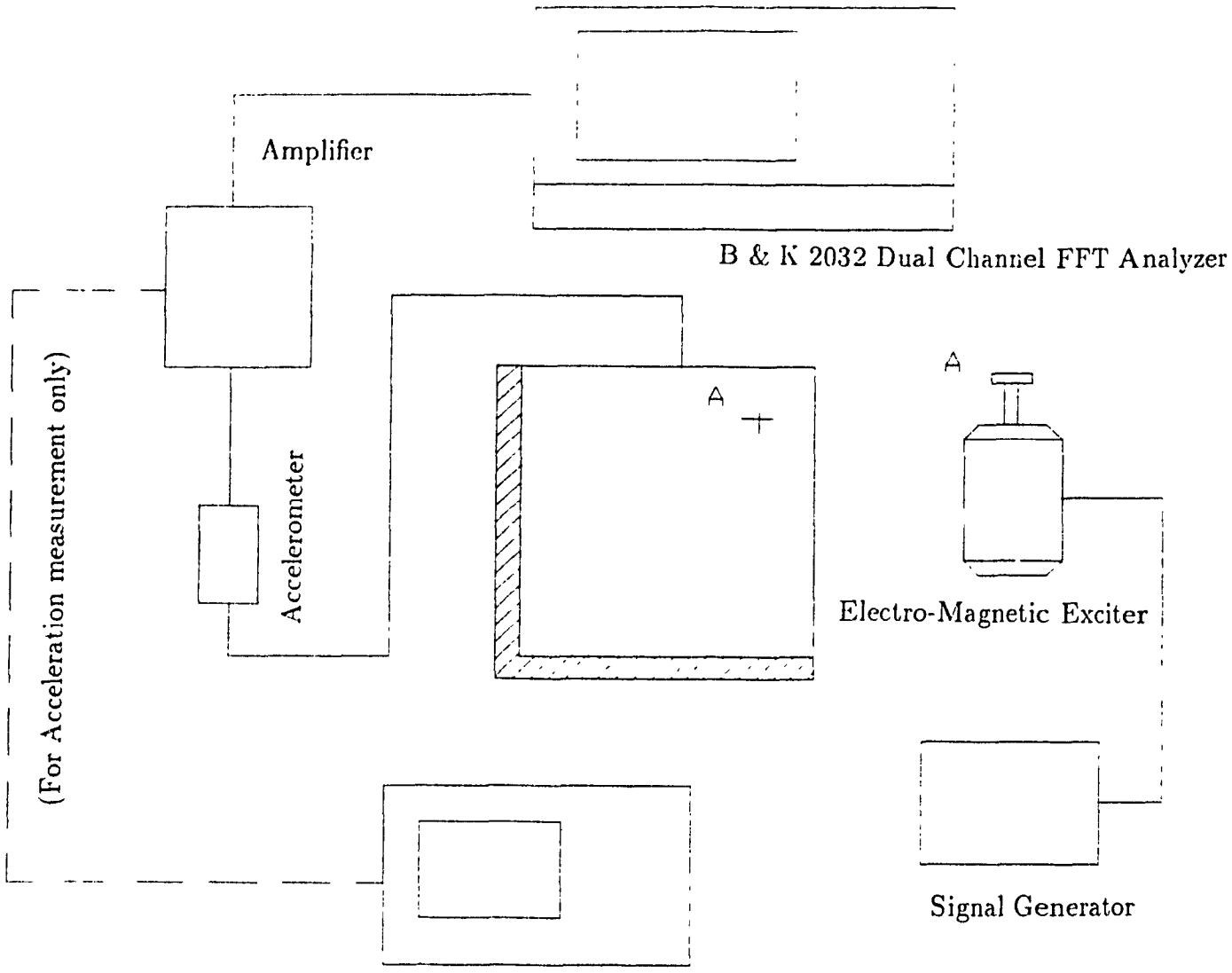

Fig. 5.2 Schematic diagram showing the instrumentation for plate response measurement.

(a)

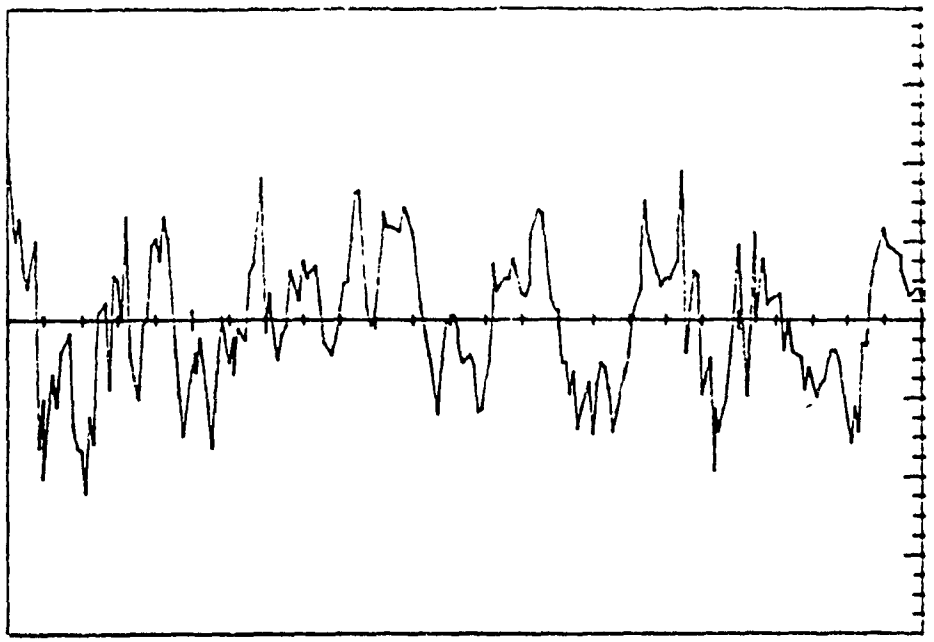

Time in seconds (0.0004 s/ div)

(b)

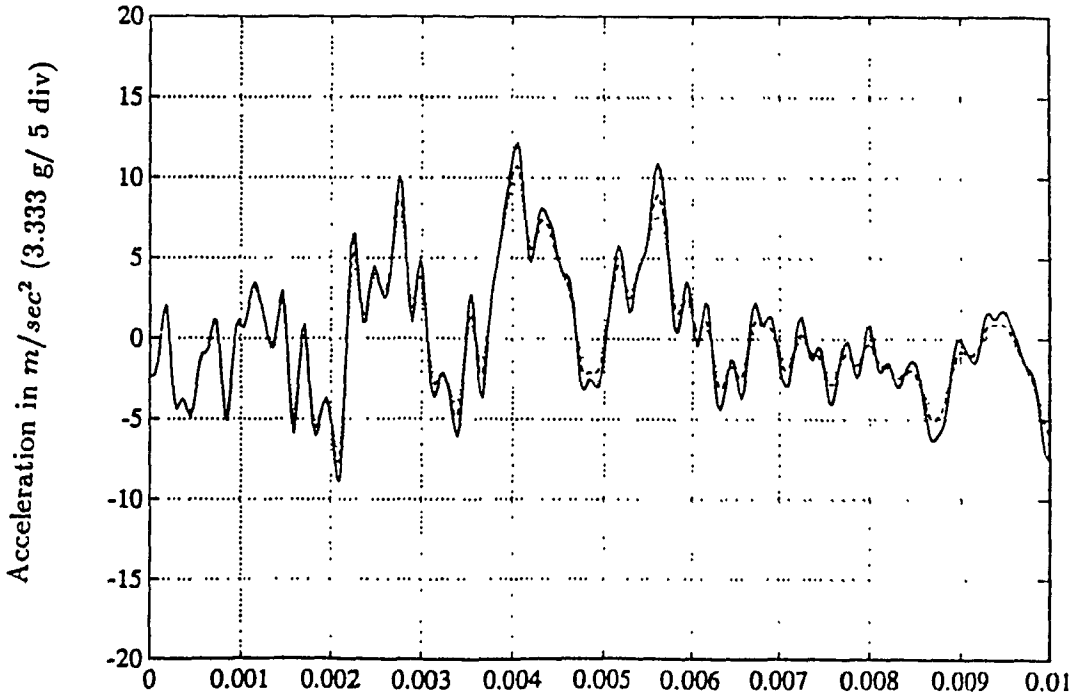

Time in seconds

Fig. 5.3 Acceleration Response of (a) test structure, and (b) mathematical model with different damping (— $\zeta = 0.005$, - - - $\zeta = 0.010$, $\cdots \zeta = 0.015$).

(a)

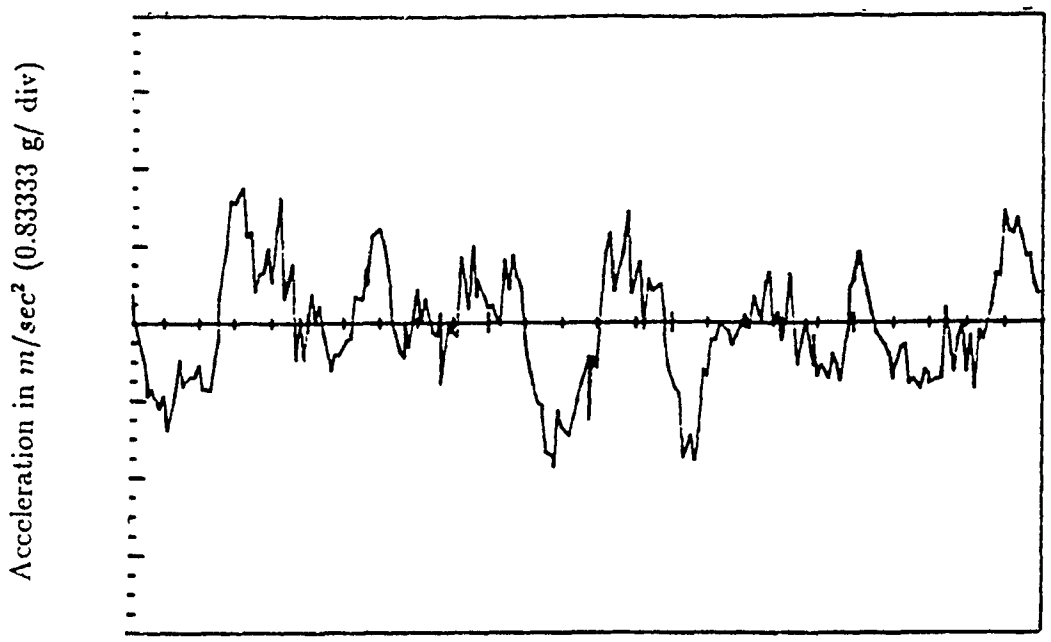

(b)

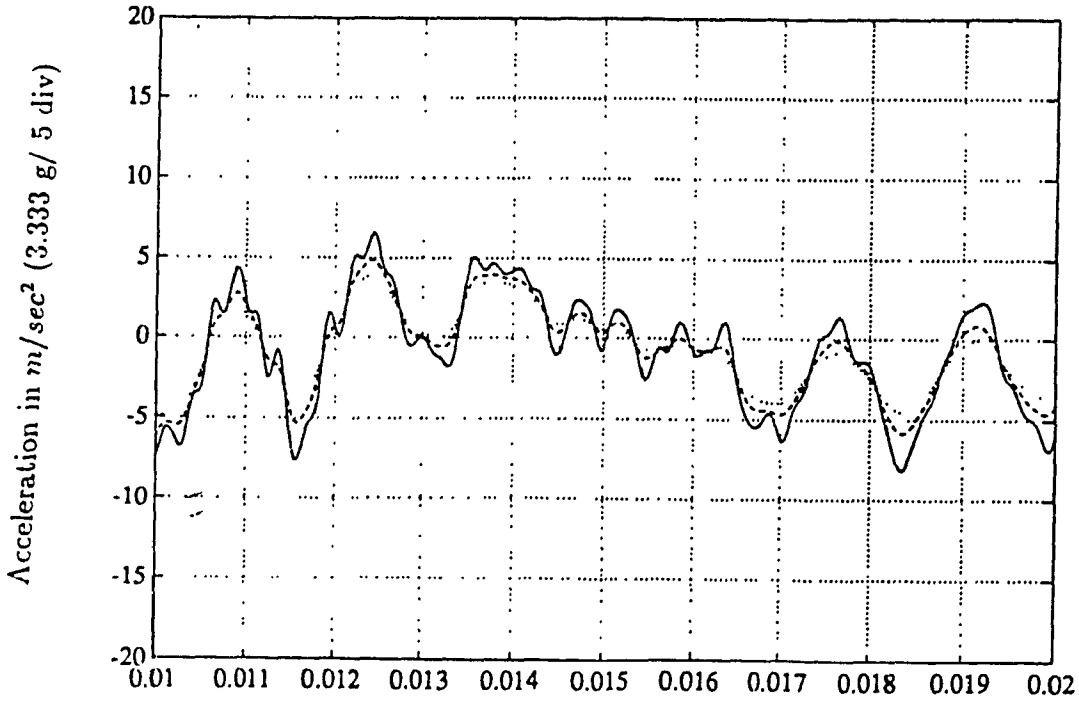

Fig. 5.4 Acceleration Response of (a) test structure, and (b) mathematical model with different damping (— $\zeta = 0.005$, - - - $\zeta = 0.010$, $\cdots \zeta = 0.015$).

Chapter 6

CONCLUSIONS AND SCOPE FOR FURTHER RESEARCH

The response of mechanical system elements such as beams and plates subjected to impact loads are analysed in this thesis. When the response is within the elastic range, normal mode analysis is employed and rigid plastic analysis is used in the plastic range.

A normal mode analysis for a simply-supported beam and cantilever beam is carried out for standard pulse loads. Similar study on plates is also carried out after solving the eigenvalue problem by Rayleigh Ritz method.

The Rayleigh-Ritz method is used in solving the plate eigenvalue problem. Improved shape functions are formulated to minimize the estimates by reduction of plate differential equation to an ordinary differential equation. The Rayleigh Ritz results obtained by using these approximate functions are compared with those values obtained by using beam orthogonal polynomials and beam characteristic functions. Plate Characteristic Functions and natural frequencies by iterative reduction of plate partial differential equation to an ordinary differential equation provides very good estimates for the natural frequencies and mode shapes. Mode shapes are much simpler when compared with those obtained using Rayleigh Ritz method and takes less time for response evaluation.

In the case of large magnitude of impact force the structure would cross the linear range of response. The rigid plastic analysis of a cantilever beam is used to study the behavior of the beam response due to an impact load at the tip.

Elastic acceleration response of a plate is observed due to a mass falling on it

by an experiment and a suitable mathematical model is formulated.

6.1 CONCLUSIONS

Based on the study of beam and plate response due to impact loads, the following conclusions could be drawn from the work presented in preceeding chapters:

6.1.1 Elastic Response

- Frequency coefficients and shape functions are more accurate, almost exact, in the case of Plate Characteristic Functions compared to those obtained using the Rayleigh-Ritz analysis.
- Approximate plate functions and Beam characteristic functions do not vary much in displacement shape but their higher derivatives do differ.
- Response evaluation time using plate characteristic function is much less since the mode shapes are simple functions as against the series form of mode shapes in the Rayleigh-Ritz method. When n terms are used, plate characteristic functions need computational time proportional to n as against n^2 with the Rayleigh-Ritz method.
- Both beam and plate response evaluations to pulse loads indicate that the contribution from the fundamental mode is dominant in the total response.

6.1.2 Plastic Response

- In the case of small approximations, the numerical and close form solutions yield very close results, indicating accuracy of the numerical method. Therefore it may be concluded that the large deformation results obtained by numerical method are also reasonably accurate.

6.1.3 Experiments

- Homogeneous edge conditions are hard to simulate in practice, and hence it is more realistic to assume flexible edge conditions.
- Mathematical model gives more realistic response to that of the test structure, and it compares well.

6.2 RECOMMENDATIONS FOR FUTURE WORK

Following recommendations are made for future research in this area:

- Mode shapes, slopes, moments, and shear forces at the plate edges should be computed to verify if the plate characteristic functions satisfy the boundary conditions exactly.
- Plates involving free edges and a free corner should be studied.
- Application of Plate Characteristic Functions in other plate shapes should be carried out.
- Plastic Analysis can be extended to plates to find the local behavior of the structure to impact loads.
- More exhaustive experimental investigations need to be carried out to analyse the plate response.

References

[1] C. .M. HARRIS and C. E. CREDE Second Edition. Shock and Vibration Handbook McGraw Hill Book Company. New York

[2] WERNER GOLDSMITH Impact The theory and physical behaviour of colliding solids, Edward Arnold Ltd., London

[3] S. CHATTOPADHYAY, 1987 The Journal of Acoustic Society of America **82** 493 497, Permanent Indentation Effects on the Impact Response of Elastic Plates.

[4] K. KARAS, 1939 Ing. Arch. **X**, 237 250 Platten Unter Seitlichem Stoss

[5] C. ZENER, 1941 Phys. Rev., **59**, 669 673, The Intrinsic Inelasticity of Plates.

[6] W. H. HOPPMANN, 2ND 1948 Journal of Applied Mechanics, Trans. ASME **70** 125 140. Impact of a Mass on a Damped Elastically Supported Beam.

[7] W. H. HOPPMANN, 2ND 1949 Journal of Applied Mechanics, Trans. ASME **71** 370 374. Impact of a Mass on a Column.

[8] W. H. HOPPMANN, 2ND 1950 Journal of Applied Mechanics, Trans. ASME **72** 409 414. Impact on a Multispan Beam.

[9] D. A. TROWBRIDGE, J. E. GRADY, R. A. AIELLO 1991 Computers and Structures **40** 977 984. Low Velocity Impact Analysis with NASTRAN.

[10] H. L. CHEN, W. LIN, L. M. KEER and S. P. SHAH 1988 Journal of Applied Mechanics, Trans. ASME **55** 887–894. Low Velocity Impact of an Elastic Plate Resting on Sand.

[11] M. SANSALONE and N. J. CARINO 1987 Journal of Research of the National Bureau of Standards **92** 355-367. Transient Impact Response of Thick Circular Plates.

[12] R. L. RAMKUMAR and P. C. CHEN 1983 AIAA Journal, **21** 1448–1452. Low Velocity Impact Response of ..minated Plates.

[13] DANA YOUNG and ROBERT P. FELGAR, JR. 1949 University of Texas Publication. Tables of Characteristic Functions Representing Normal Modes of Vibration of a Beam.

[14] A. W. LEISSA 1969 NASA SP 160. Vibration of Plates

[15] A. W. LEISSA 1973 Journal of Sound and Vibration, **31** (3), 257 293. The free Vioration of Rectangular Plates.

[16] K. VIJAYAKUMAR and G. K. RAMAIAH 1978 Journal of Sound and Vibration **56**, 127-135. Analysis of Vibration of Square Plates by the Rayleigh-Ritz Method with Asymptotic Solutions from a modified Bolotin Method.

[17] R. B. BHAT 1985 Journal of Sound and Vibration, **102** , 493 499. Natural Frequencies of Rectangular Plates using Characteristic orthogonal polynomials in Rayleigh-Ritz method.

[18] T. S. CHIHARA 1978 Introduction to Orthogonal Polynomials, Gordon and Breach Science Publishers, London

[19] R. B. BHAT 1985 Journal of Engineering Mechanics, Transactions of A.S.C.E., **111**(11) 1301 1309. Plate Deflections using orthogonal polynomials.

[20] R. B. BHAT 1990 Journal of Sound and Vibration **138** (2), 205 219. Numerical Experiments on the determination of natural frequencies of transverse vibrations of Rectangular plates of nonuniform thickness.

[21] S. M. DICKINSON and A. DI BLASSIO 1986, **108** (1), 51 62. On the use of orthogonal polynomials in Rayleigh-Ritz method for the study of flexural vibration and buckling of isotropic and orthotropic plates.

[22] C. S. KIM and S. M. DICKINSON 1987 Journal of Sound and Vibration **114** 129 -142. The flexural Vibration of line supported rectangular plate systems.

[23] P. A. A. LAURA and V. H. CORTINEZ 1988 Journal of Sound and Vibration **122** 396 398. Optimization of the Kantorovich method when solving eigenvalue problems.

[24] V. H. CORTINEZ and P. A. A. LAURA 1990 Journal of Sound and Vibration **137** , 457-461. Analysis of vibrating rectangular plates of discontinuously varying thickness by means of the Kantorovich extended method.

[25] S. M. DICKINSON 1978 Journal of Sound and Vibration **59** , 143-146. On the use of simply supported plate functions in Rayleigh-Ritz method applied to the flexural vibration of rectangular plates.

[26] S. M. DICKINSON and E. K. H. LI 1982 Journal of Sound and Vibration **80**, 292 297. On the use of Simply-Supported Plate Functions in the Rayleigh-Ritz method applied to the Flexural Vibration of Rectangular Plates.

[27] L. V. KANTOROVICH and V. I. KRYLOV 1964 Approximate Methods of Higher Analysis. New York : John Wiley and Sons, Inc. (Translated by C. D. BENSTER).

[28] G. B. WARBURTON 1979 Journal of Sound and Vibration **7** , 327-334. Response using the Rayleigh-Ritz method.

[29] D. J. GORMAN Free Vibration Analysis of Rectangular Plates. Elsevier Science Publishers B.V. Amsterdam , The Netherlands

[30] R. B. BHAT Modal Analysis of Mechanical Systems and Applications, Department of Mechanical Engineering, Concordia University, Montreal, Canada.

[31] L. MEIROVITCH 1986 Elements of Vibration Analysis, Second Edition McGraw Hill Book Company, New York

[32] L. MEIROVITCH 1967 Analytical Methods in Vibrations The Macmillan Company, New York

[33] S. TIMOSHENKO, D. H. YOUNG, W. WEAVER Jr. Vibration Problems in Engineering. Fourth Edition, John Wiley and Sons, New York

[34] W. H. LIU and C. C. HUANG Journal of Sound and Vibration **119(1)** 177-182 1987 Free Vibration of a Rectangular Plate with elastically restrained and free edges.

[35] M. MUKHOPADHYAY Journal of Sound and Vibration **67(4)**, 159 168 1979 Free Vibration of Rectangular Plates with edges having different degrees of rotational restraint.

[36] J. M. BIGGS Introduction to Structural Dynamics, McGraw Hill Book Company, New York

[37] W. JOHNSON and P. B. MELLOR Engineering Plasticity Ellis Horwood Ltd., Chichester, England

[38] S. S. RAO and K. S. RAGHAVAN 1987 Journal of Applied Mechanics, Trans. ASME **54** 228–230. Dynamic Inelastic Response of Beams and Plates Under Combined Loading.

[39] K. NAGAYA 1980 Journal of Applied Mechanics, Trans. ASME **47** 620 626 Dynamic Response of a Plate with Arbitrary Shape.

[40] W. JOHNSON Impact Strength of Materials, Edward Arnold Ltd.

[41] J. B. KENNEDY and K. J. IYENGAR 1981 Canadian Journal of Civil Engineering Vol. **8**, 409-415 Rigid-Plastic analysis of floating ice sheets under impact loads.

[42] E. W. PARKES Proceedings of Royal Society, London Series A, Vol. 228, 1955 462–476 The Permanent deformation of a cantilever struck transversely at its tip.

[43] W. J. STRONGE and T. SHIOYA 1984 Journal of Applied Mechanics Trans of ASME **51** 501–504 Impact and Bending of a Rigid-Plastic Fan Blade.

[44] N. LEVY and W. GOLDSMITH International Journal of Impact Engineering Vol. 2, No. 3 209 229 1984 Normal Impact and perforation of thin plates by hemispherically tipped projectiles. -I Analytical Considerations.

[45] N. LEVY and W. GOLDSMITH International Journal of Impact Engineering Vol. 2, No. 4 299-324 1984 Normal Impact and perforation of thin plates by hemispherically tipped projectiles. -II Experimental Results.

[46] S. R. BODNER and P. S. SYMONDS 1962 Journal of Applied Mechanics Trans. of ASME **29** 1984 501 504 Impact and Bending of a Rigid-Plastic Fan Blade.

[47] T. C. T. TING 1965 Journal of Applied Mechanics Trans. of ASME **32** 295 302 Large Deformation of a Rigid, Ideally Plastic Cantilever Beam.

[48] NORMAN JONES 1990 Structural Impact, Cambridge University Press

[49] R. M. BRACH 1991 Mechanical Impact Dynamics Rigid Body Collisions, John Wiley and Sons, New York